Deltares

Characterization of flows induced by propeller jets

Physical scale model tests report

enabling delta life

Characterization of flows induced by propeller jets
Physical scale model tests report

Author(s)
Helena dos Santos Nogueira
Christian van Nieuwenhuizen
Wout Bakker

Characterization of flows induced by propeller jets
Physical scale model tests report

Client	-
Contact	-
Reference	TKI Deltatechnologie - DEL130 SOP Schroefstraalbelasting onderzoeksprogramma
Keywords	Propeller jet, Bed protection, Quay wall, Bow thruster, Physical scale model, PIV

Document control	
Version	1.0
Date	27-03-2023
Project nr.	11206641-003
Document ID	11206641-003-HYE-0001
Pages	89
Classification	
Status	final

Author(s)		
	Helena I. S. Nogueira	
	Christian van Nieuwenhuizen	
	Wout Bakker	

The allowed use of this table is limited to check the correct order-performance by Deltares. Any other client-internal-use and any external distribution is not allowed.

Doc. version	Author	Reviewer	Approver
1.0	Helena I. S. Nogueira Helena Isabel dos Santos Nogueira	Arne van der Hout	Bas van Vossen

Summary

Propellers of ships generate high velocities in waterways near quay walls, jetties and locks. Often, bed protection is installed in order to prevent instability of hydraulic structures due to propeller scour. Large costs can be associated with its construction. Guidelines for the design of bed protection exists, but propeller-induced loads are far from fully understood and current design guidelines may not always result in optimal bed protection designs. Therefore, a working group on propeller jet research was established, headed by the CROW and Rijkswaterstaat, with the long-term aim to improve design guidelines in order to reduce design-related uncertainty, potentially save construction materials and reduce costs. The research described in the present report was carried out in the context of this propeller jet working group, aiming to increase the understanding of transversal bow thruster loads reflected off a vertical quay wall and providing validation data for numerical models.

The present report summarizes the scale model tests performed to visualize and characterize the flow field generated by a bow thruster. The work described in the present report is part of the TKI-“Schroefstraalbelasting onderzoeksprogramma” (SOP) project DEL130, which was funded by the TKI Delta technology program and project partners. The following partners participated in the TKI-SOP project: BAM infraconsult B.V., Baggermaatschappij Boskalis B.V., Deltares, DEME, MARIN, North Sea Port Flanders n.v., Port of Rotterdam, Rijkswaterstaat, and SmartPort.

Within the TKI-SOP project the following work packages have been carried out:

- Field measurements in Ghent (Rijkswaterstaat/TUDelft, 2020, [1])
- Numerical CFD simulations (MARIN, 2023, [7])
- Physical scale model measurements (Deltares, 2021/2022, [present report])

The present report describes the results of the third item listed above, namely the physical scale model measurements carried out by Deltares. In these measurements, the transverse flow induced by a 4-channel bow thruster of an inland vessel has been measured in detail. The test setup was chosen to represent the conditions as measured in the field measurements in Ghent [1]. Next to that, several systematic variations have been performed to gain better understanding of the most important parameters for design of bed protections. The variations considered in the present research include:

- Quay wall clearance
- Under keel clearance
- Applied propeller power
- Use of multiple propellers
- Influence of bed roughness.

Furthermore, some preliminary tests have been performed with a bed protection of loose rocks to illustrate the initiation of bed deformation near a quay wall.

The dataset that has been obtained within this research project is extensive and characterizes flow induced by a transverse bow thruster in very high detail. The data can therefore be used as a benchmark for numerical model validation and further optimization of design guidelines for bed protections. The research shows that highest flow velocities occur for smallest wall and underkeel-clearances. Present design guidelines predict the magnitude of max horizontal velocity near the bed well for most tested situations, however farther away from the quay wall guidelines seem to be overly conservative, providing room for optimization of bed protections.

Contents

1 Introduction

1.1 Background

Propellers of ships generate high velocities in waterways near quay walls, jetties and locks. Often, a bottom protection is installed in order to prevent instability of hydraulic structures due to propeller scour. Large costs can be associated with its construction. Guidelines for the design of bed protection exists, but propeller-induced loads are far from fully understood and current design guidelines may not always result in optimal bed protection designs. Therefore, a working group on propeller jet research was established, headed by the CROW and Rijkswaterstaat, with the long-term aim to improve design guidelines in order to reduce design-related uncertainty, save materials and costs and optimize bed protection designs. The research described in the present report was carried out in the context of this propeller jet working group, aiming to increase the understanding of transversal bow thruster loads reflected off a vertical quay wall and providing validation data for numerical models that can be used for bed protection design.

Rijkswaterstaat (RWS) has set up a roadmap with the goal of improving design guidelines for bottom protection near maritime infrastructure. In this context, a CROW working group was established to jointly develop research initiatives contributing to the knowledge gaps identified in the field of scour induced by propeller jets. The research program “Schroefstraalbelasting OnderzoeksProgramma” (SOP) was developed under the TKI Delta Technology framework to gain a better understanding of the physical processes associated with scour induced by propeller jets, combining efforts from field measurements, scale models tests and numerical modelling.

In 2020 field measurements were performed in the Port of Ghent on jets induced by bow thrusters reflected on a vertical quay-wall, where flow velocities and pressures were measured along the quay-wall and near the bottom. Field measurements provide valuable insight into the flow phenomena in prototype scale. However, due to limitations in the field, assessing the influence of all relevant parameters is practically not feasible. Therefore, using the field measurements as basis, scale model tests and numerical simulations were performed to extend the existing database by a systematic variation of parameters. The numerical simulations were developed by MARIN in 2022 (ref. [7]) and the scale model tests were performed by Deltares in the period of 2021/2022. The scale model was based on the field measurements performed in the Port of Ghent (ref. [1]).

1.2 Scope

This report focuses on the scale model tests performed at Deltares in the period of 2021/2022. The scale model tests were divided in two test series: initial series and additional series. Both test series are described in this report. The initial test series focused on testing one bow thruster over a smooth bed. The main goal of these tests was to quantify the efflux velocity at the outlet of the bow thruster and to characterize the reflected jet underneath the vessel, aiming at quantifying the location and magnitude of the maximum flow velocity near the bed. Based on the results of the initial test series, an additional test series followed focusing on testing both thrusters simultaneously active and testing with a rough bed (fixed and mobile). The aim of the additional test series was to assess the increase in flow velocities near the bed with two propellers on, and to assess how bed roughness influences the maximum velocity near the bed. The results from these scale model tests may be the basis for updating the existing guidelines for the design of bottom protection.

2 Model scale

2.1 Scaling rules

For a proper reproduction of the propeller jet flow in the model, the most important scaling criteria are:

- Froude scaling
- Reynolds scaling

Modelling based on Froude scaling means that an equal ratio between inertial and gravity forces in both the model and the prototype is assumed. This assumption is valid for flows where the gravity and inertial forces are dominant and the effect of remaining forces such as kinematic viscosity are small, which is applicable to free-surface flows. The Froude number is defined as:

$$Fr = \frac{u}{\sqrt{gh}}$$

In which u is the flow velocity (m/s), g is the acceleration of gravity (m/s^2) and h is the water depth (m).

For phenomena where viscous and inertial forces are dominant, Reynolds scaling should be applied. The Reynolds number is defined as:

$$Re = \frac{uD}{\upsilon}$$

Where v is the kinematic viscosity of the fluid (m^2/s) and D a representative length scale.

In practice, it is not feasible to satisfy simultaneously Froude and Reynolds similarity in a physical scale model. For free-surface flows, Froude scaling is typically adopted with the drawback of not representing correctly viscous effects in the scale model. However, if the Reynolds number is kept sufficiently large in the scale model, scale effects may be considered negligible. In order for scale effects due to viscosity to be negligible, the Reynolds number, as defined below, should exceed their corresponding limits (as established by ref. [2]):

- Reynolds number of the jet flow
$$Re_{flow} = \frac{u_0 D_p}{\upsilon} > 3 \times 10^3$$
- Reynolds number of the propeller
$$Re_{propeller} = \frac{nD_p L_m}{\upsilon} > 7 \times 10^4$$

Where u_o is the axial efflux velocity of a propeller, D_p the propeller diameter, n the number of revolutions per second of the propeller and L_m an characteristic length of the propeller. For a chosen model scale, n_L, the relevant scale factors following the Froude scaling law are presented below:

Length	n_L
Velocity	$n_u = \sqrt{n_L}$
Discharge	$n_Q = {n_L}^{2.5}$
Force	$n_F = {n_L}^3$

2.2 Scale factor

For the selection of the model scale, several aspects shall be considered:

- Geometrical constraints in the experimental facility
- Scale effects should be limited
- Dimensions of available propellers
- Practicality of the (PIV) measurements

In order to limit scale effects, the model should be as large as possible while fitting in the experimental facility. In the available facilities at Deltares, a model of scale up to 1:10 could be built. On the other hand, a large model will increase the difficulty of performing PIV measurements (limiting factors include cable length of PIV cameras and laser, vector field resolution, particle image quality as function of distance between camera and measurement plane, unfeasibly large fields of view, etc). The available model propeller is also a determinant factor for the model scale selection.

Based on the available propeller, a model of **scale 1300/90 = 14.44(4)** has been selected. This scale is derived by the ratio of the inlet suction diameter in the prototype and model.

2.3 Scaled parameters

The main geometric parameters of the vessel (based on the reference vessel Somtrans XXV, see [1]) and hydrodynamic conditions are summarized in the tables below, in prototype and model scale values. As the main region of interest concerns the surroundings of the bow of the vessel, it was deemed unnecessary to represent the full vessel length in the model, for which about half of the vessel length is considered.

Table 2.1 Main dimensions of the vessel and bow channel

Parameters	Prototype scale	Model scale (scale 1:14.44)
Length, L (m)	135	9.4 (~half-length: 4.5)
Beam, B (m)	17.5	1.21
Draught, D (m)	3.88	0.27
Thruster inlet suction diameter (m)	1.30	0.09
Bow thruster channel height, C_H (m)	0.82	0.06
Bow thruster channel width, C_W (m)	1.10	0.08

Table 2.2 Hydrodynamic parameters

Parameters	Prototype scale	Model scale (scale 1:14.44)
Water depth (m)	6.4	0.44
Under keel clearance of reference (m)	2.5	0.17
Maximum thrust (N)	43,760	14.5
Efflux velocity, U_0 (m/s)*	4 - 8	1 - 2
Re_0 (-)	$> 10^6$	$> 10^4$

* Estimated with the PIANC formula, see [4]

3 Physical scale model

3.1 Experimental facility

For this project the IOS1 basin at Deltares was used. This is the largest of the two facilities typically used to test intake and outfall structures. Throughout the report the dimensions are provided in prototype scale, except as otherwise indicated (model scale indicated as “m.s.”). The facility is 20 m wide (m.s.) and 12.5 m long (m.s.), allowing a maximum water depth of about 1.1 m (m.s.). The wall in the test section is equipped with glass windows over a length of 5.8 m (m.s.) for flow visualization (Figure 3.1). A raised wooden floor covers the area in front of the window section and allows the installation of instruments on the floor.

Water can flow in and out of the facility by a system of pumps to fill and empty the basin; no ambient current has been considered in the present tests. Water from the underground reservoir enters the model upstream of the permeable boundary, as shown in Figure 3.2. Two permeable boundaries are built in the basin to increase the flow resistance and to ensure well distributed flow in the basin. These are permanent features of this facility and are only relevant during filling operations. The basin can be drained by gravity. However, for this project the valve providing gravity drainage of the basin was closed to avoid seeding particles to contaminate the underground reservoir. A drainage pump was installed and connected to a filtering unit (see Figure 3.2, right) to discharge water back to the reservoir.

For safety reasons, the measurement area was covered with black cloth to ensure that laser light from the PIV system is not visible to people passing nearby the experimental facility, see Figure 3.2.

Figure 3.1 IOS basin, view of the test section before construction of the model.

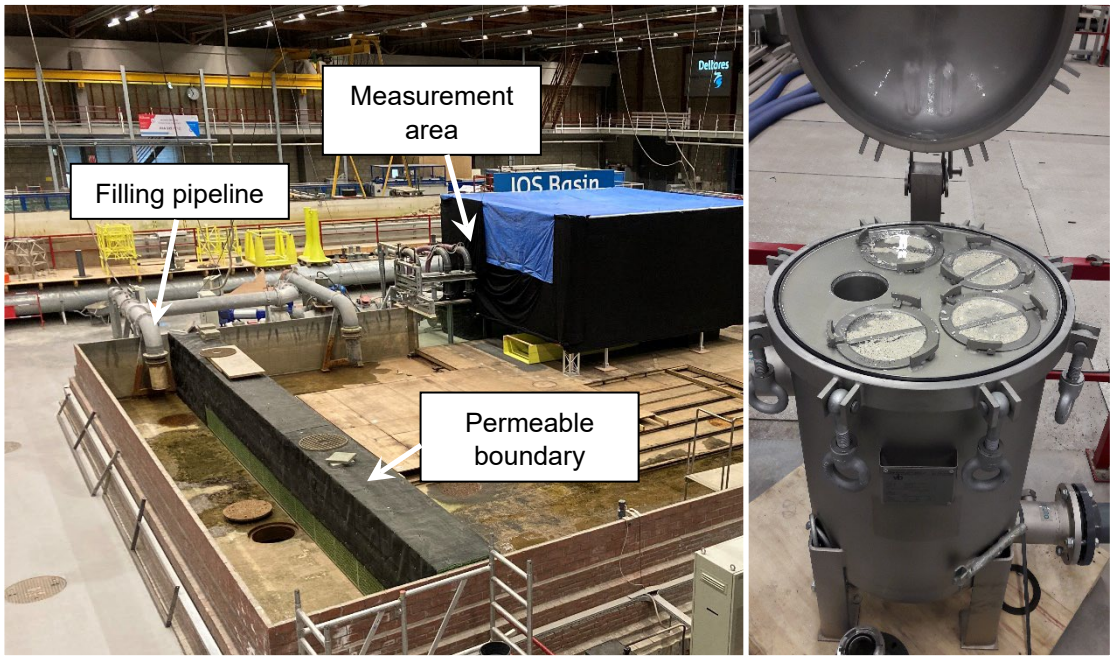

Figure 3.2 View of the Filling pipeline (left) and view of the filtering unit (right) used to filter seeding particles.

3.2 Measurement setup

The measurement setup is schematized in Figure 3.3. To correctly represent the channel width in Ghent where the field measurements were performed (see [1]), a wooden wall was installed in the model at 3.7 m (m.s.) from the windows. The wooden wall is 12 m long (m.s.) and is open at the ends to allow free flow recirculation in the basin. The first tests in the initial test series were performed without the wooden wall in place to have a more generic open situation. By performing tests with and without the wall, the influence of the channel wall could be assessed.

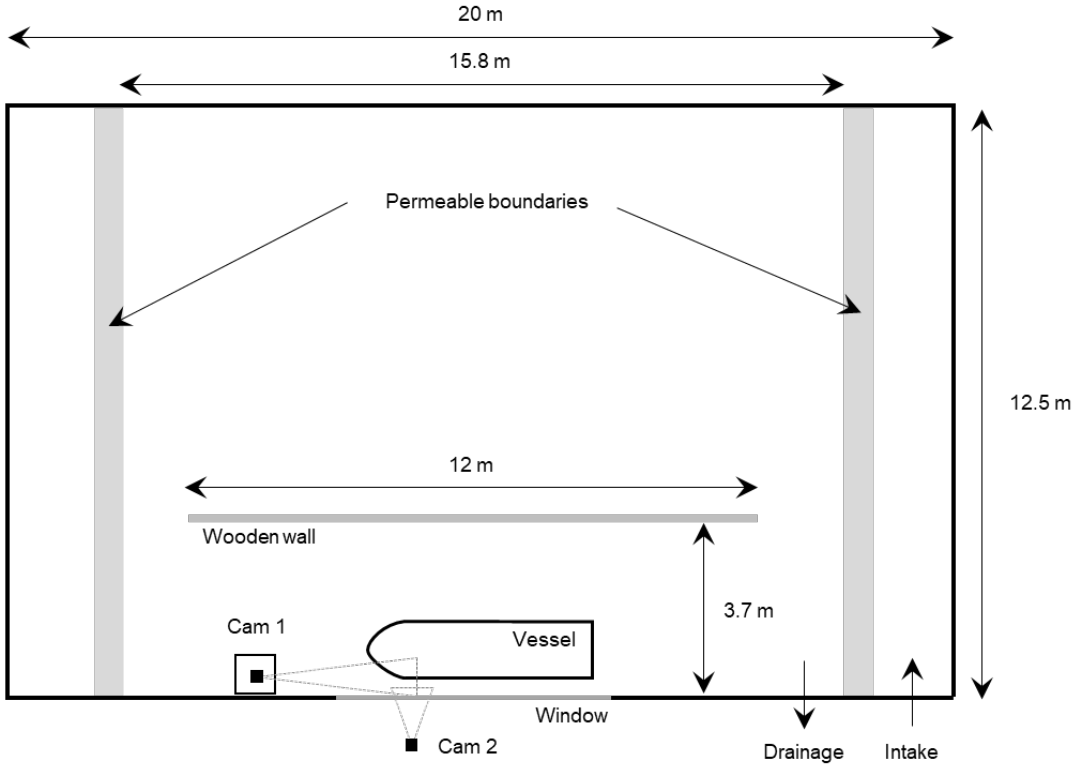

Figure 3.3 Schematic representation of the measurement setup, top view. Dimensions in model scale.

For PIV measurements it is fundamental to have optical access to the flow in the region of interest. For this reason, two cameras were installed in the model (see Figure 3.3). One camera (Cam 1) was placed inside the basin, in front of the bow of the vessel, capturing the field of view in planes perpendicular to the quay-wall (i.e., planes parallel to the jet centerline). The fields of view captured with Cam 1 are illustrated in Figure 3.4,a-b. Camera 1 was initially placed at a large distance from the jet centerline (at about 5 m, m.s.) to minimize disturbances to the flow field in the region of interest. However, after a few tests the quality of the PIV images degraded considerably due to accumulation of seeding particles in the large volume (optical path) between camera and measurement plane. To avoid this issue in future tests, this camera was placed at about 2.5 m (m.s.) from the measurement plane and the camera lens was changed to cover an equivalent field of view. During the additional test series, camera 1 was moved closer to the measurement plane, placed at about 1.6 m (m.s.), to increase the vector field resolution near the bed. A second camera (Cam 2) was placed outside of the basin, capturing the side of the vessel; with this camera the field of view focused on planes parallel to the quay-wall (see Figure 3.4,c). The two cameras were not operating simultaneously. Most of the measurements were performed with camera 1, whereas camera 2 was used for a small selection of tests.

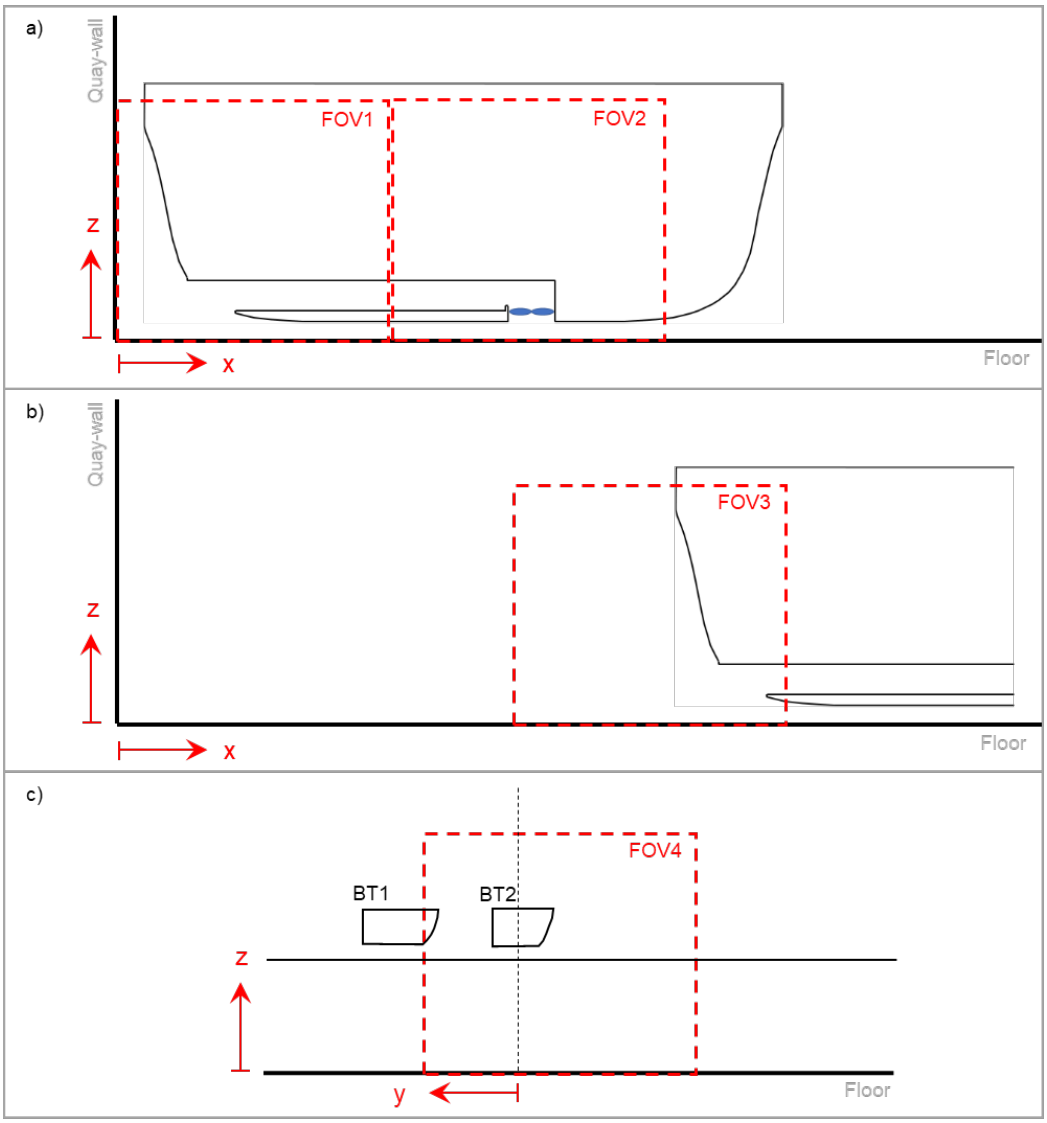

Figure 3.4 Schematic representation of the fields of view: a) fields of view 1 and 2 were captured by cam 1 for tests where the vessel is placed near the quay-wall (confined jet); b) field of view 3 was captured by cam 1 during the free jet tests and c) field of view 4 was captured by cam 2 for a selection of confined jet tests.

The PIV measurements were performed in 2D planes, so that two velocity components (x,z) or (y,z), depending on the field of view, could be derived for each measurement plane. The aimed field of view covers an area estimated of 40 cm x 40 cm (m.s., see Figure 3.4).

In addition to PIV, a series of instruments were used in the model to measure pressures and flow velocities near the bed. The location of the instruments placed on the floor are illustrated in Figure 3.5 and Figure 3.6 for the initial and additional test series, respectively. The location of the instruments in the field measurements (ref. [1]) was used as basis for the placement of the instruments in the scale model. Three Electromagnetic sensors (EMS) were installed on the floor, aligned with the axis y = 0 m, measuring flow velocities in the x and y directions. The center of the measurement volume of the EMS sensor is located at about 5.5 mm (m.s., 8 cm prototype scale) from the floor (see section 4.5 for more information on the EMS measurement volume). The location of EMS3 changed between the initial and additional test series in order to measure velocities closer to the quay-wall, as illustrated in the figures below. Ten differential pressure sensors (dP cells) were installed on the floor and only used during the initial test series. Most of the cells were placed along the y =0 m axis. The sensors were installed underneath the wooden floor and small holes on the wood plate ensured the connection between the sensors and the flow near the bed. After a couple of PIV tests the sensors stopped providing reliable signals probably due to accumulation of seeding particles in the holes above the sensors.

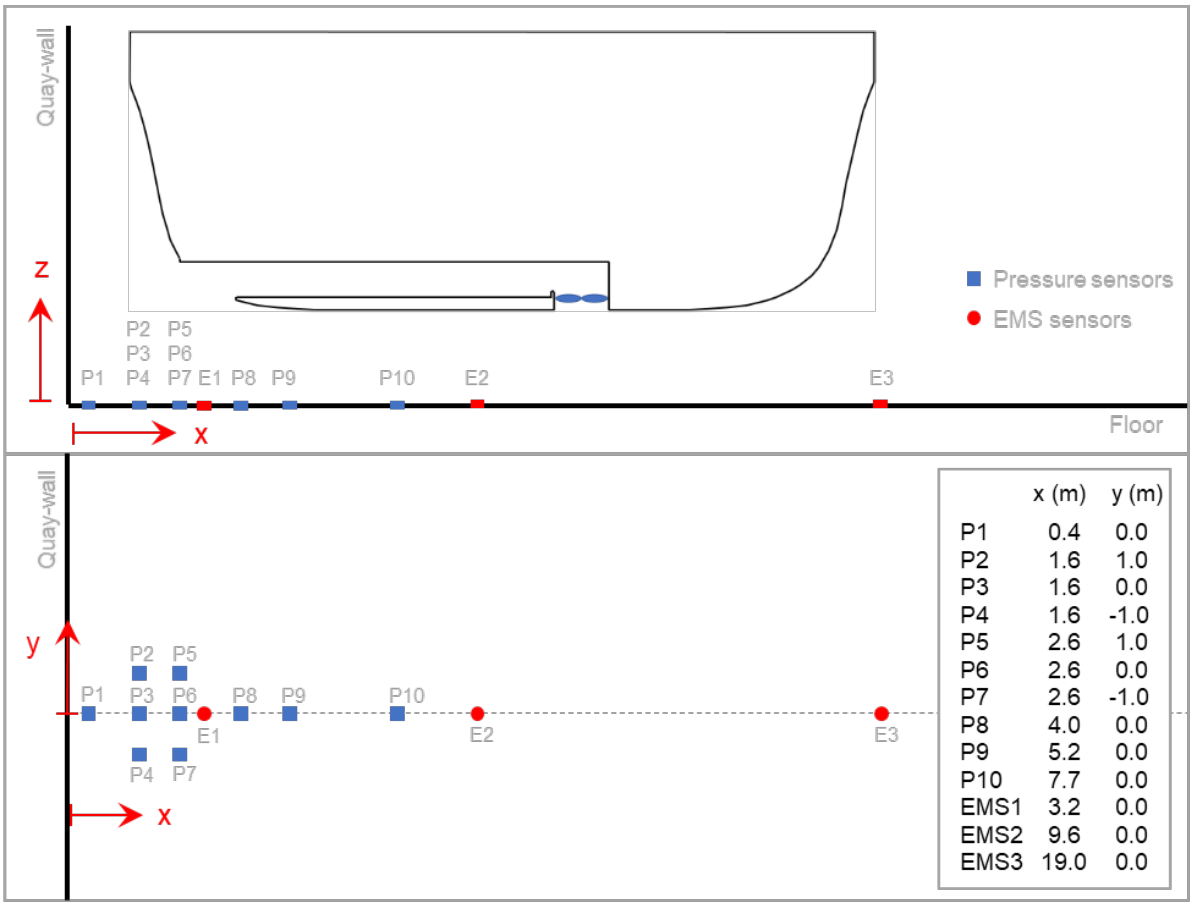

	x (m)	y (m)
P1	0.4	0.0
P2	1.6	1.0
P3	1.6	0.0
P4	1.6	-1.0
P5	2.6	1.0
P6	2.6	0.0
P7	2.6	-1.0
P8	4.0	0.0
P9	5.2	0.0
P10	7.7	0.0
EMS1	3.2	0.0
EMS2	9.6	0.0
EMS3	19.0	0.0

Figure 3.5 Position of the instruments on the floor in the initial test series.

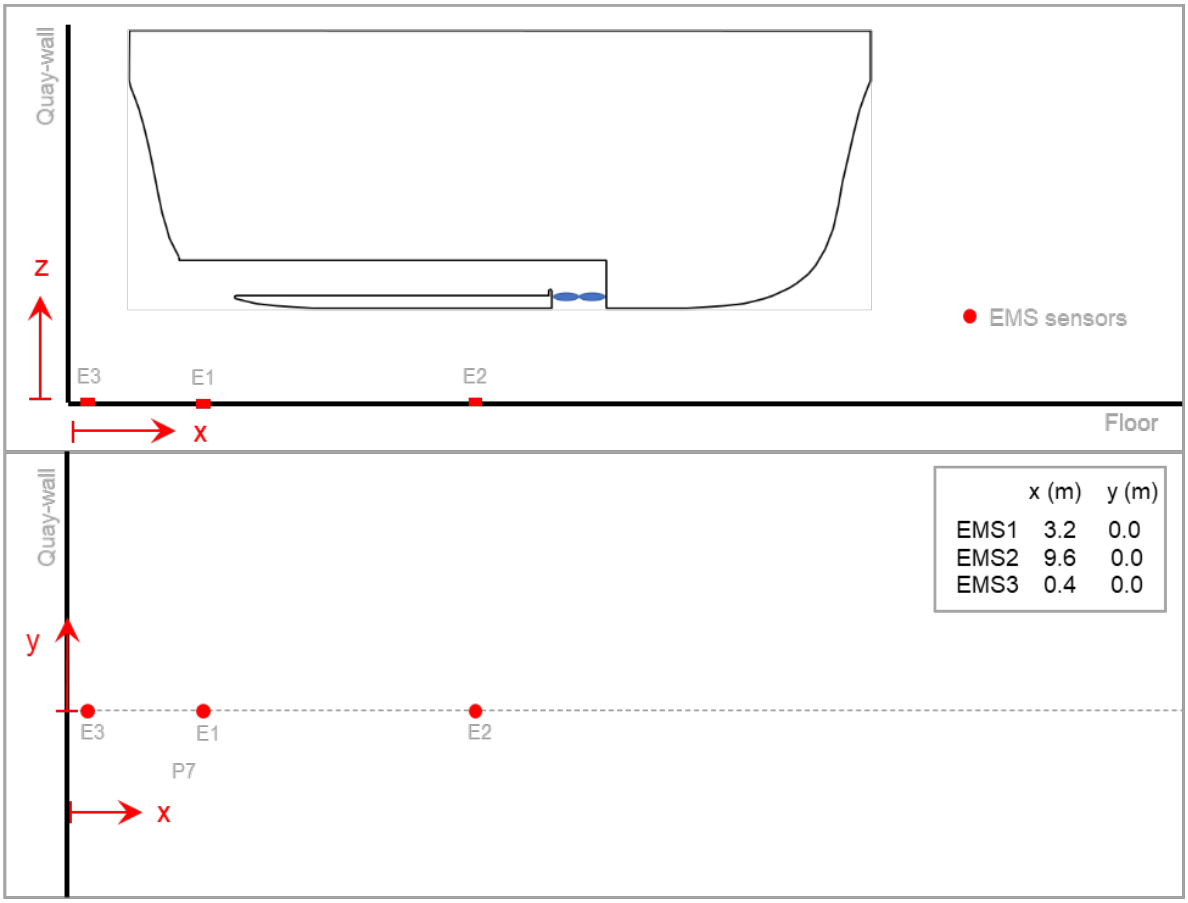

Figure 3.6 Position of the instruments on the floor in the additional test series (smooth bed tests).

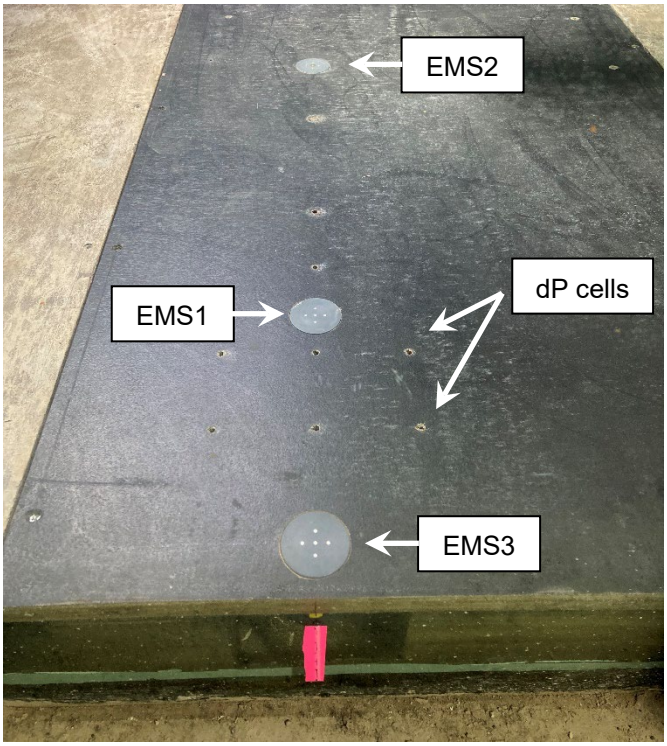

Figure 3.7 View of the instruments on the floor in the additional test series (smooth bed tests).

Three force sensors were installed on the vessel to measure forces in three dimensions (three force components in *x*-, *y*-, *z*-direction per sensor). The sensors were attached to the frame that keeps the vessel in place during testing and connected to the vessel by means of magnets (see Figure 3.9). During the measurements this captive measurement setup fixed the vessel position, such that the vessel could not displace in any direction, thereby making it possible measure the external force acting on the vessel in 6 degrees of freedom.

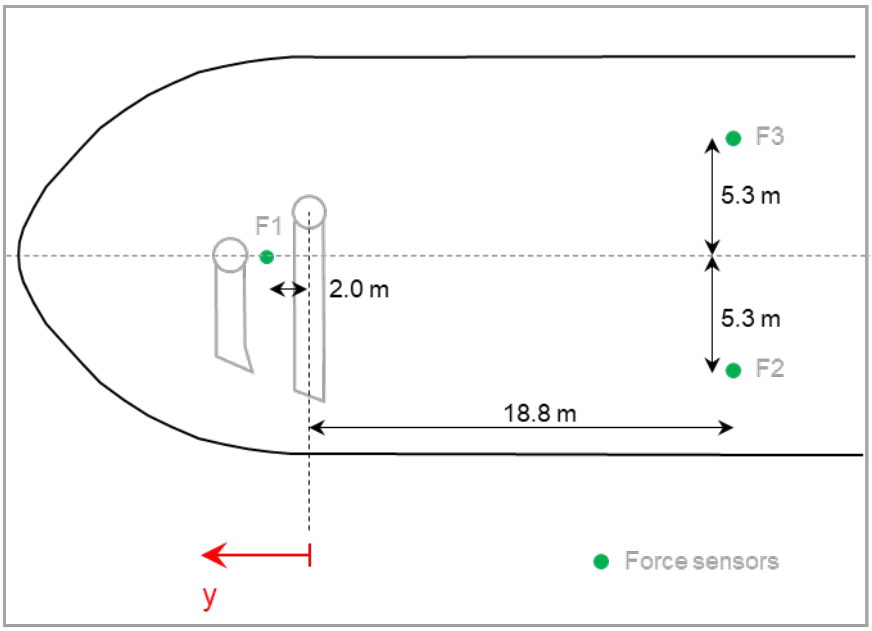

Figure 3.8 Position of the force sensors on the vessel (distances in prototype scale).

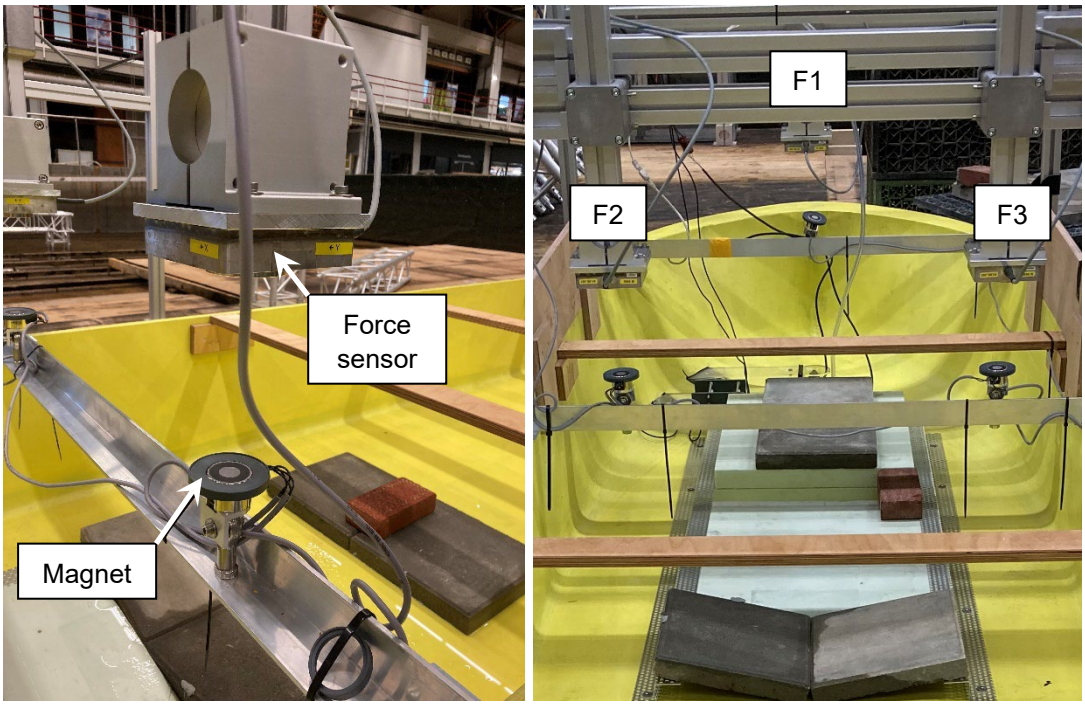

Figure 3.9 Force sensor and magnet (left) and overview of the force sensors when detached from the vessel (right).

3.3 Model vessel

The details of the hull of the vessel used in the field measurements were not available, therefore a similar and representative hull shape has been used in the scale model tests. A 3D hull geometry has been provided by MARIN and is based on a sistership of the Somtrans XXV, with a slightly different bow shape. The geometry used in the physical scale model tests is the same as used by MARIN in their CFD numerical model. Figure 3.10 presents the geometry of the model vessel.

The model vessel is made of wood and is open at the rear allowing water to flow into the model. This allows a simplified ballasting procedure and a simplified supporting system in the scale model. Ballasting of the vessel was achieved by a combination of heavy elements (bricks) and light elements (Styrofoam), distributed in the model so that the correct draught could be achieved. The target draught is 0.27 m (m.s., 3.88 m prototype scale) and it was kept constant throughout all measurements. When testing with different under-keel clearances only the water depth in the model was changed.

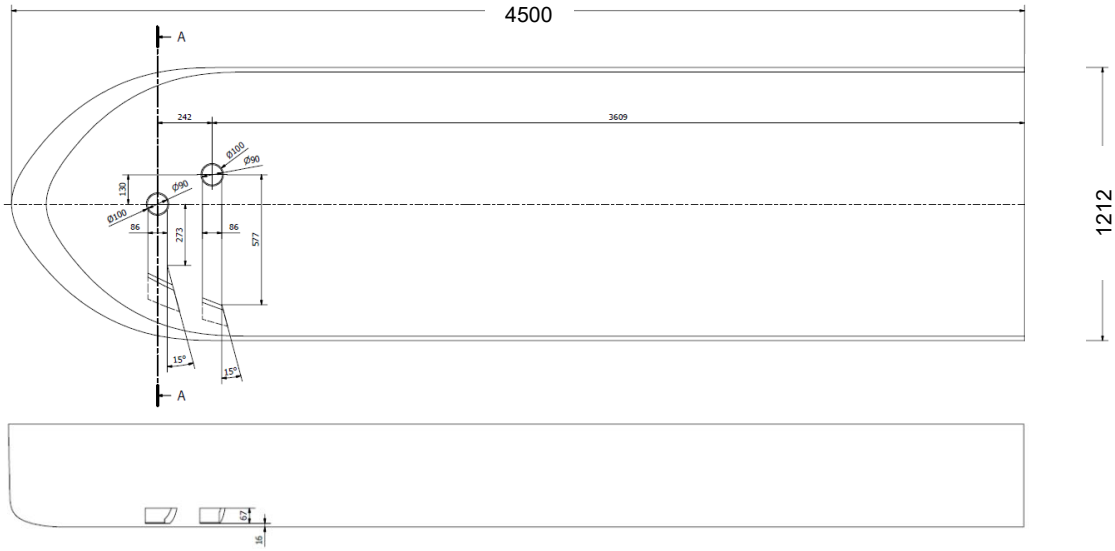

Figure 3.10 Top and side view of the model vessel with main dimensions in model scale.

The model vessel was fixed to a captive support system. The supporting frame keeps the vessel in place at a selected position (Figure 3.11); the supporting frame allows changing the vessel position between tests in three directions, in the vertical and in the horizontal plane. The connection between the supporting frame and the vessel is made at three points via force sensors and magnets, one force sensor per supporting point. Under each force sensor there is a magnet that attaches to another magnet placed on the vessel. To prevent damage to the force sensors in case of (accidentally) overloading, the magnets disconnect when the force acting on them exceeds 70N (m.s.).

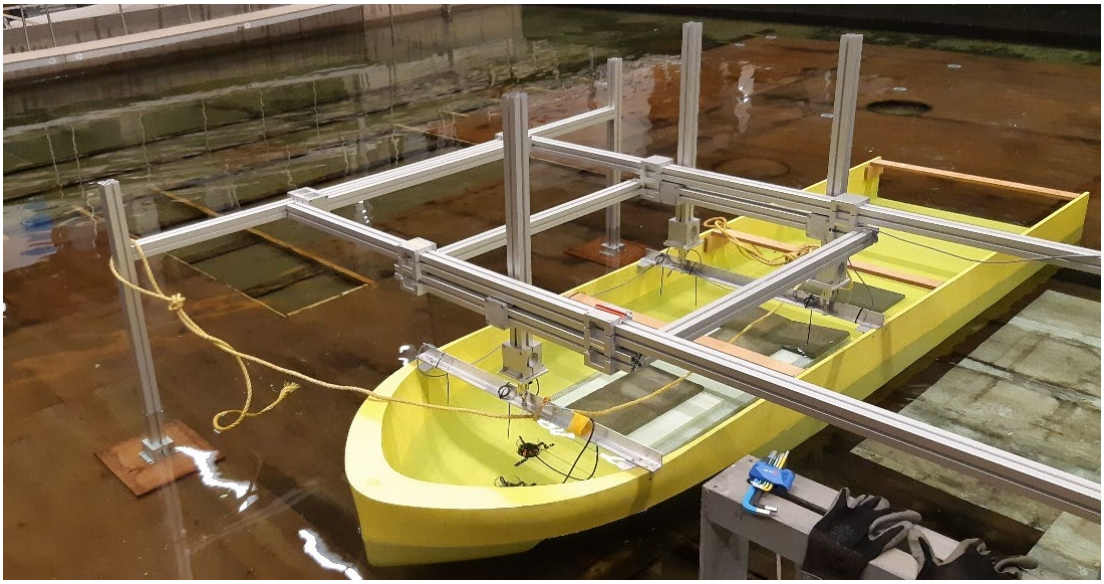

Figure 3.11 Model vessel attached to the supporting frame.

3.4 Bow thrusters

The model vessel was equipped with two bow thrusters (BT1 and BT2), with BT1 the most forward thruster and BT2 the aft one. These elements were geometrically scaled down from the prototype thrusters of Somtrans XXV (see section 2.3) and made of transparent Perspex. The two thruster channels have the same cross-section (57 mm x 76 mm, m.s., 0.82 m x 1.10 m prototype scale) but different lengths and outlet geometries. The inlet diameter of both bow thrusters is 90 mm (m.s., 1.3 m prototype scale). Each channel was made by two separate pieces, i.e., a straight rectangular section and a diverging section, so that it could fit in the model vessel. Figure 3.12 and Figure 3.13 show the main dimensions of the bow channels BT1 and BT2, respectively. The outlet of the bow channels was milled after installation to make it flush with the hull of the vessel, as shown in Figure 3.14 (right).

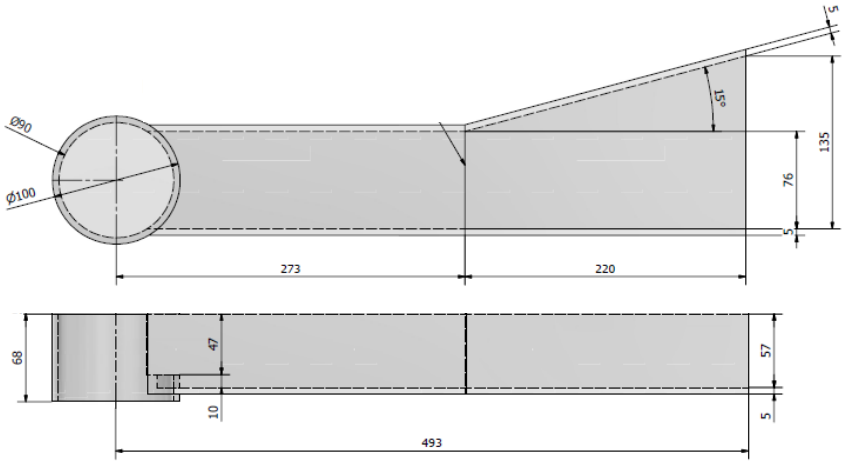

Figure 3.12 Bow channel BT1.

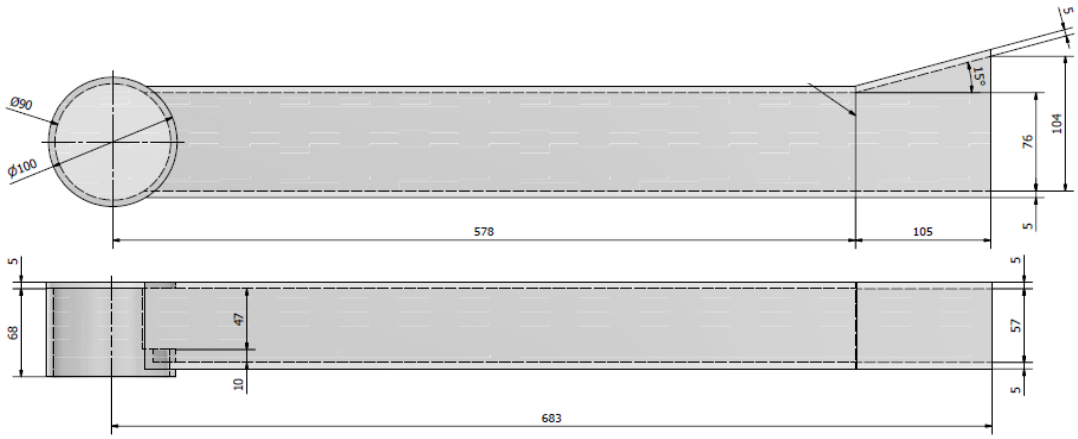

Figure 3.13 Bow channel BT2.

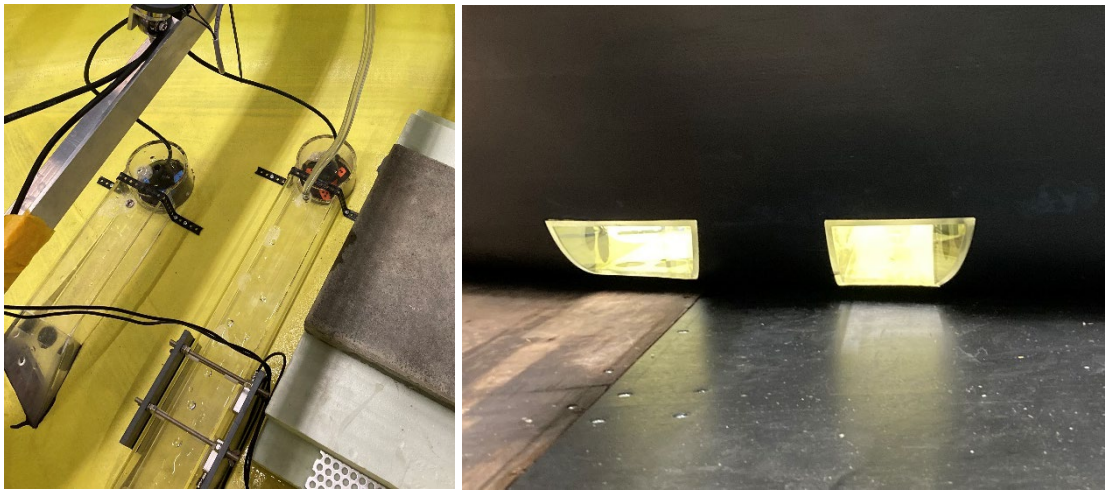

Figure 3.14 Top view of the bow channels after installation in the vessel (left) and view from the outlets (right).

3.5 Propeller

A schematized propeller was used in the scale model instead of a geometrically scaled propeller. A commercially available propeller was used, model T200 of BlueRobotics, with the characteristics as summarized in Appendix C.

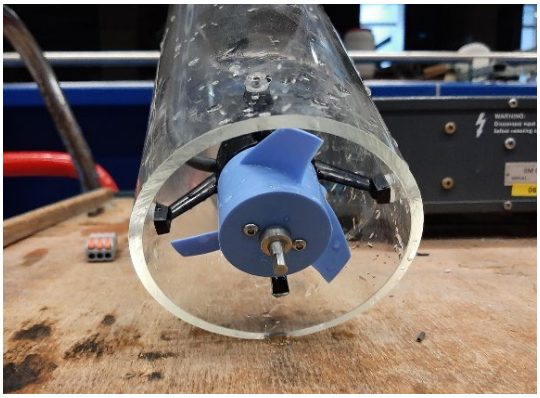

The propeller diameter is 76 mm (m.s., 1.10 m prototype scale). The propeller thrust was used for scaling, i.e., the target thrust in the scale model is the Froude scaled thrust in the field. The total thrust that is delivered by the propeller is measured by force sensors, measuring global hydrodynamic hull forces (see also Section 4.4.3). So, the actual propeller characteristics,

typically described by KT and KQ coefficients, are of less importance to our research objectives and will not be measured directly. Only global propeller loads will be measured, in line with the approach followed in the field measurements where a load cell was used to determine propeller induced mooring line loads.

In essence, the main objective in these tests is to characterize the flow field produced by the thruster given a certain efflux velocity at the outlet plane of the bow thruster channel. The actual performance of the propeller itself (i.e.: efficiency, thrust and torque) and how the flow in the thruster channel is being generated is thereby of less importance. This is also in line with how the design guidelines of bed protections are generally set-up: given a certain efflux velocity U_0 the maximum near bed velocity can be calculated.

The model thruster includes an electric motor and a system to control and measure the propeller rotational speed.

3.6 Bed roughness

During the initial test series one test was performed to assess the influence of the measurement frame used in the field measurements in Ghent on the resulting flow velocities near the bed. For this purpose, a scaled frame was placed underneath the vessel, aligned with the centerline of BT2, mimicking the measurement setup in the field measurements in Gent. Figure 3.15 illustrates the frame used in the model.

Figure 3.15 Scaled measurement frame. Top: view of the frame from the top; Bottom: frame as installed in the model during testing.

Based on the results of the test with the measurement frame, it was decided to investigate the effect of the bed roughness further by performing additional tests using a more realistic bed roughness. In this context, fixed rock and loose rock tests were performed during the additional test series. For the fixed rock tests a grading 10-60kg was selected, whereas for the loose rock tests a 90-250 mm grading was used, both normal density gradings. Figure 3.16 presents both rock gradings as installed in the model. The rock gradings were scaled down to model scale according to Froude scaling, with the target and achieved characteristic diameters as presented in Table 3.1. For the fixed rock tests the bed material was glued on the floor of the basin; the loose rock material was simply laid on the floor. Both gradings covered a thickness of about 40 mm (m.s.), with an extent (width x length) of about 1.0m x 1.0m (m.s.).

The selection of the gradings to use in the scale model was made in cooperation with the project partners. The loose rock grading selection was based on the expected mobility for the flow velocities achievable in the model. The aim of the loose rock tests was to see some level of deformation for the largest flow velocities tested. PIV measurements were only performed for the fixed rock tests, whereas for the loose rock tests deformation tests with underwater cameras and stereophotography measurements were performed.

Figure 3.16 Rock gradings used during the rough bed tests. Left: fixed rock 10-60 kg, right: loose rock 90-250 mm.

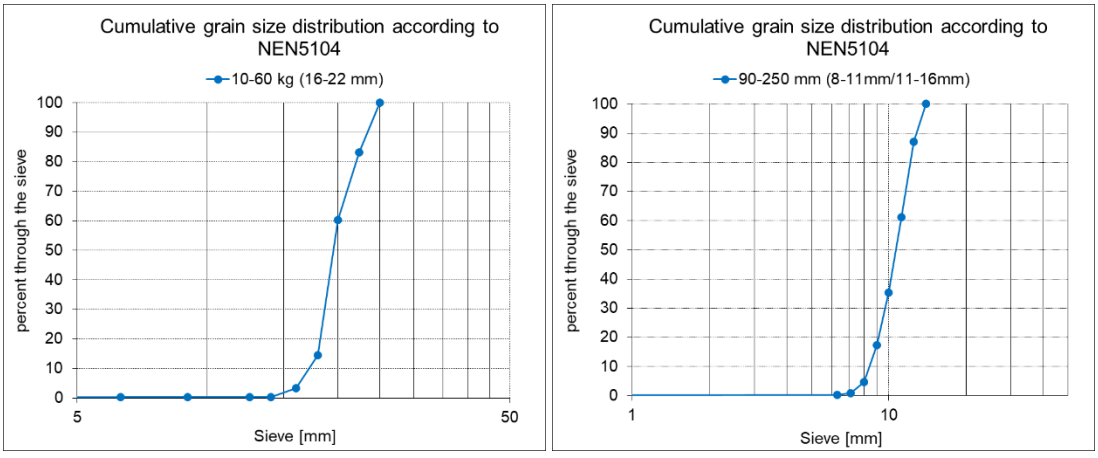

Figure 3.17 Sieve curves for 10-60 kg fixed rock (left) and for 90-250 mm loose rock (right).

Table 3.1 Characteristic diameters in prototype and model scale.

Characteristic diameter	10-60 kg, ND			90-250 mm, ND		
	Reference prototype	Target model	Achieved model	Reference prototype	Target model	Achieved model
D_{15}	0.22 m	15.2 mm	18.0 mm	0.10 m	7.1 mm	8.8 mm
D_{50}	0.28 m	19.4 mm	19.5 mm	0.16 m	11.1 mm	10.7 mm
D_{85}	0.32 m	22.2 mm	22.7 mm	0.22 m	15.0 mm	12.4 mm

4 Measurement techniques and instrumentation

This chapter elaborates on the measurement techniques and equipment used during the scale-model tests.

4.1 Particle image velocimetry (PIV)

The main technique used for flow velocity quantification is planar-PIV. This is a basic form of PIV where a two-dimensional velocity measurement (throughout a measurement plane) is performed. The basis of this PIV technique is to determine the displacement of small tracer particles (seeding) in the flow. These tracer particles which are assumed to follow the flow due to their relatively small size and small velocity decay compared to the flow velocity. A laser sheet repeatedly illuminates the particles in the flow while a camera captures an image on each laser pulse. The displacement of the particles can be determined with the aid of post-processing software. The software determines the spatial correlation of groups of particles between two image frames, where the highest correlation peak gives the most likely displacement. An instantaneous, spatially distributed particle displacement is obtained. As the timestep between the frames is known, the displacement can be translated to a velocity vector. Both instantaneous and time-averaged flow fields can then be derived from the measurements. In addition, some statistics such as the standard deviation of the flow are obtained. The standard deviation gives insight in how ‘stable’ the flow is. A high standard deviation tells that there are large fluctuations in the flow velocity that often indicates high levels of turbulence.

4.1.1 Seeding

The seeding applied in the PIV measurements consists of white 100-micrometer Polyamide spheres of the type Vestostint® 1101. The seeding has an average density of 1060 kg/m3. In a tank, 30 grams of dry seeding material is mixed with 10 L of water. A circulation pump ensures that the suspension stays well mixed. A peristaltic pump injects the seeding mixture directly into the bow thruster channel to reach a sufficient number of particles in the flow to enable PIV, see Figure 4.1.

Figure 4.1 Seeding distribution system. Left: Mixing tank with submerged mixing pump and peristaltic injector pump. Right: Seeding is injected into the bow thruster channel.

4.1.2 Cameras

The cameras used to capture the PIV images are LaVision Imager MX cameras with a resolution of 4MP and a 1” sensor. They are connected to the PIV system by a CamLink connection which enables time-synchronisation with the laser pulses. The lenses used are 35mm Fujinon C-mount TV lenses.

4.1.3 Calibration

The obtained flow fields are discretized in pixel coordinates. To convert the fields to a cartesian frame of reference, calibration is required. This calibration is performed by aligning a calibration board (1 m x 0.5 m (m.s.)) with a printed pattern of known dimensions (in this case dots that are spaced 10x10 mm (m.s.) apart) with the laser sheet. An eye-safe construction laser aids to align the calibration plate with the measurement plane, see Figure 4.2. An image with the aligned calibration plate is acquired, after which the PIV processing software (Davis 8.4.0.) converts the pixel coordinates to real world coordinates in millimetres using a calibration routine.

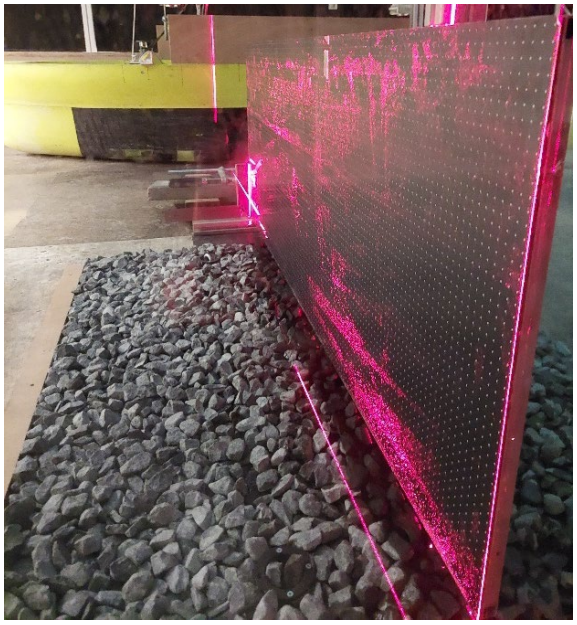

Figure 4.2 The calibration plate aligned with the PIV measurement plane with the aid of a building laser.

4.1.4 Laser

A pulsed laser (Litron Nano L 50-100 PIV) is used to illuminate the seeding particles in the measurement plane. It was outfitted with a convex lens to diverge the laser beam into a laser sheet. The laser is located outside the basin on the dry side of the glass wall. For FOV1, FOV2 and FOV3, the laser sheet was oriented vertically and transmitted perpendicular through the glass wall. For a small number of tests with FOV4, the laser sheet was first orientated horizontally. Then the laser sheet was radiated through the glass after which it was reflected downwards by the means of a mirror to align with FOV4. The laser pulses were logged simultaneously with the other measurement equipment data to allow for time-synchronisation of the PIV data with the other signals.

4.2 Bathymetry (stereophotography)

To accurately observe and quantify the deformation of the tested mobile bed protection, before and after each test a 3D-stereophotography measurement is done to obtain a 3D image of the protection and the surrounding bathymetry. This technique provides a 3D image of the bathymetry as well as a 3D colour photo, as illustrated in Figure 4.3. In ref. [3] it is explained how this technique works. This technique was also extended to consider a refraction surface, such as the water surface (see [3]), although this is not relevant for its application within the present research. The stereo-images must be coupled to a cartesian coordinate system by the means of a calibration. Markers with fixed dimensions are therefore placed around the region of interest to convert the pixel coordinates to real-world dimensions.

Figure 4.3 Left: The stereophotography setup with on the left the stereo box used to take the images. The region of interest is surrounded by markers to calibrate the images. Right: Example of stereophotography measurement of a loose rock test: bathymetry difference plot on the lower side showing bathymetry changes relative to the initial rock protection level and colour image on the top side, also obtained with stereophotography.

4.3 Rock displacement (cameras)

For the deformation tests, continuous monitoring of the movement of the rocks is essential since the underlying flatbed may temporarily become exposed during the rock motion. A 3D-measurement after the test does not provide this information, but it is captured by the cameras installed in the model. To provide continuous observations during the experiments two cameras (FLIR Blackfly BFLY50H5C-C) (Cam1 and Cam2) were placed in a watertight housing in the basin and a GoPro camera (Hero 9) was placed outside the basin capturing the field of view just in front of the active bow thruster, as illustrated in Figure 4.4. The underwater cameras are used to monitor the rock stability during each test. By taking regular snapshots from the underwater cameras, a qualitative analysis of the stability of the protection can be made. Cam2 was placed such that it monitored the rocks underneath the bow thruster channel intake as it could be expected that a suction vortex might form, potentially displacing rocks at that location. Some lamps were placed around the model to illuminate the regions of interest. One lamp was placed underwater behind Cam2 to illuminate the bed underneath the suction inlet.

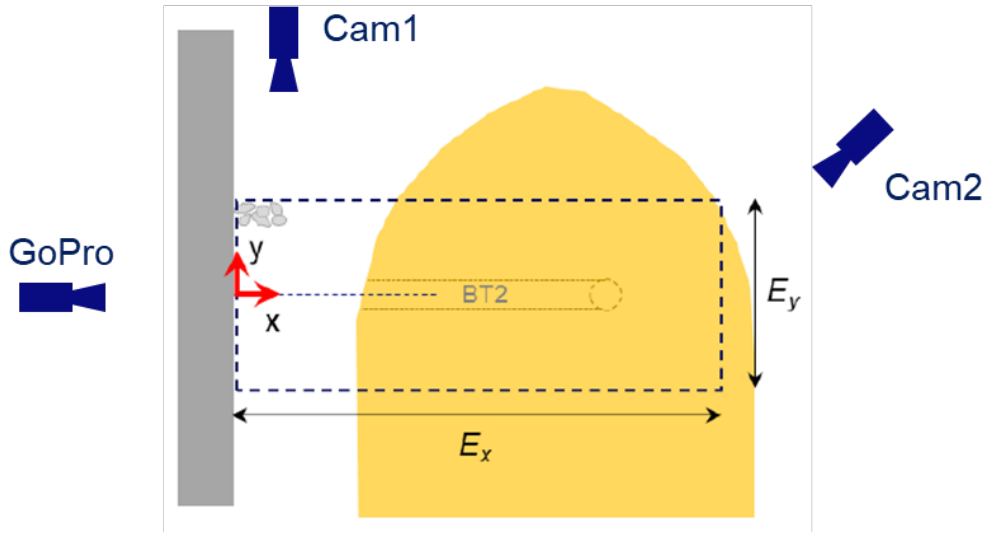

Figure 4.4 Camera setup used in the deformation tests.

4.4 Thruster flow rate (acoustic flow meter)

An acoustic flow meter was installed to measure the flow passing through the bow thruster channel. The working principle of this device is that the transit time of an acoustic signal (sound) along a known path is altered by the fluid velocity: It travels quicker with the flow than against it. Often, these devices are applied to measure flows in pipelines and are placed at sufficient distances from pumps, valves, bends and other obstacles such that the flow is uniform in the measurement volume. However, the flow in the bow channel is not expected to be uniform as the measurement location is too close to the propeller. Hence, a calibration of the flow meter in the configuration used during the scale model tests was necessary to derive a relationship between measured flow velocity and the corresponding cross-section averaged flow velocity (or equivalently discharge).

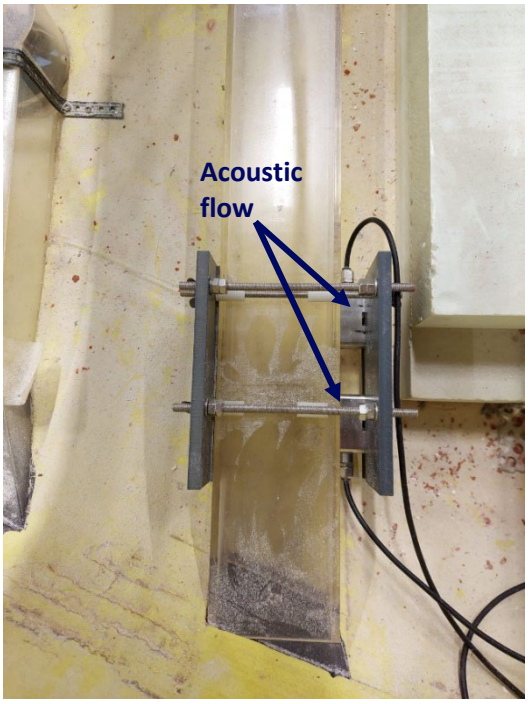

Figure 4.5 The acoustic flowmeter (consisting of the two metal transducers) attached to the bow thruster channel. They are clamped to the Perspex channel by the means of a grey PVC clamp.

For the calibration, the propeller with the thruster channel attached was placed in a flume with the suction side on one side of a separation wall, pumping the water through the wall to the other side. During the calibration, the water level was kept constant on both sides by the means of an overflow weir on the downstream side and slowly adding water to the upstream side. The water passing the weir was collected in a third compartment where the rate of increase of the water level was measured with a water level meter. A schematization of the calibration setup can be found in Figure 4.6.

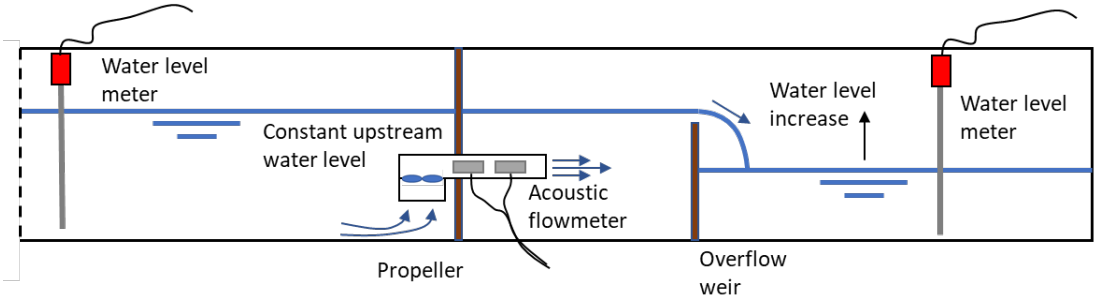

Figure 4.6 Schematization of the acoustic flow meter calibration setup.

The discharge was then derived by multiplying the rate of change of the water level with the surface area of the collecting basin. From the calibration procedure, the relation between the discharge (and its accuracy) and the measured flow velocity signal of the acoustic flow meter was derived. Appendix D contains the calibration results of the flow rate.

4.5 Water velocity (EMS)

In addition to the PIV measurements, electromagnetic flow velocity meters (EMS type E40 Flush) were used to measure the flow velocity near the bed. These electromagnetic flow meters work on the principle that when charged particles (free electrons in the water flow) pass through a magnetic field (created by a coil in the EMS), they induce a potential difference in the direction perpendicular to the flow (Faraday's law of induction). This potential difference (voltage) is measured by platina electrodes on the surface of the probe. Since the magnetic field is non-uniform (its strength decreases with distance from the probe), there is not an exact measurement point but more of a measurement volume. To have an indication of a representative location at which the velocity is measured, the location is used that splits the magnetic field in two parts of equal magnitude. For the probes used, this location lies around 5.5 mm (m.s., 8 cm prototype scale) above the center of the electrodes. One can refer to ref. [5] for a more elaborate overview of the EMS measuring volume and a description of the calibration procedure of these flush mounted EMS's. Figure 4.7 shows the EMS's built into the experimental setup. Figure 3.5 and Figure 3.6 show the locations of the instruments for the initial test series and during the additional test series respectively. The measurement range of the EMS's during the initial test series was set to 0-1 m/s (m.s.). For the additional test series, the location of EMS3 was changed from furthest from the wall to next to the wall to verify the flow magnitude there. As the flow velocities at the new location of EMS3 near the wall turned out to be higher than the original measurement range of 1m/s (m.s.), the measurement range was increased to 2.5 m/s (m.s.).

Figure 4.7 Left: Three electromagnetic flow meters mounted flush in the smooth bed. Right: Flow meters seen from the bottom of the bed.

4.6 Force measurements

The forces acting on the vessel induced by the bow thruster jet were measured with force sensors (type ME-K3D120e) with a measurement range of -50-50N (m.s.). These were placed at the three connection points between the vessel and the supporting frame allowing for the measurement of three force components (xyz). Figure 3.8 shows the position of the instruments. The connection between the force sensors and the vessel is made by means of electromagnets. The magnets keep the vessel attached to the force sensors until a limit of 70N (m.s.) is reached. In this way, the instruments are protected against damage for the occasion that their maximum allowable force of 100N (m.s.) would be reached.

Figure 4.8 The xyz force sensor can be seen on the top. It is attached via an electromagnet below it to the vessel. It disconnects before the maximum allowable force is reached.

4.7 Pressure fluctuations (differential pressure transducers)

Differential pressure (dP) transducers (Type SensorTechnics RPOP001D6A) were installed along the bottom at locations corresponding to the field measurements. A total of ten dP transducers were installed in the smooth bed with one side of the sensor looking ‘up’ in the water column where the other side was in contact with the water below the double bottom of the setup. Without flow, the water column has a hydrostatic pressure distribution and there is no pressure difference over the dP transducers. However, when the bow thruster is in use, velocity fluctuations arising from instabilities of the jet can lead to pressure fluctuations, primarily above the double bottom floor. These pressure fluctuations can give rise to local (under)pressure pockets which can mobilise bed material. Moreover, the fluctuations give some insight into the turbulent statistics of the flow. The dP transducers have a measurement range of 60 millibar (m.s.). The locations of the instruments can be found in Figure 3.5.

Unfortunately, during the initial test-series, excess PIV seeding material entered the dP transducers and deposited on the internal membranes of the devices, rendering them useless (see the schematisation in Figure 4.9). As a result, the measurement data from the dP-transducers became spurious and unreliable and is therefore omitted from the results.

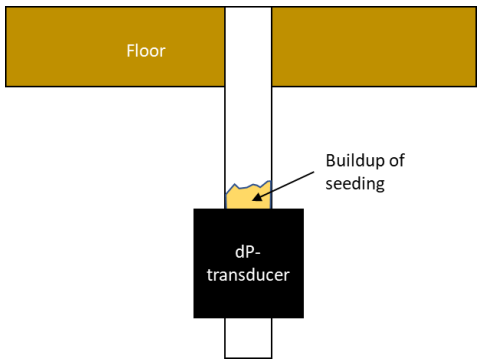

Figure 4.9 Schematization of the PIV seeding clogging the dP-transducer membrane.

4.8 Water level (Temposonic)

The water level in the basin is acquired with an MTS Temposonic® (R-Type) position transducer. It consists of a vertical stainless-steel rod with a floater around it that holds a permanent magnet. The physical measurement principle is that of magnetostriction. A magnetic pulse is sent down the rod and interferes with the permanent magnet. A magnetic torsion wave is reflected and returns to the probe head. The time is measured between the pulse and the arrival of the wave. From the transit time, the position of the floater can be determined with high accuracy. The Temposonic® has a measurement range of 0 to 1.2 m (m.s.).

4.9 Propeller rotation rate

The propeller in the bow thruster is driven by a synchronous 3-phase permanent magnet motor. This means that the rotation of the motor rotor follows the electrical alternating driving current frequency synchronously. Thus, by measuring the driving frequency, one measures the propeller RPM. One of the three motor phases was therefore connected with a frequency-to voltage converter which converts the driving frequency to an analog voltage via a known relationship. This voltage was subsequently logged simultaneously with the other measurement signals in the data acquisition system, providing a reliable measure for the rotation rate of the propeller. The propeller operates in the range of 0-3200 RPM (m.s.). Appendix C contains the specifications of the propeller and motor.

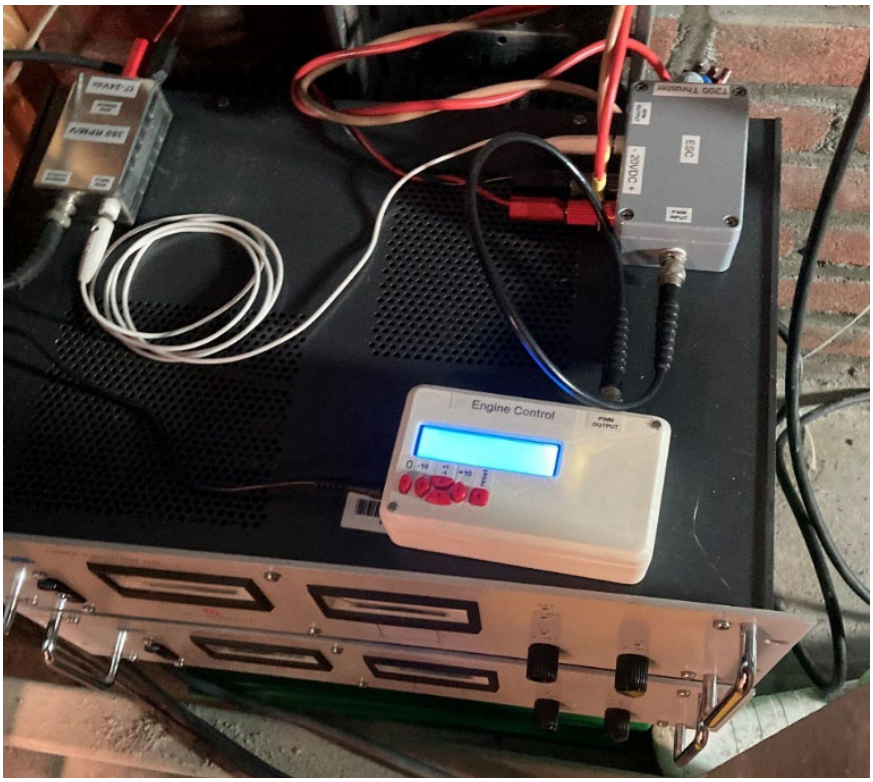

Figure 4.10 The engine controller on the bottom right sets the thruster power. The box on the top left converts the motor drive frequency to an analog voltage.

5 Testing

5.1 Variables

Table 5.1 summarizes the parameters that were varied during testing and the range of parameter variation. The dimensions are provided in prototype scale, except as otherwise indicated. The schematization of the parameters is presented in Figure 5.1 and Figure 5.2.

Table 5.1 Parameters varied during testing (values in prototype scale)

Parameters	Values / Range of variation
Under-keel clearance – UKC (m)	0.5, 1.0, 1.5, 2.5
Height thruster above the bed – h_{BT} (m)	1.22, 1.72, 2.22, 3.22
Distance quay-wall and port side – Δx (m)	0.8, 3.0, 5.0, 23.0
Quay-wall clearance - L_{BT} (m)	3.7, 5.9, 7.9, 25.9 (BT1) 2.6, 4.8, 6.8, 24.8 (BT2)
Distance bow thruster centreline to PIV measurement plane – Δy (m)	-4.0, -2.0, 0.0, 2.0, 3.5
Distance PIV meas. plane and quay-wall – $\Delta x_{PIVplane}$ (m)	0.3, 0.6
Rotational speed of the propeller – RPM (-)	400 - 830
Bow thrusters active	BT1, BT2, BT1&BT2
Direction of rotation of the thrusters (viewed from the top)	Clockwise / counterclockwise
Bed roughness	Smooth bed / fixed rock / loose rock

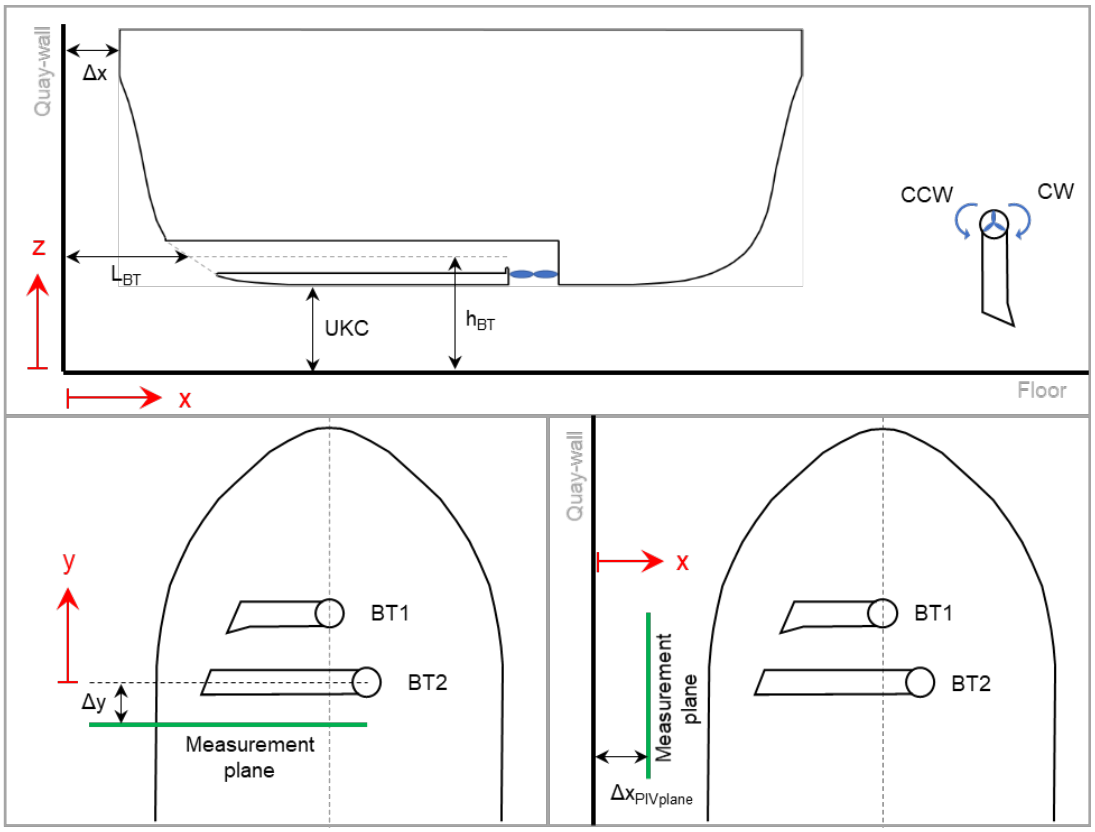

Figure 5.1 Schematization of the parameters changed between tests. Direction of rotation as seen from top.

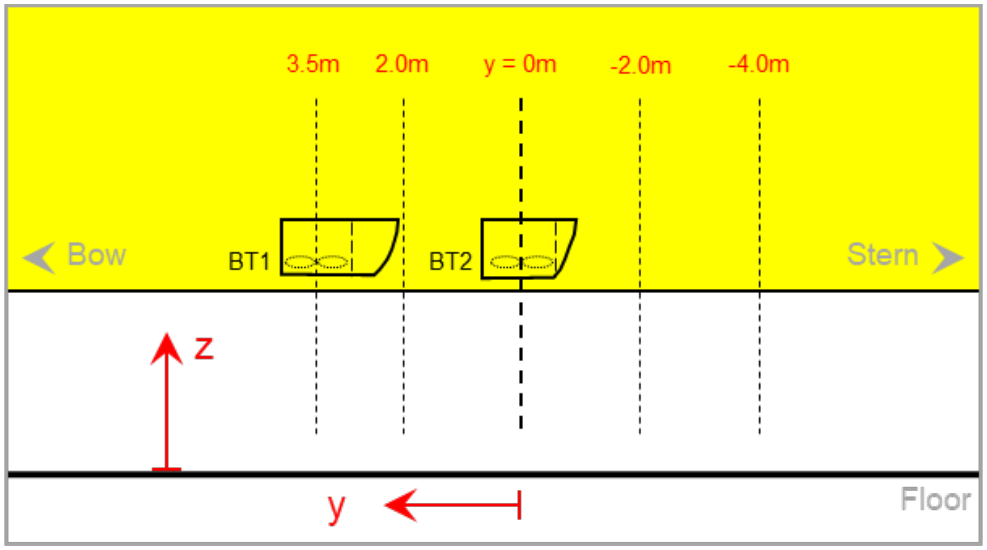

Figure 5.2 Schematization of the different measurement planes in the y-direction (Δy).

All tests were performed for a constant draught of the vessel (3.88 m). The under-keel clearance (UKC) was varied in the scale model by changing the water level in the basin, keeping the draft of the vessel constant. The distance between the vessel and the quay-wall (Δx) was measured between the vessel's vertical sidewall and the quay-wall. This distance was set by using PVC spacers that were made for this purpose. The spacers were removed before starting testing, the magnets hold the ship in place during testing. The centreline of bow thruster 2 is used as reference for y = 0 m. Positive values for Δy indicate that the measurement plane is located towards the bow; similarly, negative values for this parameter indicate measurement planes located towards the stern of the vessel. The rotational speed of the propeller was varied by changing the power given to the motor. The selected power and corresponding rotational speed were determined during calibration of the acoustic flow meter as function of the target velocity to be tested.

In addition to the variations summarized in
Table 5.1, two other variations were considered:

- With/without channel wall
- With/without measurement ladder

The first tests in the initial test series were performed without the (wooden) channel wall, simulating open water conditions. Once the wall was built, it remained in the model until the end of the project. All tests in the initial test series were performed without the measurement ladder, representing the measurement ladder used in the field measurements, apart from one test.

5.2 Test program: initial test series

The main purpose of the initial test series was to verify in a scale model the results from the field measurements. Therefore, a test program was defined to repeat a selection of tests with the same variations of parameters as in the field. In addition, it was decided to expand the dataset by including additional variation of parameters (such as UKC) and to assess the efflux velocity by performing free jet tests. In this test series only bow thruster 2 (BT2) was active and all tests were performed for smooth bed conditions. One test was performed with a model ladder underneath the vessel to reproduce the effect of the measurement ladder in the field measurements.

Regarding the flow velocity to be tested, the aim was to test in the scale model velocities corresponding to the velocities tested in the field. However, in the field the efflux velocity could not be measured directly but was estimated based on applied power and rotational speed of the propeller, by making use of Equation 8-6 to 8-10 of the PIANC guidelines [4]. It was estimated that in the field test a maximum efflux velocity of about 8 m/s could be expected. However, when performing the calibration of the flow meter in the scale model it was observed that the maximum achievable flow velocity in the bow channel with the available propeller and motor was about 5 m/s. In order to test a variation of velocities, three velocity values were then selected (3.0, 4.0 and 5.0 m/s). During the test program it was decided to test only the two extreme (3.0 and 5.0 m/s) velocity values since the flow patterns and results for the intermediate (4.0 m/s) velocity were not providing additional new information.

Note that a direct comparison between the scale model tests and the field tests [1] is not straightforward, mainly because of two reasons:

1. The actual efflux velocity achieved in the field test was not measured and is therefore uncertain
2. The efflux velocities in the scale model (converted to prototype scale) are generally lower than the efflux velocities achieved in the field.

However, by presenting the measured near bed flow velocities as a ratio of the efflux velocity, still a valuable comparison can be made between scale model and field measurements. Specifically, since the observed flow patterns proved to be generally independent of the absolute magnitude of the efflux velocity.

Table 5.2 summarizes the test program for the initial test series. For the location of the PIV plane see Figure 3.4.

Table 5.2 Test program – initial test series. Values in prototype scale.

PIV plane	Δx (m)	Δy (m)	UKC (m)	Target mean flow velocity thruster (m/s)			Note
FOV1	0.8	0.0	2.5, 0.5	3.0	4.0	5.0	Confined jet tests
	0.8	0.0	1.5, 1.0	-	-	5.0	
	0.8	3.5, 2.0 -2.0, -4.0	2.5	3.0	4.0	5.0	
	3.0	2.0, 0.0, -2.0	2.5	3.0	-	5.0	
	3.0	0.0	1.5, 1.0	-	-	5.0	
	3.0	0.0	0.5	3.0	-	5.0	
	5.0	2.0, 0.0, -2.0	2.5	3.0	-	5.0	
FOV2	0.8	0.0, -2.0	2.5	3.0	-	5.0	
FOV3	23.1	0.0	2.5, 0.5	3.0	4.0	5.0	Free jet tests
FOV4	0.8	0.0	2.5	3.0	-	5.0	Confined jet tests

5.3 Test program: additional test series

The main purpose of the additional test series was to investigate the effect on the flow patterns and maximum flow velocity of two thrusters simultaneously active, assess the influence of the

bed roughness on the magnitude and location of the maximum flow velocity and to identify the regions of the bottom where main deformation occurs.

In this series it was decided to repeat some of the tests of the initial test series for reproducibility purposes. During testing it was decided to bring camera 1 closer to the measurement plane to increase the resolution of the flow near the bed (see section 3.2).

Table 5.3 summarizes the test program for tests performed with smooth bed and Table 5.4 summarizes the test program for tests with fixed rock and loose rock tests are presented in Table 5.5. All tests with rough bed were performed with BT2 active. PIV measurements were performed for the fixed rock tests focusing on FOV1.

Table 5.3 Test program – additional test series with smooth bed.

Active thruster	Direction of rotation (BT1 / BT2)	Δx (m)	Δy (m)	UKC (m)	Target mean flow velocity thruster (m/s)	Field of view	Note
BT1	CCW	0.8	3.5, 2.0, 0.0, -2.0	2.5	5.0	FOV1	Confined jet tests
BT2	CCW	0.8	0.0	0.5, 1.5	5.0	FOV1	
BT2	CW	0.8	0.0	0.5, 1.5, 2.5	5.0	-	NO PIV
BT2	CCW	0.8	-2.0, -4.0	0.5	5.0	-	NO PIV
BT1 & BT2	CCW/CW	0.8	3.5, 2.0, 0.0	2.5	5.0	FOV1	Confined jet tests
BT1 & BT2	CW/CW	0.8	3.5, 2.0, 0.0, -2.0	2.5	5.0	FOV1	
BT1 & BT2	CCW/CW	0.8	-2.0	2.5	5.0	FOV1	
BT1 & BT2	CCW/CW	0.8	2.0	1.5	5.0	FOV1	
BT1 & BT2	CCW/CW	0.8	2.0	0.5	3.0, 5.0	FOV1	
BT1 & BT2	CCW/CW	3.0	2.0	0.5	5.0	FOV1	
BT1 & BT2	CCW/CW	23.1	2.0	0.5, 2.5	5.0	FOV3	Free jet tests

Table 5.4 Test program – additional test series with fixed rock (FOV1).

Δx (m)	Δy (m)	UKC (m)	Target mean flow velocity thruster (m/s)	Rock grading	Target diameter		
					D15 (m)	D50 (m)	D85 (m)
0.8	2.0, 0.0, -2.0	2.5	5.0	10-60 kg	0.22	0.28	0.32
0.8	0.0	0.5, 1.5	5.0				
3.0	0.0	0.5, 2.5	5.0				

Table 5.5 Test program – additional test series with loose rock. Parameters in prototype scale.

Δx (m)	UKC (m)	Target mean flow velocity thruster (m/s)	Rock grading	Target diameter		
				D15 (m)	D50 (m)	D85 (m)
0.8	2.5	5.0	90-250 mm	0.10	0.16	0.22
0.8	0.5	5.0				

5.4 Test procedure

5.4.1 Filling the basin

A typical test starts by filling up the basin to the desired water level. A target level is set in the control software of the basin filling system and the model fills up until reaching the desired level, after which the filling pump is automatically stopped. The water level in the basin is measured by a Temposonic® floater (see section 4.8) whose signal is read in the data acquisition system and can be also be checked visually by marks made on the glass walls of the basin with the target levels for each test.

5.4.2 Placement of the vessel

The placement of the vessel in the x-direction is aided by spacers that have the exact distance (Δx) to be tested. The placement of the vessel in the y-direction is done by using a cross-laser (see Figure 5.3), aligned with the PIV laser, that indicates with a red laser beam where the (PIV) measurement plane is located. Vertical lines made on the sidewall of the vessel indicate the different target positions. By moving the vessel, the target position for a certain test is aligned with the laser beam. The vessel is then attached to the supporting frame by activating the magnets underneath the force sensors.

Figure 5.3 Cross-laser used to align the vessel in the y-direction..

5.4.3 Zero measurement

A zero measurement is performed at the start of the measurement day in order to get a reference for the signals of the instruments in an undisturbed situation (no flow in the basin). When modifications to the setup have been applied, such as changing the water level in the basin to test a different UKC, a new zero measurement is performed. The zero measurement has a duration of 5 minutes (m.s.).

5.4.4 Start-up measurement

After the zero measurement, a start-up measurement follows with a duration of 10 min. The aim of this measurement is to capture the start-up phase of the propeller and its influence on the measured signals. After a few seconds of starting the acquisition system, the propeller is turned on. The seeding pump is also turned on during this test to ensure that enough particles are suspended in the flow for the PIV measurement.

5.4.5 PIV measurement

The PIV measurement commences by starting the acquisition system. After checking the PIV system and deciding on the parameters for PIV acquisition, the PIV measurement starts. The acquisition system records a test for 15 min (m.s.), during which an 8-minute (m.s.) PIV measurement is performed. For all tests 1000 frame pairs were recorded with an interval of 2 Hz. The choice for 1000 frame pairs was made based on the concept of convergence of statistics: after this amount of frame pairs, the averaged flow field has settled down to stable values. The time between two laser pulses within one frame-pair was varied between tests and is a function of the flow velocity. For example: when testing with lower flow velocities, the displacement of the seeding particles may become so small that the displacement lies within one camera pixel, then the displacement cannot be observed any more. Consequently, the time between the pulses must be increased to have sufficient particle displacement.

6 Postprocessing

6.1 PIV postprocessing

The postprocessing phase deals with all processing that is performed after the test acquisition. On a dedicated PIV computer, a series of operations are performed to go from raw PIV images to velocity-vectors. These operations are listed below:

- image rotation: most tests were performed with upside-down camera for setup convenience purposes.
- derive minimum intensity of the raw images and subtract the minimum from all frames: the aim of this procedure is to obtain sharp images with a good contrast between seeding particles and dark background.
- masking: apply a mask to the frames where the PIV algorithm should be applied; the aim of this procedure is to reduce the processing time by masking out areas that are not relevant for the analysis.
- PIV algorithm: apply the PIV cross-correlation algorithm to derive instantaneous velocity vectors for each image pair. Based on the instantaneous maps, time-averaged velocity and standard deviation maps can be obtained.
- export data: velocity maps are exported in .vc7 format which will be read and used by a MATLAB script to create standard figures.

6.2 Time series postprocessing

Some basic postprocessing was performed on the time series signals. The EMS-signals were time-averaged over the duration of the tests for the sake of presenting average values in overview plots. Only the force sensor signals required some filtering as the signal showed high frequency fluctuations which are not representing relevant physical processes for this study. Thus, a simple moving average filter was used to filter the high frequency noise.

6.3 Parameters for normalization of results

Based on the free jet tests a relationship was derived between the maximum velocity of the jet as measured by the PIV and the velocity measured by the acoustic flow meter installed in the bow channel. On average, the velocity of the jet is about 10% higher than the velocity measured by the flow meter (see Table 6.1). The velocity used for the normalization of the results, as an estimation for U_0, the efflux velocity, is obtained by: $U_0 = 1.1\ U_{BT}$

Table 6.1 Free jet tests – relation between maximum velocity of the jet and velocity measured by the acoustic flow meter in the bow channel.

Test ID	UKC (m)	U_{BT2} (m/s)	Max Ux jet outflow (m/s)	Max Ux / UBT2
8	2.5	2.6	2.9	1.13
14	2.5	5.6	5.9	1.06
17	2.5	3.9	4.2	1.08
20	0.5	2.6	2.8	1.07
23	0.5	3.7	4.2	1.14
26	0.5	5.3	5.9	1.10

7 Results

7.1 Presentation of results

The main results and observations are summarized in this chapter. For that, a selection of tests that best illustrate the main observations are presented. The results from all performed scale model tests are summarized in Appendix A and Appendix B. The results (tables) from the initial test series can be found in Appendix A.1 and in Appendix A.2 the results from the additional test series are presented. The overview figures summarizing the results of all tests are presented in Appendix B.

For each test, the results are presented in a maximum of 11 figures. The name of the figures is composed by the prefix “PIVSOP”, followed by test number as listed in the tables in Appendix A, followed by a letter (A to K). Below follows a brief description of the information presented in each figure. All results are presented in prototype scale.

Figures in Appendix B
Figures A to C present time-series of the signals measured by the different instruments in the model (EMS, Forces, etc), whereas Figures D to J illustrate the results obtained from the PIV measurements. For FOV 1, 2 and 3 the vertical velocity profiles in Figures D and E present the U_x and U_z components, respectively; for FOV 4 the vertical profiles present the U_y and U_z components.

Fig “test name”A:
This figure presents a schematization of the test configuration and the location of the EMS sensors relative to the vessel and the time-averaged flow velocity (x and y components combined) measured by these sensors.

Below the schematization plots three graphs present the time-series of the measured signals with EMS1, EMS2 and EMS3 (x and y components presented separately). The time-averaged velocity measured for the duration of the PIV test is presented in each graph, for each component. In tests in which a PIV measurement was not performed, the value for the time-averaged velocity corresponds to the entire duration of the acquisition period after the start-up test (see section 5.4.4).

Listed below the third graph, near the bottom of the figure, are presented the active thruster used in the test, the distance between vessel and quay-wall (Δx), the distance between measurement plane and centerline of BT2 (Δy), measured under-keel clearance (UKC) and time-averaged velocity measured inside the channel of the active bow thruster. In the tests where both propellers are active, the flow velocities were measured in the channel of BT2 only.

Fig “test name”B:
In this figure a schematization of the location of the force sensors on the vessel is presented at the top. The three graphs below the schematization present the time series of the measured force signals by the three sensors F1, F2 and F3 (see Figure 3.9), with x, y and z components presented separately. The time-averaged force for the duration of the PIV test is presented in each graph.

Fig “test name”C:
This figure presents the time-series of the water level measured in the basin, the flow velocity measured in the active bow thruster with the acoustic flow meter and the RPM’s of the motor(s).

When both thrusters are simultaneously active the acoustic flow meter was mounted on BT2. In this way, when both propellers are on flow velocities are presented for BT2 only.

Fig “test name”D:
In figure D two graphs are presented: the map with the measured time-averaged velocity magnitude (m/s) is presented at the top, where the two measured velocity components (x and z, or y and z) are combined; on the bottom graph the vertical velocity profiles of the U_x-component, or U_y- component, taken at selected x-locations (or y-locations, for FOV 4) are presented. The absolute maximum velocity value in each profile, and the vertical location where it is measured, is illustrated by a red dot. The locations of the vertical profiles are illustrated by vertical dashed lines on the top graph.

Fig “test name”E:
This figure is the same as figure D with the exception of the graph at the bottom which presents the vertical velocity profiles for the U_z-component.

Fig “test name”F:
In figure F the standard deviation of the U_x component (or U_y component for FOV 4) is presented. The graph at the top of the figure present the standard deviation map, whereas the graph at the bottom presents vertical profiles at the selected locations.

Fig “test name”G:
This figure presents the standard deviation of the U_z component. At the top the standard deviation map is presented, whereas at the bottom vertical profiles at the selected locations are provided.

Fig “test name”H:
In this figure the turbulence intensity map and vertical profiles are presented.

Fig “test name”I:
This figure focuses on the flow velocities measured near the bed. The top graph shows the velocity profiles measured with PIV at selected locations, zoomed at 1m distance from the bottom. The graph below presents the decay of the maximum velocity measured near the bed with the distance to the quay-wall and comparison with the design guidelines [4]. In this figure the time-averaged velocities measured with EMS are also presented for comparison. The last graph presents the distance from the floor where the maximum velocity was measured.

Fig “test name”J:
This figure presents the turbulent intensities measured near the bed. The top graph shows the velocity profiles measured with PIV at selected locations, zoomed at 1 m distance from the bottom. The graph below presents the decay of the maximum turbulence intensity measured near the bed with the distance to the quay-wall. The turbulence intensities measured with EMS sensors are also presented for comparison. The last graph presents the distance from the floor where the maximum turbulence intensity was measured.

Fig “test name”K:
This figure is dedicated to the results from the stereophotography measurements.

Presentation of the results in the report
For the presentation and discussion of the results we selected figures that illustrate the time-averaged flow patterns, the maximum flow velocity near the bed and maximum turbulence near the bed. An overview of the different figures that are used throughout this report is presented in this section. For this overview, the reference confined jet configuration was selected,

represented by test PIVSOP107 (FOV1) and test PIVSOP186 (FOV4). This configuration corresponds to the following selection of parameters:

Reference confined jet configuration: Δx = 0.8m, UKC = 2.5m, BT2 active, smooth bed;

Test PIVSOP107 is used throughout the report as basis for comparison with other tests to assess the influence of the different parameters. Some of the initial tests were repeated at a later stage, during the additional test series, with a slightly higher vector resolution and improved seeding distribution in the basin. Test PIVSOP300 is the repetition of test PIVSOP107 and is also here presented to illustrate the influence of the different setup conditions on the results. The prefix “PIVSOP” is dropped whenever necessary for simplification purposes.

The discussion of results presented in the following sections is organized according to the parameters varied during the tests (e.g. RPM, UKC).

7.1.1 Time-averaged flow patterns

Figure 7.1 and Figure 7.2 present the time-averaged velocity magnitude obtained for tests 107 and 186. The velocity magnitude is obtained by combining the two measured velocity components in each field of view: x and z components in FOV1 and y and z components in FOV4. The velocity maps presented in this Chapter are normalized by $1.1U_{BT}$ to make it easier for comparison between tests. Similar figures were generated for all tests and are presented in Appendix B (Fig “test name”D); the figures in Appendix B are not normalized.

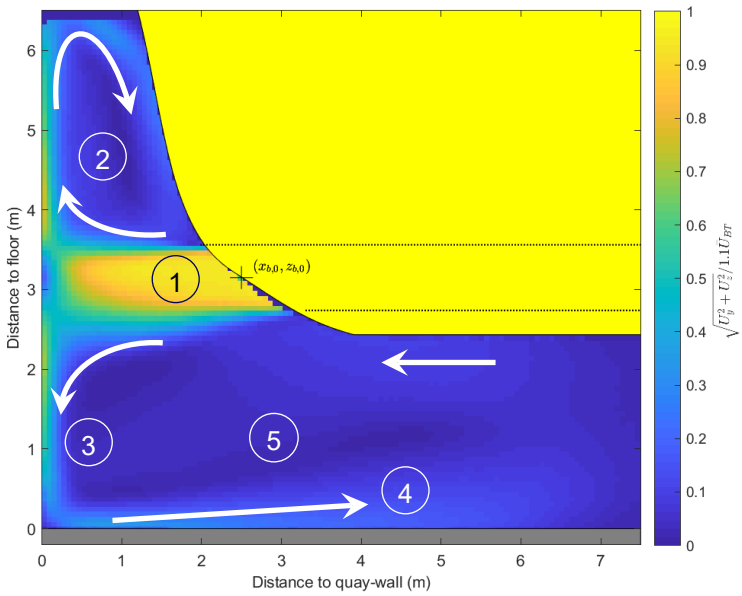

Figure 7.1 Time-averaged flow patterns for the confined jet situation. Plane x,z (FOV1), test 107. Map of the normalized velocity magnitude.

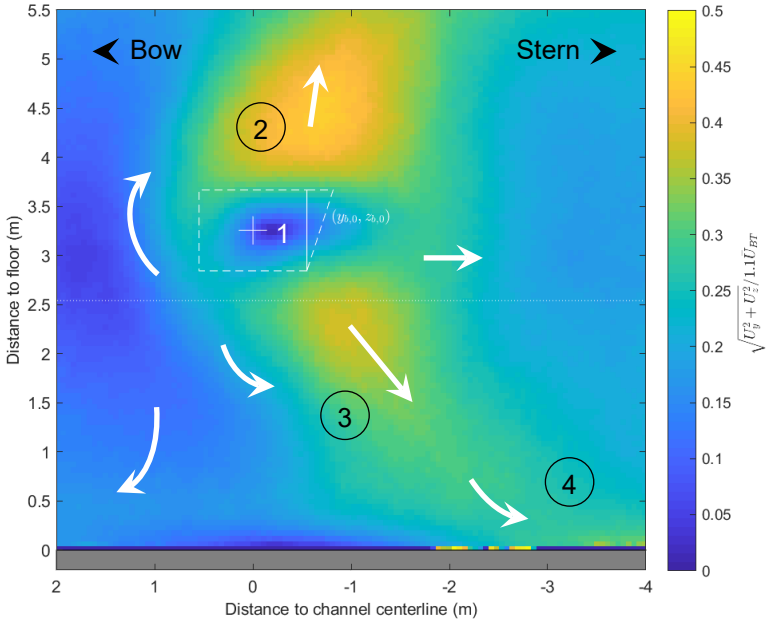

Figure 7.2 Time-averaged flow patterns for the confined jet situation. Plane y,z (FOV4), test 186, captured at a distance of 0.3 m from the quay-wall. Maps of the normalized velocity magnitude.

In this Chapter only a qualitative description of the flow patterns is provided, i.e., the length/size of the schematic arrows presented in the figures are only illustrative, i.e., they do not represent the relative magnitude of the flow patterns observed. Also, the instantaneous flow behavior is highly turbulent and variable, therefore the instantaneous flow patterns are expected to deviate from the time-average description provided.

The following flow patterns can be distinguished in Figure 7.1 and Figure 7.2:

① Jet outflow

This is the area of the flow with the highest flow velocities. The shape of the bow channel outlet influences the jet behavior. The channel is shorter at the bottom than at the top and shorter on the left (front of the vessel) side than on the right (aft of the vessel) side, i.e. the outlet shape is influenced by the hull shape of the vessel. This geometrical asymmetry promotes asymmetric mixing and momentum reduction of the jet: the jet attaches to the longer walls of the bow channel. In other words, mixing and momentum reduction occur earlier on the side of the shorter channel walls. This effect is also noticeable in the vertical velocity profiles of the u_x-component (see Figure 7.4); the distribution of u_x (z) is not symmetrical relative to the bow channel centerline; instead, the zone of maximum flow velocity is shifted slightly towards the top (when looking at the x,z plane). The plane y,z, shows the jet core (near zero velocity) slightly shifted towards the right side (longer side) of the bow channel.

② Upward flow and recirculation

The confined geometrical situation forces the jet to spread along the quay-wall. The velocity maps obtained for both planes (x,z and y,z) show that the upward flow is stronger than the downward flow, and that there is a generalized flow towards the stern of the vessel. This follows from the geometrical asymmetry of the bow channel outlet and, by consequence, of the jet flow. The boundaries (quay-wall, free-surface and vessel hull) impose changes in the flow direction, creating a recirculation pattern in between these boundaries. This is a strong and permanent pattern observed in all tests performed in this plane (Δy = 0.0m).

③ Downward flow

Part of the jet reflected on the quay-wall is directed downwards. In the y,z plane (FOV4) the direction of the downward flow is predominantly between 30 and 60 degrees towards the stern; only a small portion of the downward flow goes in the direction of the bow.

④ Return flow near the bed

The downward flow is forced to change direction upon reaching the bed. In the x,z plane (FOV1), in the centerline of the jet (Δy = 0.0m), the direction of the reflected jet is mostly towards the vessel, as also shown by the EMS signals measured along that plane (see Figure 7.3). The return flow along the bed spreads in the vertical and horizontal planes, losing momentum.

⑤ General recirculation

In the area between quay-wall, bed and vessel a generalized recirculation pattern takes place, with opposite direction to the recirculation pattern observed above the jet.

Figure 7.3 Time-averaged flow velocity near the bed measured by the EMS sensors in test 300 (a repetition of test 107). See Figure 3.6 for the exact location of the sensors.

7.1.2 Maximum flow velocity near the bed

The maximum flow velocity near the bed is determined based on the PIV measurements by taking the maximum time averaged U_x measured near the bed (0m < z < 1m). Only two velocity components are measured with PIV (U_x and U_z, in FOV1, FOV2 and FOV3, and U_y and U_z in FOV4). Since U_z is negligible in comparison with U_x near the bed region, only the U_x component is presented for discussion in this Chapter.

Figure 7.5 presents the decay of the maximum U_x near the bed. The measured flow velocities with the EMS sensors (x,y-components, and combined velocity magnitude) are also presented for comparison. Please note that only the x-component of the EMS measurements (represented by circles in the figures) should be compared with the PIV results (U_x).

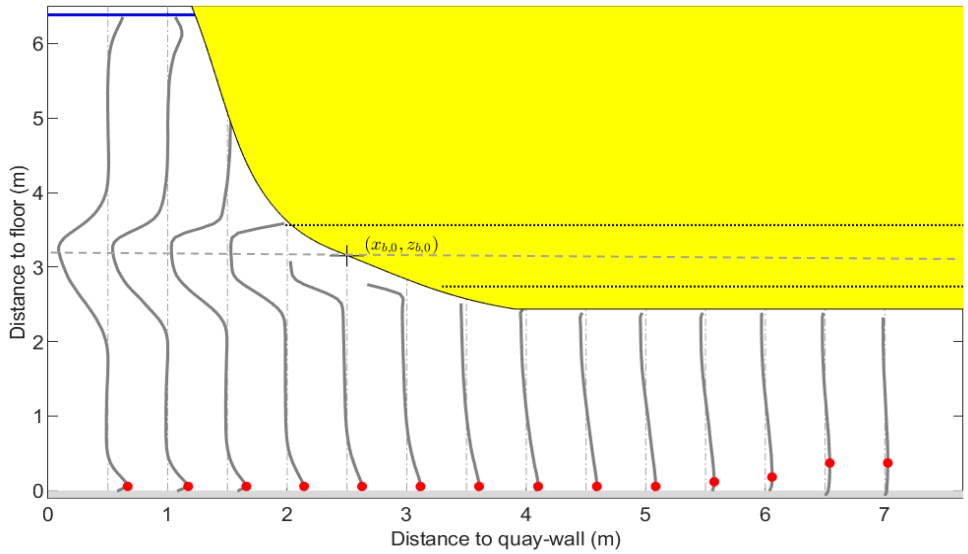

Figure 7.4 Vertical profiles of U_x plotted every 0.5m. Red dots represent the maximum velocity measured near the bed for test 107.

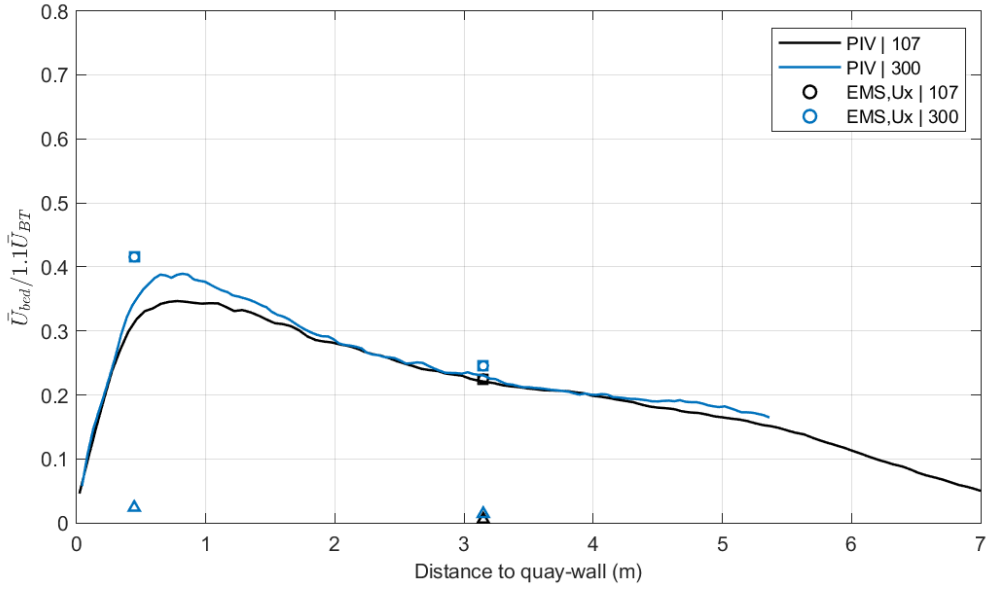

Figure 7.5 Decay of the maximum velocity Ux component (PIV) near the bed for tests 107 and 300; Velocities measured with EMS1 and EMS 3 plotted for comparison (○ - Ux, △ - Uy, □ - combined Ux and Uy).

The measured magnitude and location of the maximum flow velocity is dependent on the PIV measurement resolution, as illustrated by Figure 7.5. Test 300 was performed with a slightly higher vector resolution (one vector every ~4 cm, p.s.), when compared with test 107 (one vector every ~6 cm, p.s.). With a higher vector resolution, larger flow velocities could be measured and a better match with the velocities measured with the EMS's is obtained.

Since only a selection of conditions were repeated with a higher vector resolution, most of the comparison and discussion of results presented in the report is based on the lower resolution tests. This approach is sufficient for comparison purposes, however when determining the absolute velocity magnitude and derived quantities, the results obtained from the measurements performed with a higher resolution should be leading since they have higher accuracy.

7.1.3 Maximum turbulence intensity near the bed

The turbulence intensity was determined as follows:

$$TI = \sqrt{\sigma_1^2 + \sigma_2^2}/1.1U_{BT}$$

Where σ_1 and σ_2 represent the standard deviation of the two measured velocity components (PIV: x and z or y and z, depending on the FOV; EMS: x and y). The maximum velocity measured in the outflow (jet core) is about 10% higher the mean velocity measured in the bow thruster (U_{BT}), based on the free jet tests, and is here used as the bulk velocity.

In most figures TI is presented for both PIV and EMS measurements, for comparison. Please note that PIV and EMS are different instruments that have different measurement volumes and different acquisition frequencies which influence the resulting TI.

The maximum turbulence intensity near the bed is obtained by taking the maximum measured value near the bed. The maximum TI is not necessarily located at same vertical location as the maximum velocity near the bed. As a conservative approach, in the report we present the maximum measured TI value near the bed. At some locations, this is located at the lowest measured point in the vertical, but not always. Figure 7.6 presents the turbulence intensity profiles obtained for test 107 for an example.

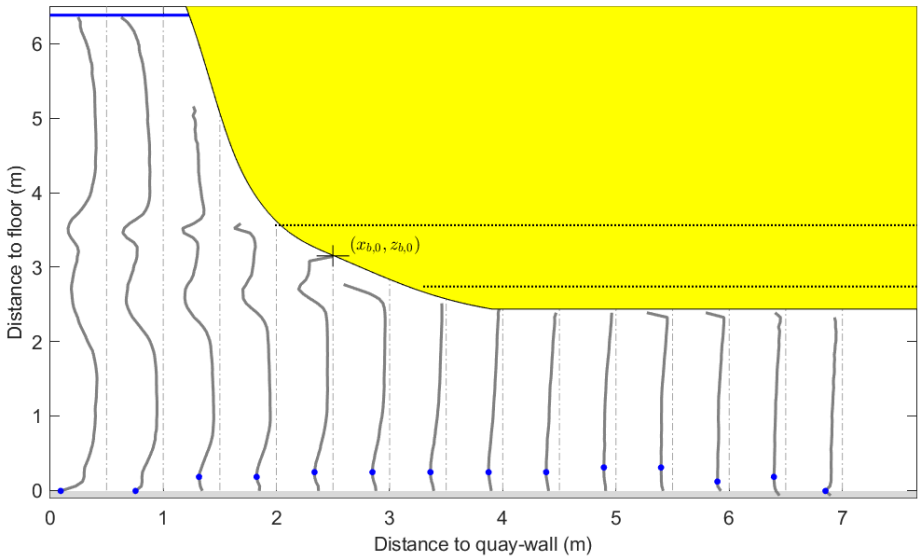

Figure 7.6 Vertical profiles of TI plotted every 0.5m. Blue dots represent the maximum turbulence intensity measured near the bed for test 107.

The turbulence intensity, as being a second-order parameter, is very much influenced by the quality of the velocity measurements. The challenge with the lower resolution PIV tests is on the one hand the lower vector resolution (or larger measurement volume), but also the insufficient seeding quantity near the bed, in the area of interest, combined with a highly 3D flow. In general, the larger the flow velocity and the more three-dimensional the flow is, the more PIV particles are lost between image pairs for the same PIV settings. Loss of particles, or insufficient number of particles, leads to erroneous vectors which are not always possible to filter out in the processing algorithm. This typically leads to bias-to-zero velocities near the bed. As a consequence, the time-averaged velocities measured at the bed for the lower resolution tests tend to underestimate the maximum velocity, especially in the conditions where large flow velocities are expected over a relatively limited area (e.g. low UKC tests, see Figure 7.7,left). Not only are the time-averaged values lower than expected, when compared with repeated tests and EMS measurements (see Figure 7.7,right) but also the variability of the instantaneous

velocity compared to the mean, or velocity fluctuations, is larger for the tests performed with a lower resolution. This directly contributes to higher turbulence intensities, as shown in Figure 7.8, which may not give a correct representation of the true turbulence intensities in that region. Therefore, the results presented should be carefully interpreted bearing in mind the limitations of the measurement setup. However, the good match of the higher resolution PIV results compared to the velocity measured independently by the EMS sensors gives confidence in the obtained level of accuracy.

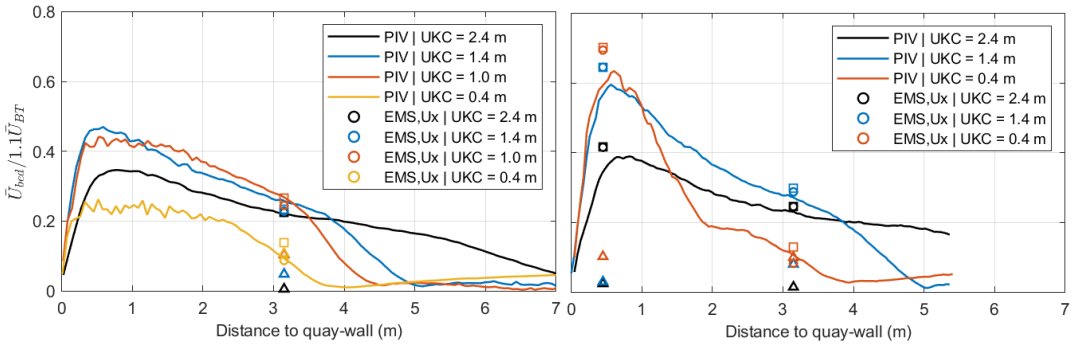

Figure 7.7 Decay of the maximum U_x velocity component (PIV) near the bed for tests performed with different vector resolutions and setup conditions; tests performed with a lower vector resolution (left) and tests repeated with a higher vector resolution (right). Velocities measured with EMS1 and EMS 3 plotted for comparison (○ - Ux, △ - Uy, □ - combined Ux and Uy).

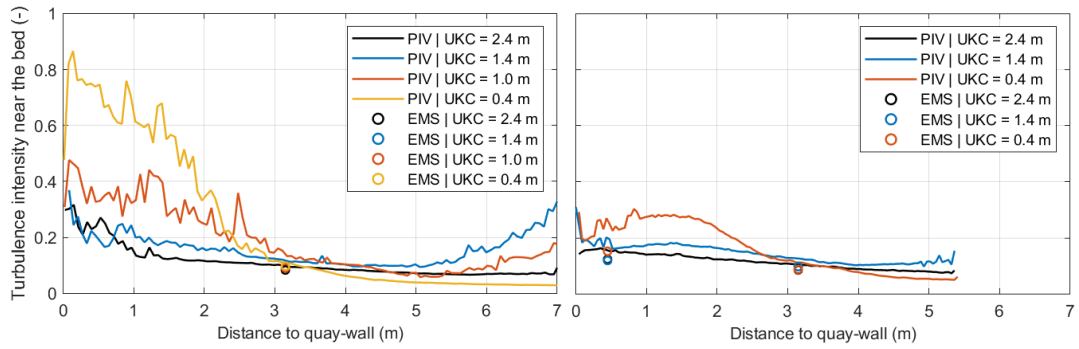

Figure 7.8 Decay of the maximum turbulence intensity for tests performed with different vector resolutions and setup conditions; tests performed with a lower vector resolution (left) and test repeated with a higher vector resolution (right). TI measured with EMS1 and EMS 3 plotted for comparison.

7.2 Results from PIV and EMS tests

7.2.1 Variation in bow thruster

Figure 7.9 shows the flow patterns obtained in the centerline of the jets created by BT1 and BT2 when the individual propellers are active. The main difference observed in the flow field relates to the space between the vessel and the quay-wall. Due to the shape of the hull of the vessel, there is a larger distance between the outlet and quay-wall at the section of BT1 than at the section of BT2. This extra space allows for further dissipation of energy of the jet before reaching the wall. Consequently, lower velocities are expected near the bed when BT1 is active, which is shown in Figure 7.10.

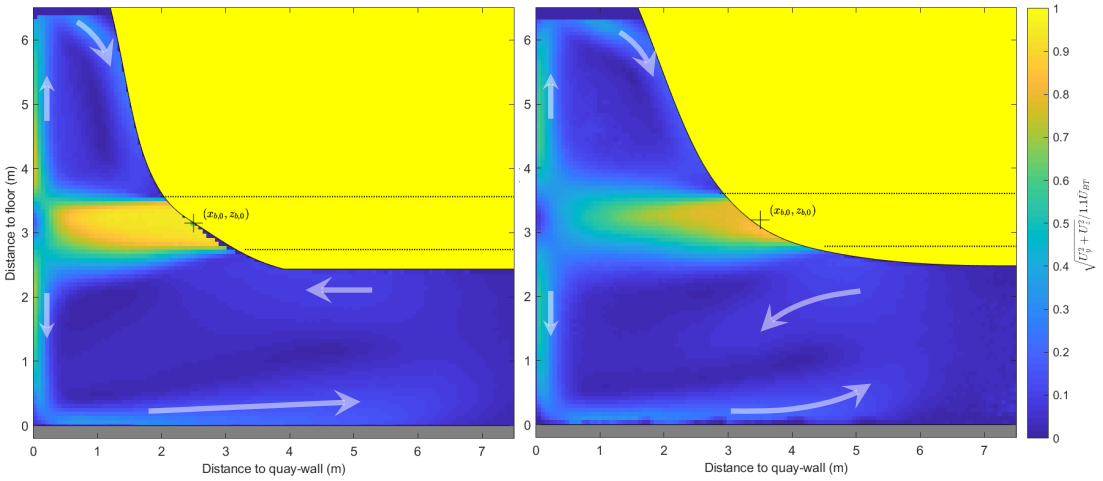

Figure 7.9 Time-averaged flow patterns in the x,z plane for BT2 and BT1, centerline of the respective jets; left: BT2 active, Δy = 0.0m (test 107); right: BT1 active, Δy = 3.5m (test 221). Map of the normalized velocity magnitude.

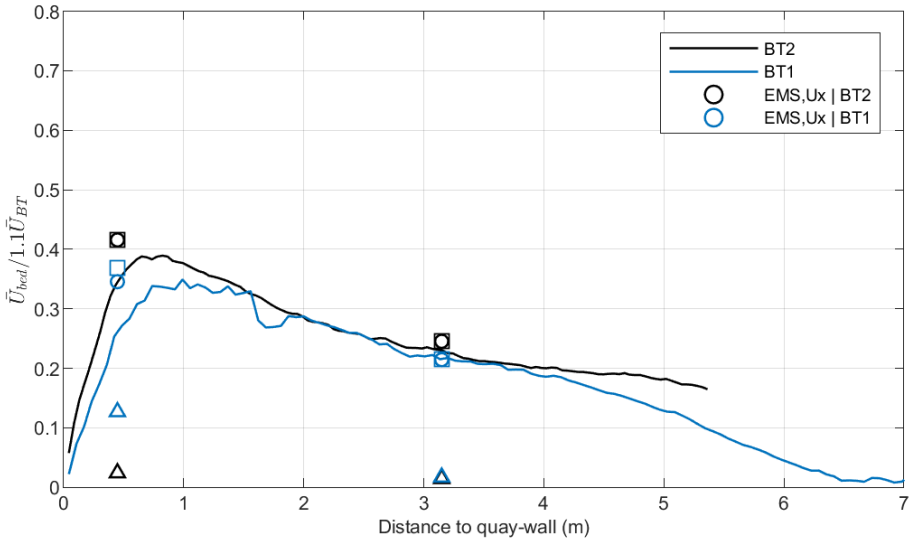

Figure 7.10 Decay of the maximum U_x velocity component (PIV) near the bed for tests performed with different bow thruster active: BT2 active (test 300) and BT1 active (test 221). Velocities measured with EMS1 and EMS 3 plotted for comparison (○ - Ux, △ - Uy, □ - combined Ux and Uy).

7.2.2 Two thrusters simultaneously active

When testing two thrusters simultaneously active two different direction of rotations were considered: propellers rotating in the same direction (clockwise, as seen from above the propeller) and in opposite directions (BT1 in counterclockwise direction and BT2 in clockwise). Figure 7.11, Figure 7.12 and Figure 7.13 present a comparison of the flow patterns for different measurement planes (variation in Δy) for both directions considered. These figures show that there are subtle changes in the flow patterns depending on the direction of rotation of the propellers. Regarding the maximum flow velocity near the bed, the direction of rotation does not seem to have an important effect. For planes Δy = 3.5 m and Δy = 2.0m, although the maximum velocities near bed are comparable between tests with different direction of rotation, the decay away from the quay is slightly faster when propellers rotate in opposite directions.

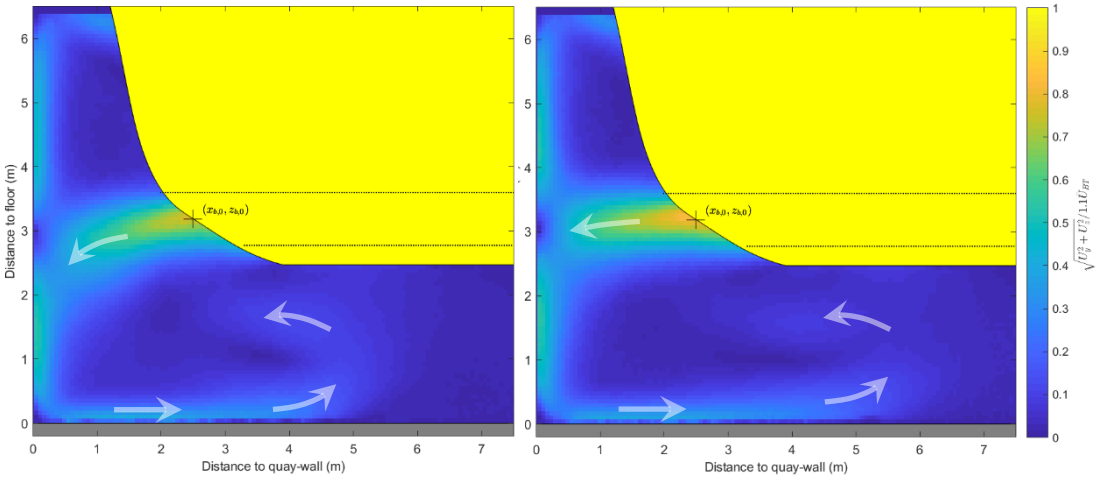

Figure 7.11 Time-averaged flow patterns in the x,z plane for both propellers active, plane Δy = 3.5m. Opposite direction of rotation (test 235, left) and same direction of rotation (test 238, right). Map of the normalized velocity magnitude.

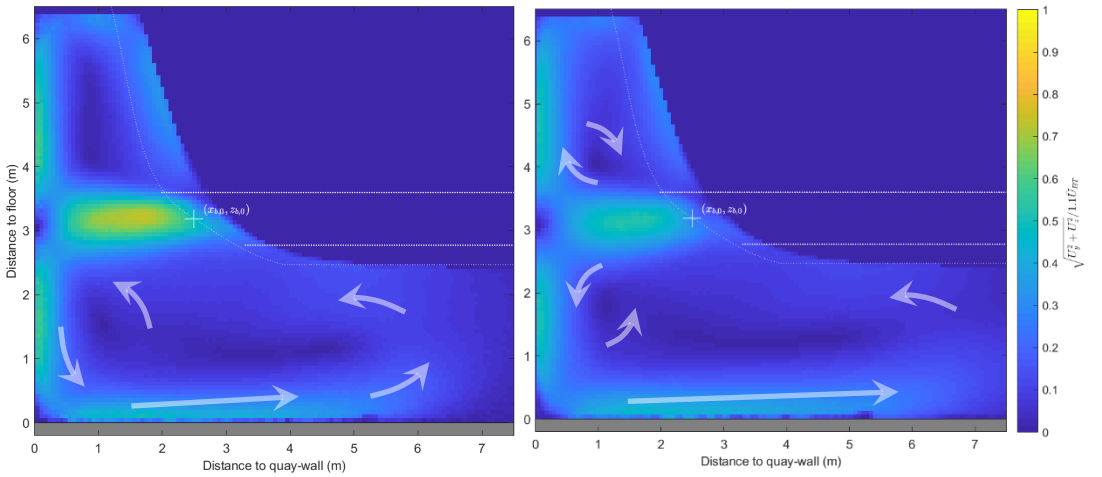

Figure 7.12 Time-averaged flow patterns in the x,z plane for both propellers active, plane Δy = 2.0m. Opposite direction of rotation (test 233, left) and same direction of rotation (test 244, right). Map of the normalized velocity magnitude.

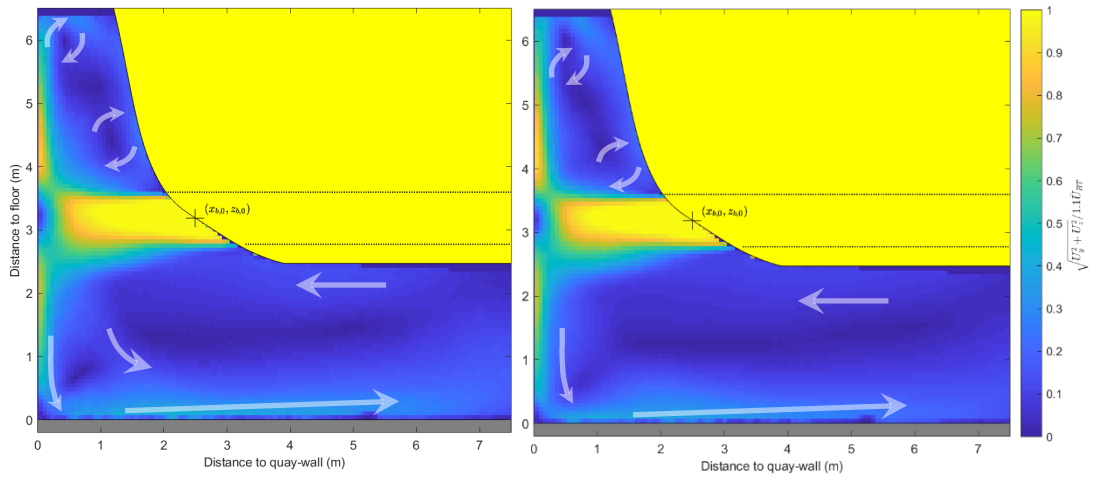

Figure 7.13 Time-averaged flow patterns in the x,z plane for both propellers active, plane Δy = 0.0m. Opposite direction of rotation (test 231, left) and same direction of rotation (test 242, right). Map of the normalized velocity magnitude.

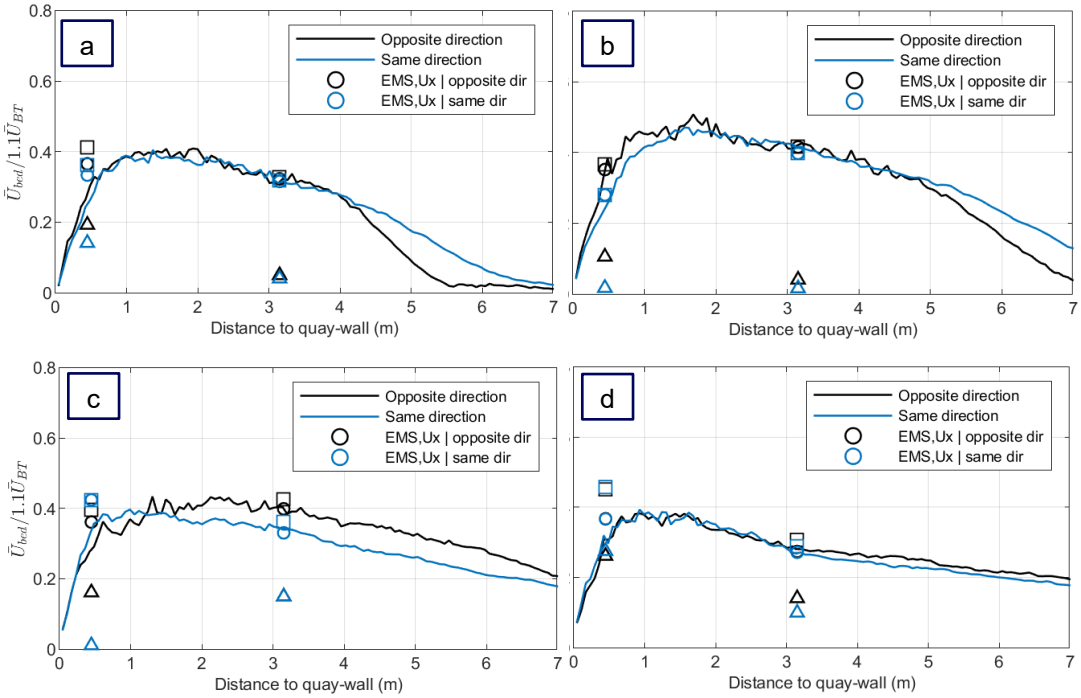

Figure 7.14 Decay of the maximum U_x velocity component (PIV) near the bed for tests performed with both propellers simultaneously active. Variation of the measurement plane and direction of rotation of the propellers. a) Plane Δy = 3.5m (opposite dir.: test 235, same dir: test 238); b) plane Δy = 2.0m (opposite dir.: test 233, same dir: test 234); c) plane Δy = 0.0m (opposite dir.: test 231, same dir: test 242) and d) plane Δy = -2.0m (opposite dir.: test 252, same dir: test 247). Velocities measured with EMS1 and EMS 3 plotted for comparison (○ - Ux, △ - Uy, □ - combined Ux and Uy).

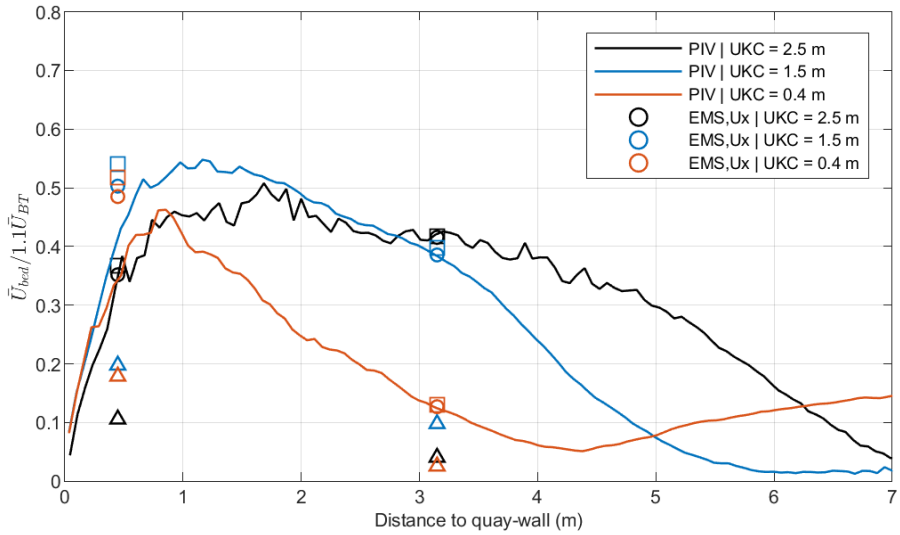

Figure 7.15 Decay of the maximum U_x velocity component (PIV) near the bed for tests performed with both propellers simultaneously active. Variation of the UKC for plane Δy = 2.0m. UKC = 2.5m (test 233), UKC = 1.5m (test 263) and UKC = 0.4m (test 269). Velocities measured with EMS1 and EMS 3 plotted for comparison (○ - Ux, △ - Uy, □ - combined Ux and Uy).

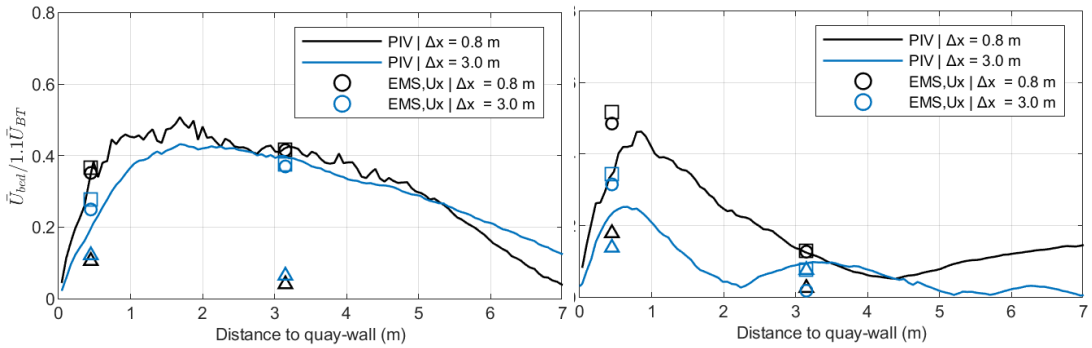

Figure 7.16 Decay of the maximum U_x velocity component (PIV) near the bed for tests performed with both propellers simultaneously active. Variation of the distance to quay-wall (Δx) for plane Δy = 2.0m, for two different UKC. UKC = 2.5m, left (Δx = 0.8m: test 233; Δx = 3.0m: test 254) and UKC = 0.5m, right (Δx = 0.8m: test 269; Δx = 3.0m: test 272). Velocities measured with EMS1 and EMS 3 plotted for comparison (○ - Ux, △ - Uy, □ - combined Ux and Uy).

7.2.3 Variation in Δy

BT2

Figure 7.17 illustrates the time-averaged flow velocities measured for tests performed on different PIV measurement planes in the y-direction for the reference confined jet configuration (see section 7.1). See Figure 5.2 for a schematization of the different measurement planes. This figure shows that the flow at planes located closer to the bow (plane Δy = 3.5 m and Δy = 2.0 m, Figure 7.17 a,b) is weaker than at planes towards the stern. This is in line to what was observed in section 7.1.1 e.g, the flow is predominantly towards the stern of the vessel.

In Figure 7.18 the decay of the maximum velocity near the bed is presented, illustrating that the highest flow velocities in the x-direction near the bed are measured in the plane Δy = -2.0 m. The measurements with the EMS's (see Figure 7.19) provide an indication of the direction of the mean flow velocity at the bed, near the quay-wall. It shows that away from the centerline of bow thruster 2 (Δy = 0.0m), the velocity y-component becomes relevant as a consequence of the jet spreading sideways. At the location of EMS2 (x_{EMS2} = 9.6 m) a relatively large-scale counter-clockwise flow is present, indicating the influence of the inlet of BT2 ($x_{inlet,center}$ = 11.4 m).

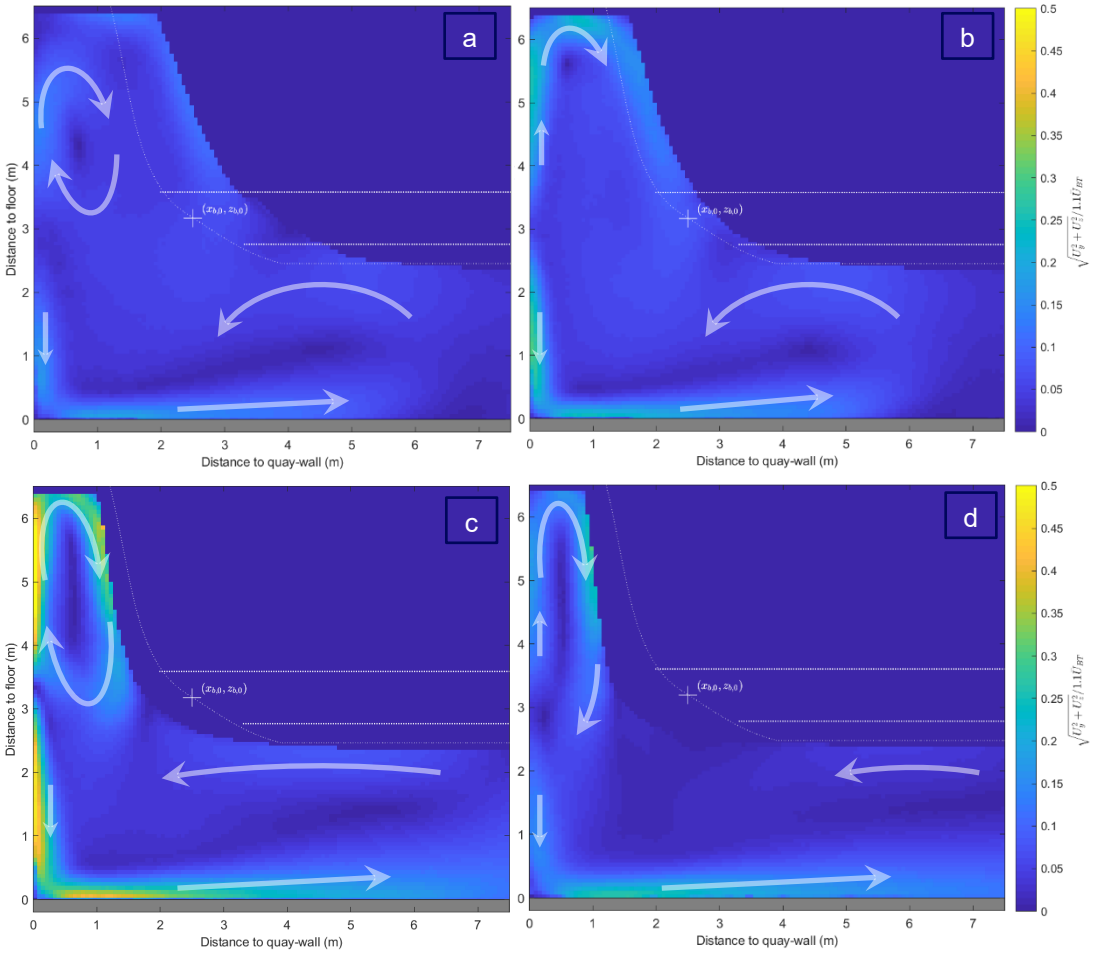

Figure 7.17 Time-averaged flow patterns in the x,z plane for different Δy for BT2. a: Δy = 3.5 m (test 102); b: Δy = 2.0 m (test 99); c: Δy = -2.0 m (test 96) and d: Δy = -4.0 m (test 93). Map of the normalized velocity magnitude. White lines correspond to the cross-section of the vessel and bow channel BT2 for Δy = 0.0 m. Map of the normalized velocity magnitude.

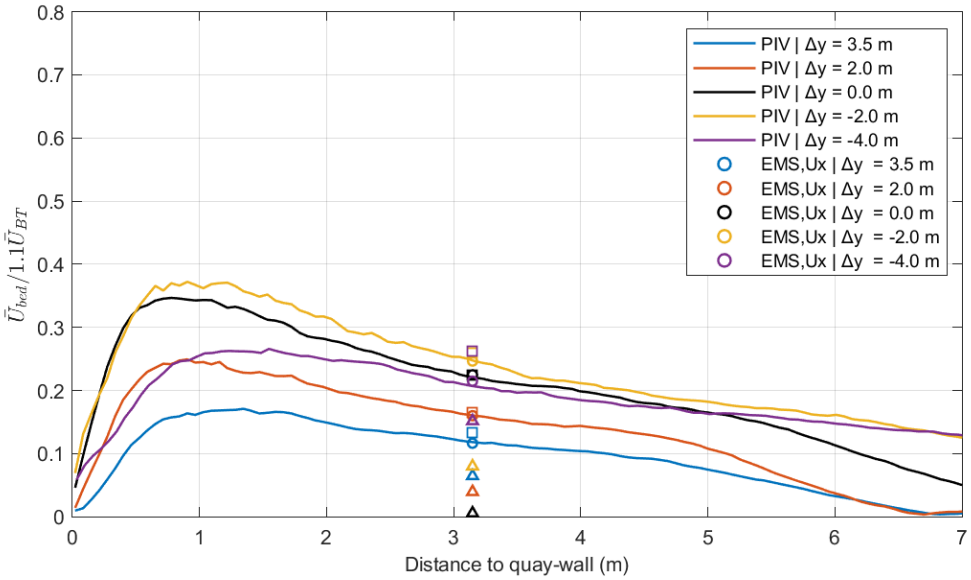

Figure 7.18 Decay of the maximum U_x velocity component (PIV) near the bed for different Δy for BT2: Δy = 3.5m (test 102), Δy = 2.0m (test 99), Δy = 0.0m (test 107), Δy = -2.0m (test 96) and Δy = -4.0m (test 93); Velocities measured with EMS1 plotted for comparison (○ - U_x, △ - U_y, □ - combined U_x and U_y).

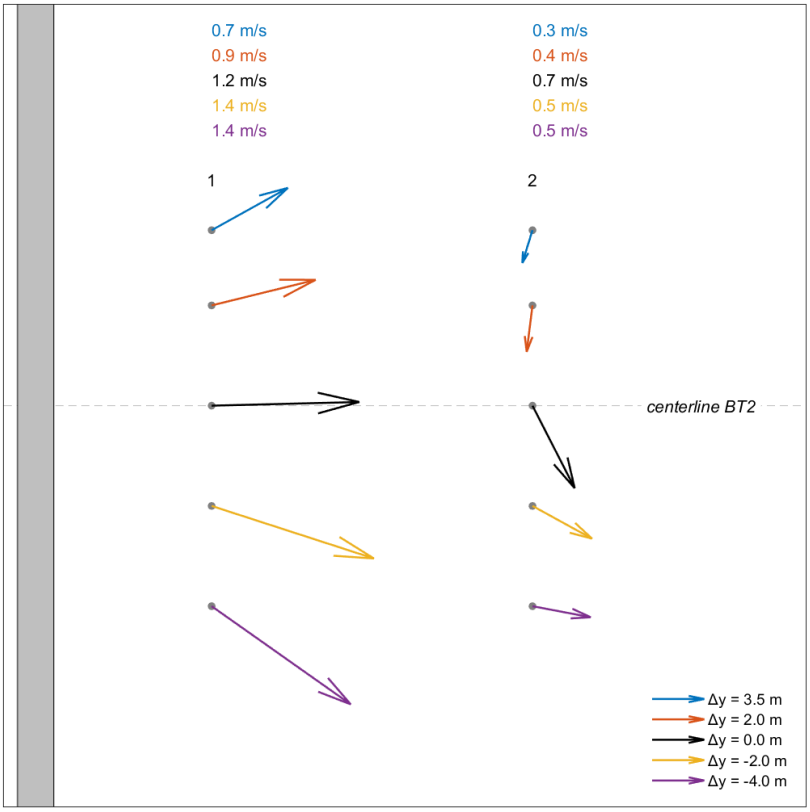

Figure 7.19 Velocity magnitude and direction measured with EMS's near the bed for different Δy for BT2: Δy = 3.5m (test 102), Δy = 2.0m (test 99), Δy = 0.0m (test 107), Δy = -2.0m (test 96) and Δy = -4.0m (test 93). x_{EMS1} = 3.2 m, x_{EMS2} = 9.6m.

The maximum turbulence intensities measured at the different planes is presented in Figure 7.19. This figure shows that in plane Δy = -2.0m is where the maximum TI values are measured in comparison with the other planes (please note that the absolute magnitude of TI may be overestimated for these low-resolution PIV tests).

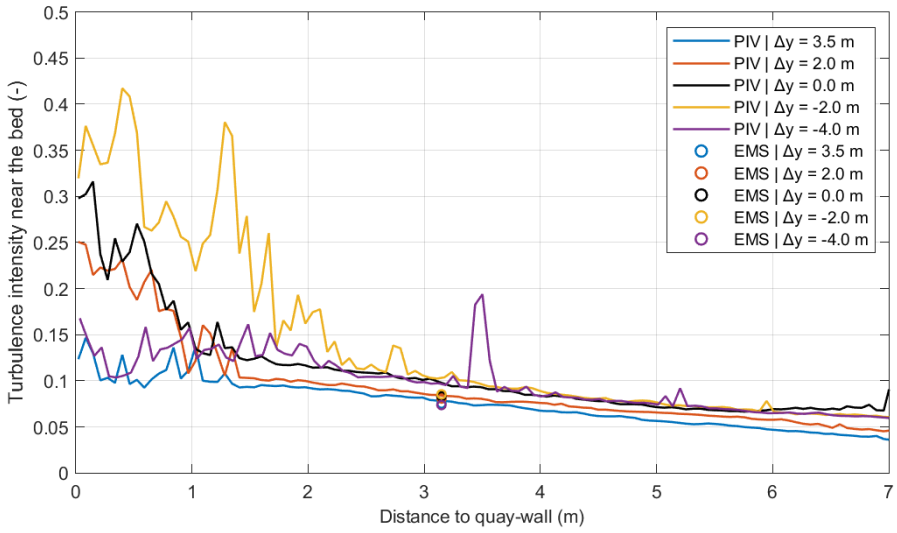

Figure 7.20 Decay of the maximum turbulence intensity (PIV, TI based on U_x and U_z components) near the bed for different Δy for BT2: Δy = 3.5m (test 102), Δy = 2.0m (test 99), Δy = 0.0m (test 107), Δy = -2.0m (test 96) and Δy = -4.0m (test 93). TI measured with EMS1 plotted for comparison (EMS, TI based on U_x and U_y components).

BT1

Figure 7.21 illustrates the time-averaged flow velocities measured with BT1 active, for the reference confined jet configuration (see section 7.1). The main flow patterns observed with BT1 active are generally similar to the patterns observed for BT2, e.g., rotational flow above the jet between vessel and quay-wall and return flow near the bed predominantly flowing towards the vessel. In Figure 7.22 the decay of the maximum U_x velocity component is presented, showing that the maximum measured velocity is in line with what was measured with BT2 active: $U_{x,max}/1.1U_{BT} < 0.4$; the maximum velocity near the bed occurs in the plane $\Delta y = 2.0$m, i.e., off-center, towards the stern of the vessel, as also observed for BT2 active.

The EMS's in Figure 7.23 illustrate the predominant flow direction at each measured point. These tests were performed during the additional test series where EMS3 was placed very close to the quay-wall (see section 3.2). Although the maximum U_x is measured in the plane $\Delta y = 2.0$m, the maximum velocity magnitude (U_x and U_y combined) was measured in the plane $\Delta y = 0.0$m.

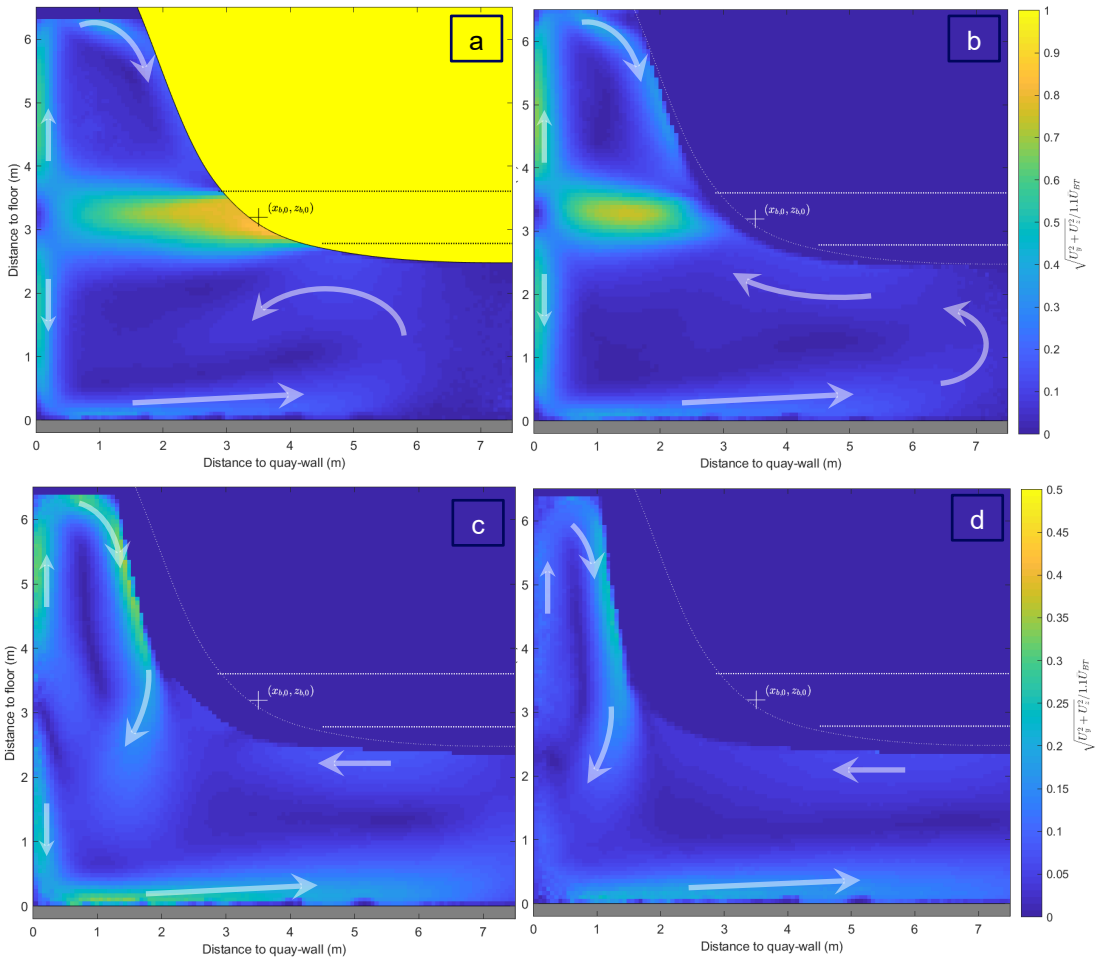

Figure 7.21 Time-averaged flow patterns in the x,z plane for different Δy for BT1. a: Δy = 3.5m (test 221); b: Δy = 2.0 m (test 218); c: Δy = 0.0 m (test 223) and d: Δy = -2.0 m (test 225). Map of the normalized velocity magnitude. White lines correspond to the cross-section of the vessel and bow channel BT1 for Δy = 3.5 m.

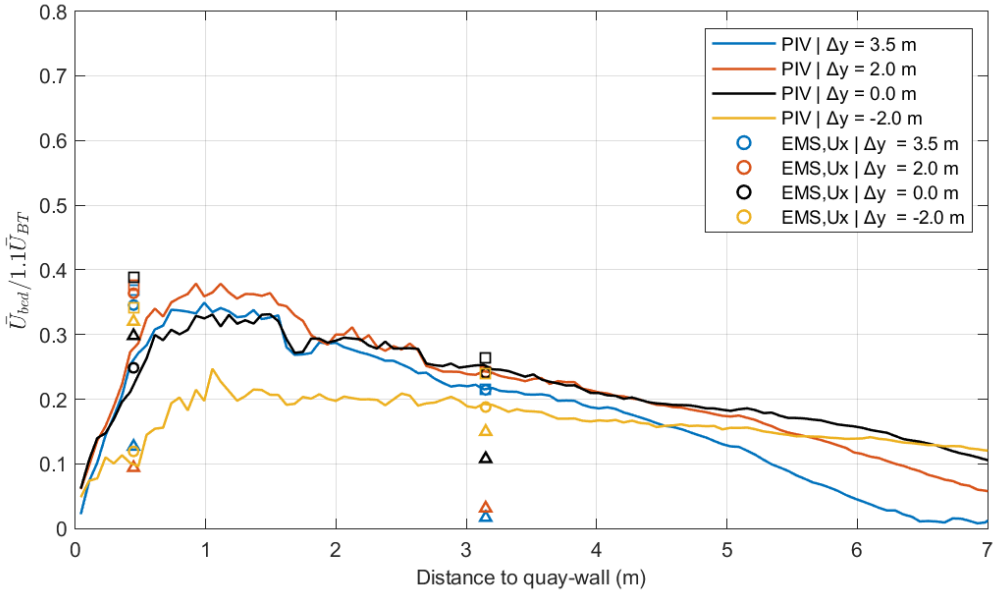

Figure 7.22 Decay of the maximum Ux velocity component (PIV) near the bed for different Δy for BT1: Δy = 3.5m (test 221); Δy = 2.0 m (test 218); Δy = 0.0 m (test 223) and Δy = -2.0 m (test 225). Velocities measured with EMS1 plotted for comparison (○ - U_x, △ - U_y, □ - combined U_x and U_y).

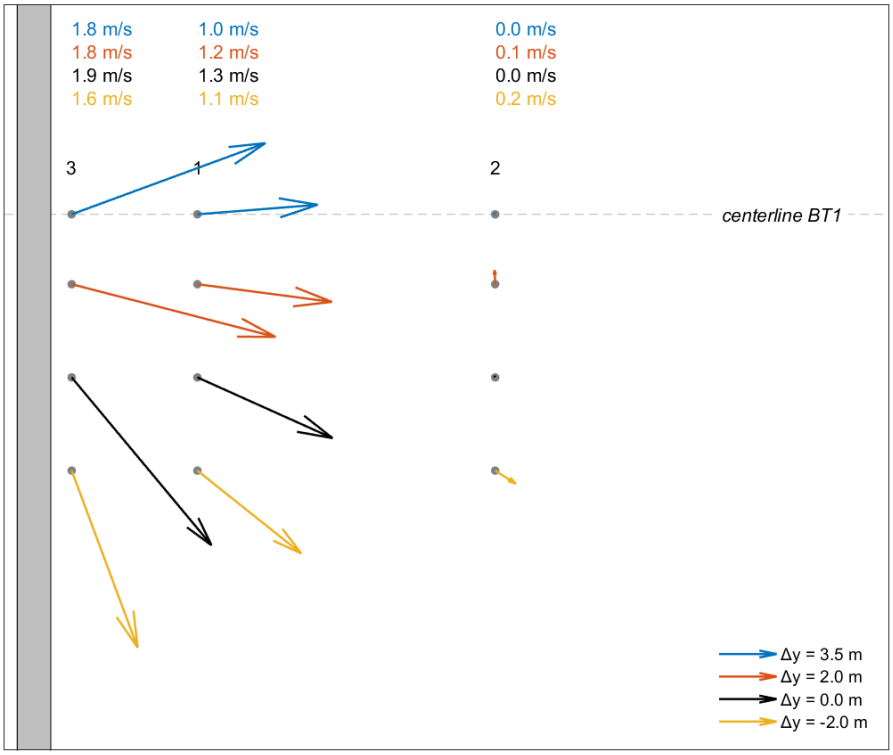

Figure 7.23 Velocity magnitude and direction measured with EMS's near the bed for different Δy: Δy = 3.5m (test 221), Δy = 2.0m (test 218), Δy = 0.0m (test 223), Δy = -2.0m (test 225). x_{EMS3} = 0.4 m, x_{EMS1} = 3.2 m, x_{EMS2} = 9.6m.

7.2.4 Variation in RPM

Figure 7.24 presents the time-averaged flow patterns for the reference confined jet configuration (see section 7.1) for two tests performed with different RPMs, and consequently different flow velocities in the bow channel: 445 RPM (test 105) and 800 RPM (test 107). The figure shows that the flow patterns are very similar in both tests; the main difference is observed

in the spreading of the reflected jet near the bed: for a higher flow velocity (Figure 7.24 right) the jet spreads further underneath the vessel.

Figure 7.25 presents the decay of the maximum velocity near the bed for three tests with varying RPM's. This figure shows that the maximum near bed velocity increases linearly within the first ~0.50 m from the quay-wall, reaching the maximum value in the region 0.50 < x < 1.0m. For x > 1.0m, the velocity near the bed starts to gradually decrease. A sharper decrease in the maximum velocity is observed at a certain point in each test, the distance from the wall at which it happens depends on the RPM. This sharper velocity decrease relates to a change in flow direction, which happens earlier for a lower RPM. The velocities measured with EMS's (see Figure 7.26) show that near the quay-wall the flow is predominantly directed towards the vessel, however at the second sensor (EMS2) the y-component is larger, meaning that the flow is predominantly towards the stern.

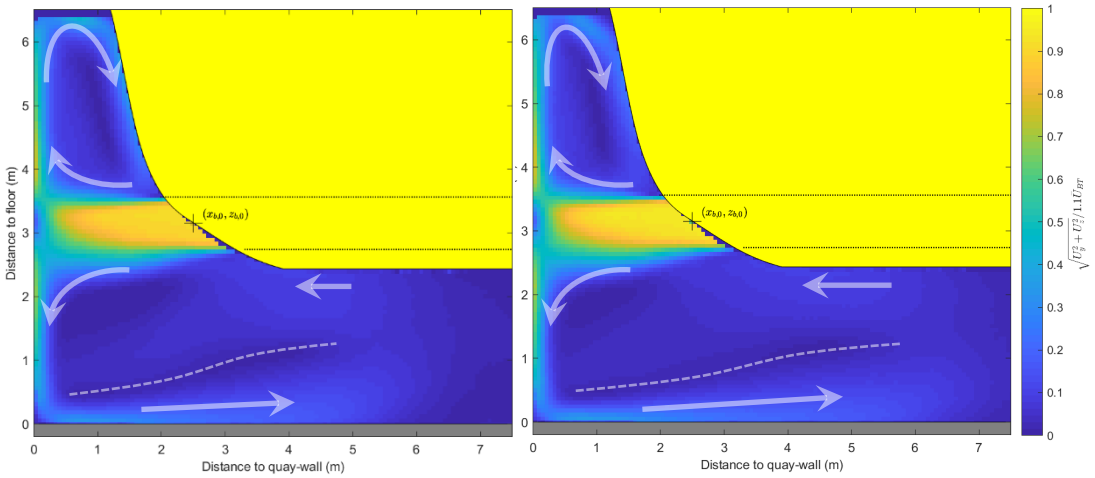

Figure 7.24 Time-averaged flow patterns in the x,z plane for different RPM for BT2. Left: 445 RPM, U_{BT} = 2.6 m/s (test 105); right: 800 RPM, U_{BT} = 4.8 m/s (test 107). Map of the normalized velocity magnitude. Dashed line: extent of the zone with near zero flow velocities.

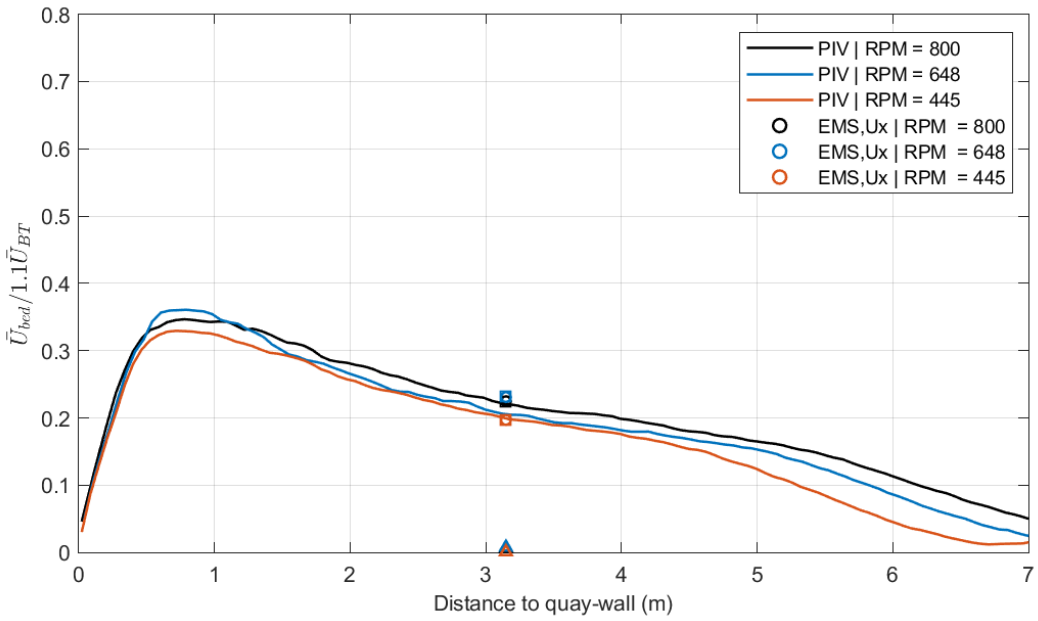

Figure 7.25 Decay of the maximum Ux velocity component (PIV) near the bed for different RPM for BT2: 800 RPM (test 107), 648 RPM (test 55) and 445 RPM (test 105); Velocities measured with EMS1 plotted for comparison (○ - U_x, △ - U_y, □ - combined U_x and U_y).

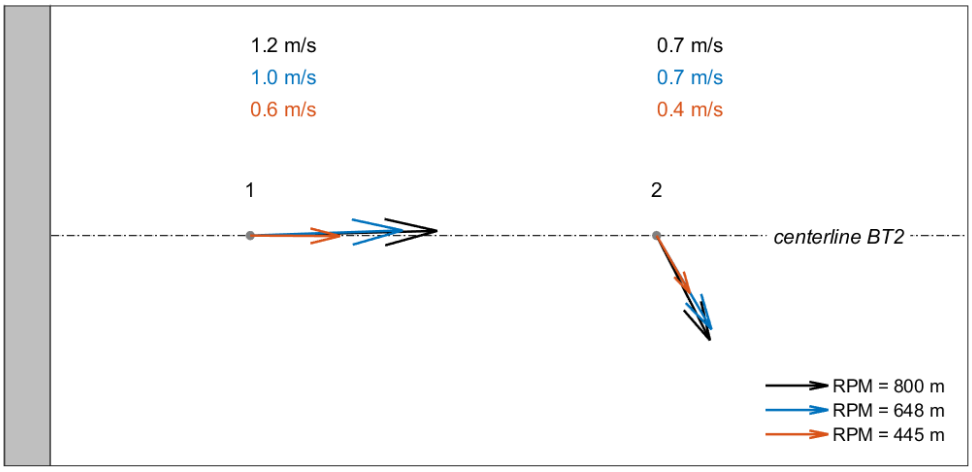

Figure 7.26 Velocity magnitude measured with EMS's near the bed for different RPM for BT2: 800 RPM (test 107), 648 RPM (test 55) and 445 RPM (test 105). x_{EMS1} = 3.2 m, x_{EMS2} = 9.6m.

Figure 7.27 presents the maximum turbulence intensity measured for the tests with different RPM's. As mentioned in section 7.1.3, the turbulence intensities for the test with the highest expected velocities (highest RPM, black line in Figure 7.27) may be overestimated in the region near the wall where larger flow velocities are hard to measure in the low resolution PIV tests. For all tests an almost linear decaying trend characterizes the region 1.5m <x< 5m.

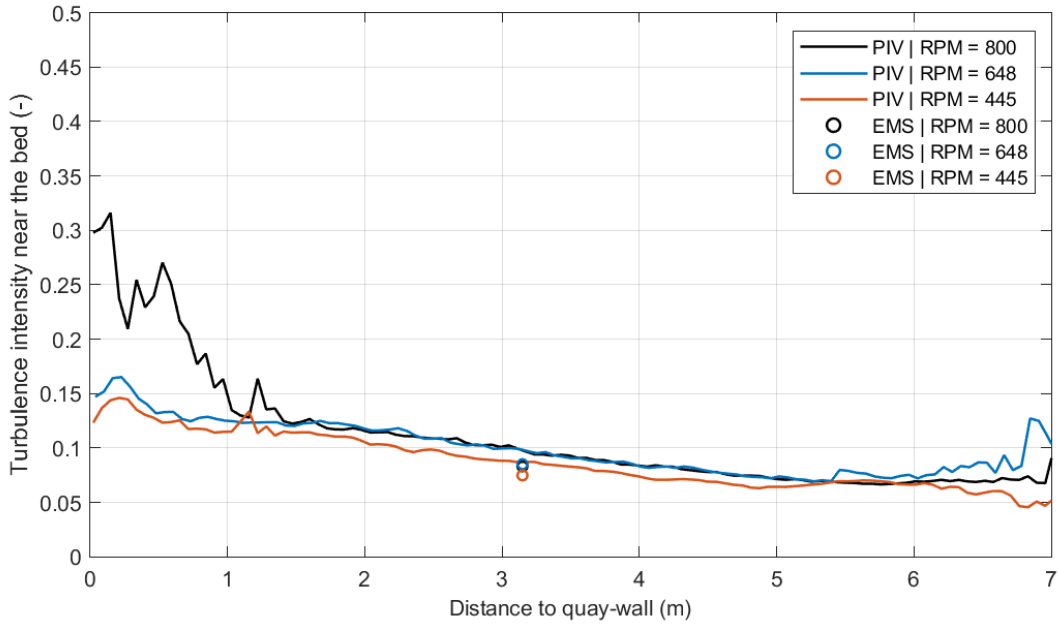

Figure 7.27 Decay of the maximum turbulence intensity (PIV, TI based on U_x and U_z components) near the bed for different RPM for BT2: 800 RPM (test 107), 648 RPM (test 55) and 445 RPM (test 105). TI measured with EMS1 plotted for comparison (EMS, TI based on U_x and U_y components).

7.2.5 Variation in UKC

Figure 7.28 illustrates the measured flow patterns for different UKC's (2.5m, 1.5m, 1.0m and 0.5m), for Δx = 0.8m, BT2 active and max RPM. The larger the UKC, the more space is available for the reflected jet to propagate underneath the vessel. As the space underneath the vessel becomes more confined, the return flow near the bed will gradually spread more in the direction along the quay-wall (y-direction), as shown in Figure 7.29 (EMS1). However, very close to the quay-wall (EMS3, x_{EMS3} = 0.4m) the flow direction is mostly towards the vessel and the velocity magnitude increases as UKC becomes smaller.

The decay of the maximum velocity near the bed is shown in Figure 7.30. In this figure, the tests repeated with higher vector resolution are presented. This figure shows that the maximum flow velocity is measured in the test with the lowest UKC tested (0.5m). For all tests, the maximum velocity is measured within the region of 0< x < 1m. The rate of velocity decay is dependent on the UKC: as the UKC decreases and the influence of the main jet, and the hull of the vessel, start blocking the flow under the vessel, a faster velocity decay in the x-direction is observed. So, compared to higher UKC values, a low UKC gives the higher velocities near the quay wall, but the velocity reduces faster farther away from the quay wall.

Regarding the turbulence intensity (see Figure 7.31), this is larger for the test with the smaller UKC, where the maximum TI measured with PIV is in the order of 30%.

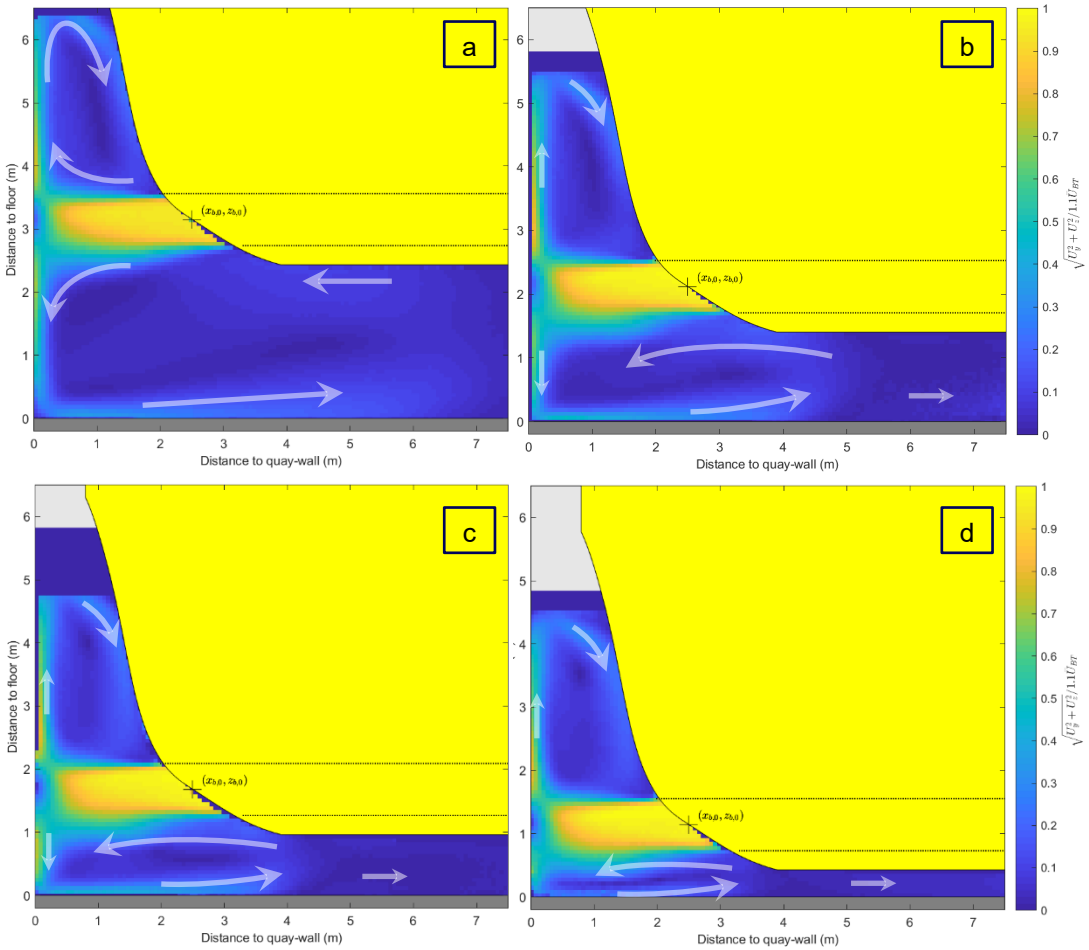

Figure 7.28 Time-averaged flow patterns in the x,z plane for different UKC for BT2 and Δx = 0.8m. a: UKC = 2.5 m (test 107); b: UKC = 1.5 m (test 150); c: UKC = 1.0 m (test 162) and d: UKC = 0.5 m (test 146). Map of the normalized velocity magnitude.

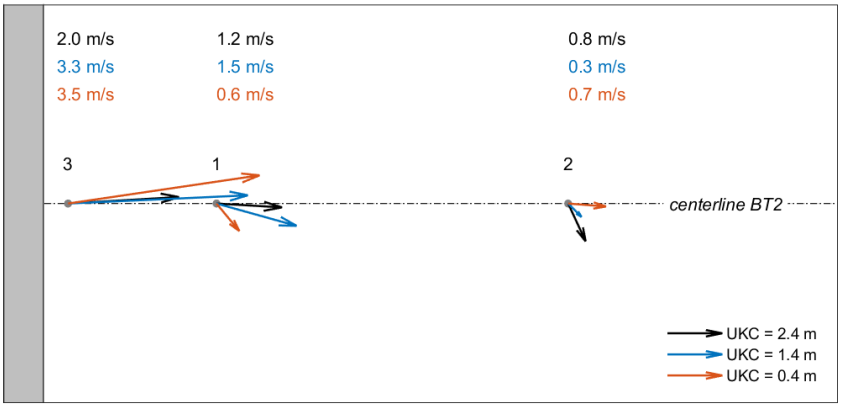

Figure 7.29 Velocity magnitude and direction measured with EMS's near the bed for different UKC for BT2 and Δx = 0.8m: UKC = 2.4m (test 300), UKC = 1.4m (test 298) and UKC = 0.4m (test 291). x_{EMS3} = 0.4m, x_{EMS1} = 3.2 m, x_{EMS2} = 9.6m.

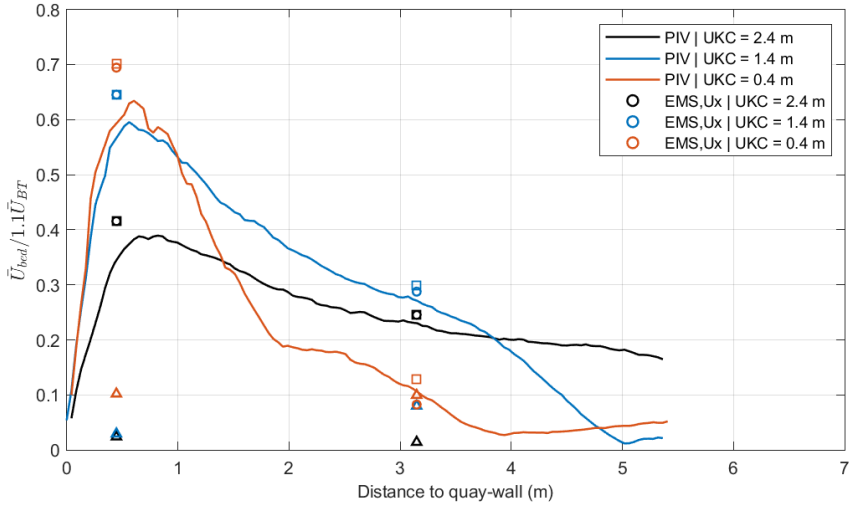

Figure 7.30 Decay of the maximum U_x velocity component (PIV) near the bed for different UKC for BT2 and Δx = 0.8m: UKC = 2.4m (test 300), UKC = 1.4m (test 298) and UKC = 0.4m (test 291); Velocities measured with EMS1 and EMS 3 plotted for comparison (○ - U_x, △ - U_y, □ - combined U_x and U_y).

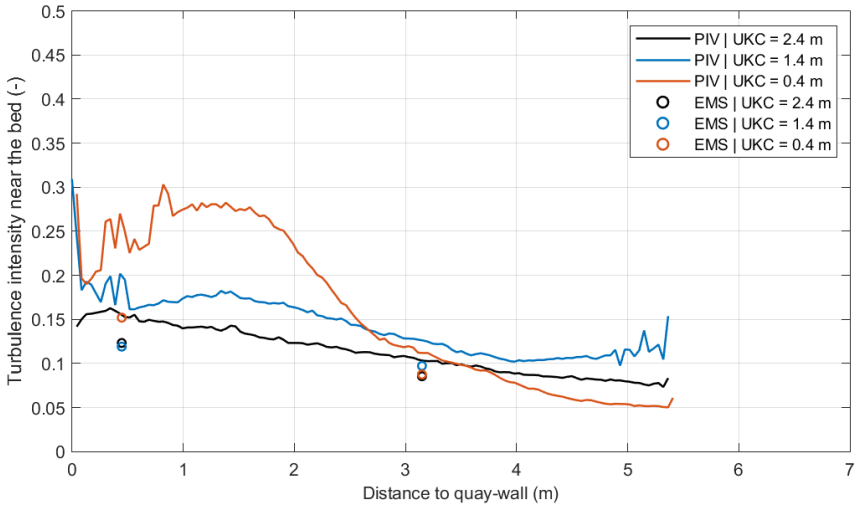

Figure 7.31 Decay of the maximum turbulence intensity (PIV, TI based on U_x and U_z components) near the bed for different UKC for BT2 and Δx = 0.8m: UKC = 2.4m (test 300), UKC = 1.4m (test 298) and UKC = 0.4m (test 291); TI measured with EMS1 and EMS 3 plotted for comparison (EMS, TI based on U_x and U_y components).

7.2.6 Variation in Δx

Figure 7.32 presents the velocity maps for a variation in the distance to the quay-wall (Δx) for BT2 active and UKC = 2.5m. The test performed for Δx = 23m (free jet test) is here presented to illustrate that no influence from the boundaries is observed in the flow patterns at this distance. The more space there is between vessel and quay-wall the more space is available for the main jet (outflow) to spread and decrease momentum before reaching the quay-wall. At a distance of Δx =5m from the quay-wall, the wall still has an effect on the jet propagation, highlighted by the return flow above and below the jet outflow.

Regarding the maximum flow velocities near the bed in the x-direction, these occur for the smallest quay-wall clearance, however there is not a large difference between tests for a large UKC (2.5m, Figure 7.34 left). For a small UKC (0.5m, Figure 7.34 right) the maximum velocity is also observed for the smaller quay-wall clearance, and the difference between tests is much more pronounced. For the small UKC (0.5m), for Δx = 0.8m the velocity decay near the bed is promoted by the interaction with the main jet (first decay trend, 1m < x < 2m) and then by the blockage of the hull of the vessel (second decay trend, 2m < x < 4m), as shown in Figure 7.33 (left). For Δx = 3.0m (Figure 7.33, right), the main blockage to the return flow is promoted by the main jet.

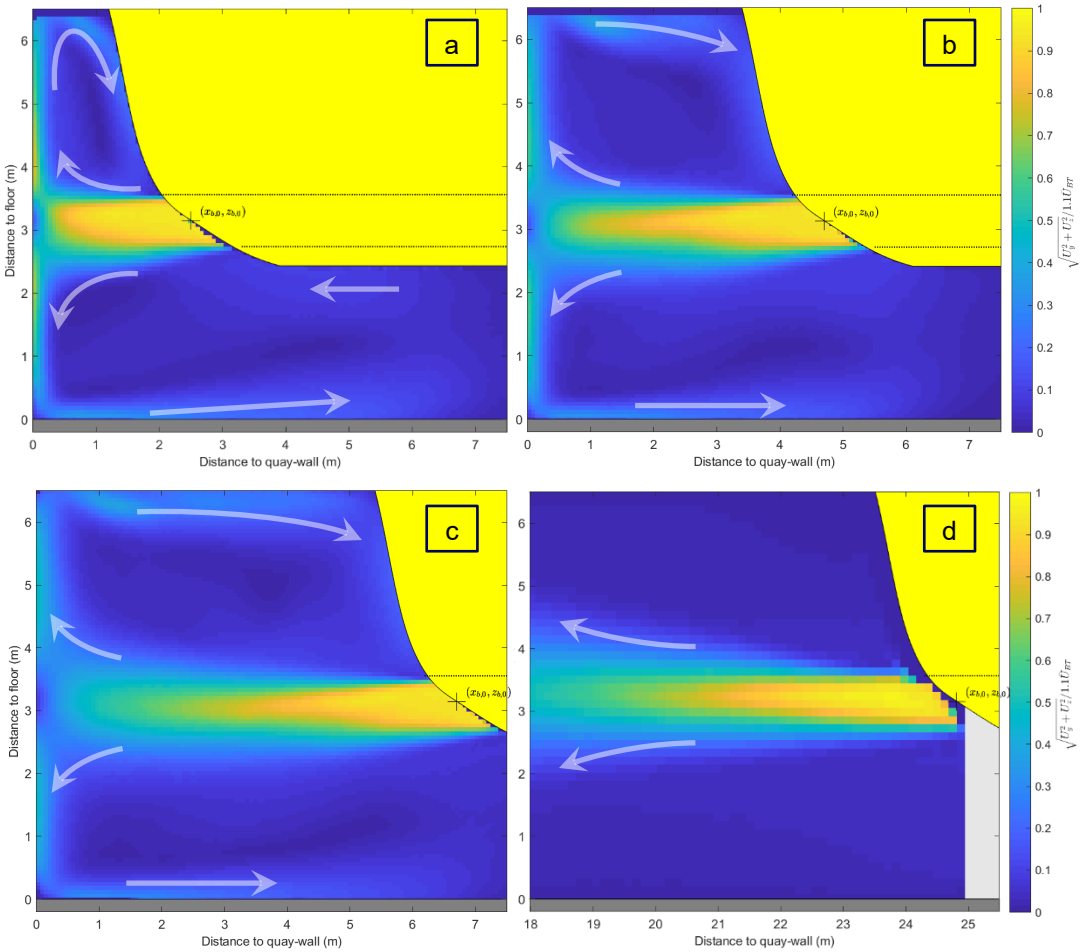

Figure 7.32 Time-averaged flow patterns in the x,z plane for different distance to the quay-wall for UKC = 2.5m. a: Δx = 0.8 m (test 107); b: Δx = 3.0 m (test 133); c: Δx = 5.0 m (test 112) and d: Δx = 23.0 m (test 14). Map of the normalized velocity magnitude.

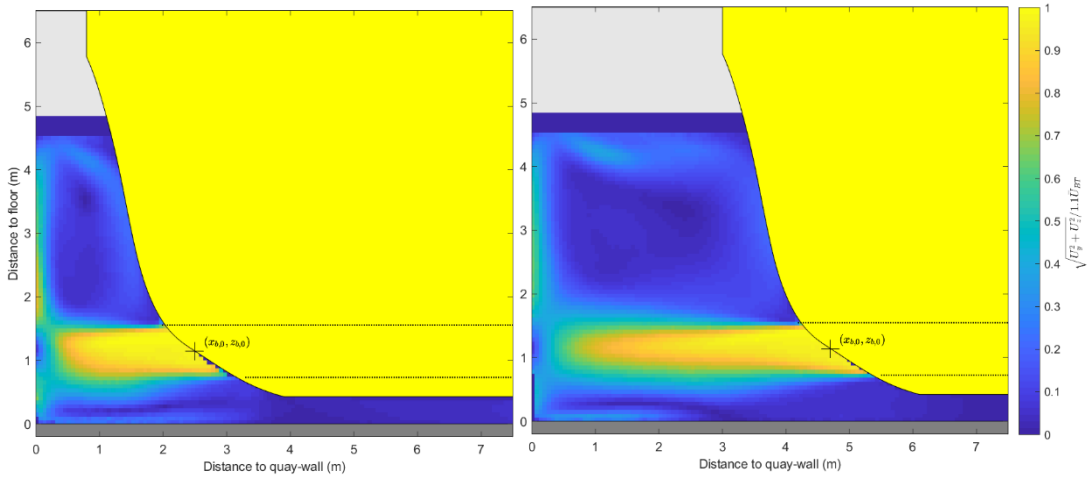

Figure 7.33 Time-averaged flow patterns in the x,z plane for different distances to the quay-wall for UKC = 0.5m. Δx = 0.8 m (test 146), left; Δx = 3.0 m (test 142), right. Map of the normalized velocity magnitude.

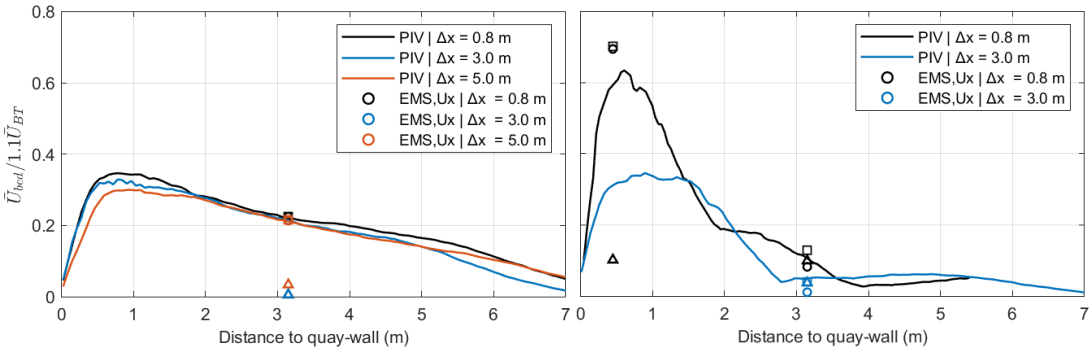

Figure 7.34 Decay of the maximum Ux velocity component (PIV) near the bed for different Δx and different UKC, for BT2. UKC = 2.5m (left), Δx = 0.8m (test 107), Δx = 3.0m (test 133), Δx = 5.0m (test 112); UKC = 0.5m (right), Δx = 0.8m (test 291) and Δx = 3.0m (test 142); Velocities measured with EMS1 and EMS3 plotted for comparison (○ - U_x, △ - U_y, □ - combined U_x and U_y).

7.2.7 Variation in bed roughness

Figure 7.35 shows the decay of the maximum flow velocity for the test performed with the measurement frame (Figure 3.15) placed underneath the vessel. This figure shows that the initial velocity increase near the quay-wall is similar between tests. After reaching the peak in the area 0.5m < x < 1.0m, the velocity starts to decrease, quicker with the frame in place. This test has shown that an increased roughness plays a role in decreasing the resulting velocities near the bed for which further exploratory tests were performed with more realistic bed roughness.

Figure 7.36 illustrates the time-averaged flow patterns captured for smooth and rough beds (fixed rock, 10-60 kg), for the smallest distance to the quay-wall tested (Δx = 0.8m), for the two extreme under-keel clearances tested: UKC = 2.5m (Figure 7.36 a,c) and UKC = 0.5m (Figure 7.36 b,d). This figure shows that bed roughness significantly changes the flow patterns. With smooth bed (Figure 7.36 a,b), the return jet spreads along the bed, in the horizontal and vertical planes, in a seemingly linear way towards the vessel. In the presence of a rough bed (Figure 7.36 c,d), the reflected jet detaches from the bed moving upwards in the vertical direction. Part of the upward flow is incorporated by the main jet, creating a localized recirculation cell. As a consequence, the flow underneath the vessel in the presence of a rough bed is directed towards the quay-wall; this is an opposite direction to what has been observed for smooth bed and is a direct consequence of the change in flow behavior with rough bed, i.e., by continuity,

the flow underneath the vessel will move towards the separation point created by the upward flow.

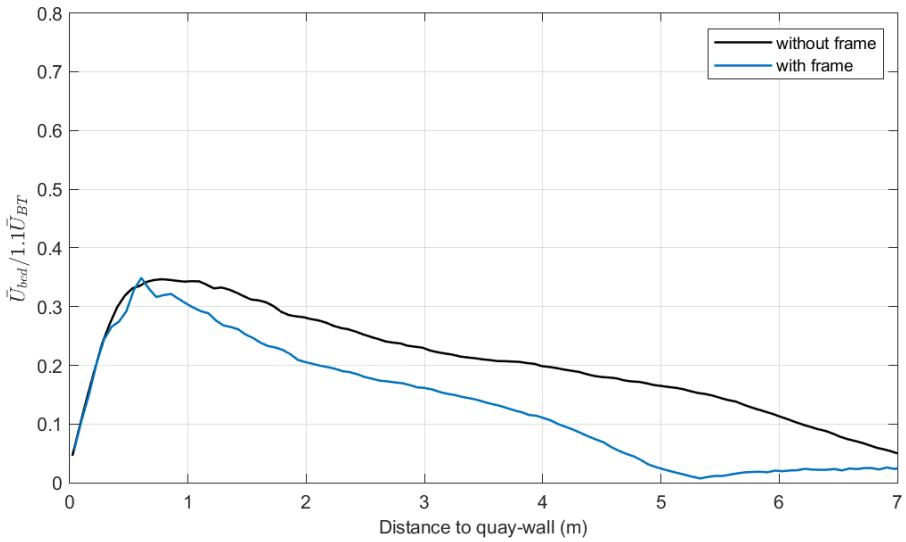

Figure 7.35 Decay of the maximum Ux velocity component (PIV) near the bed for BT2 active, with and without the measurement frame (tests 60 and 107, respectively).

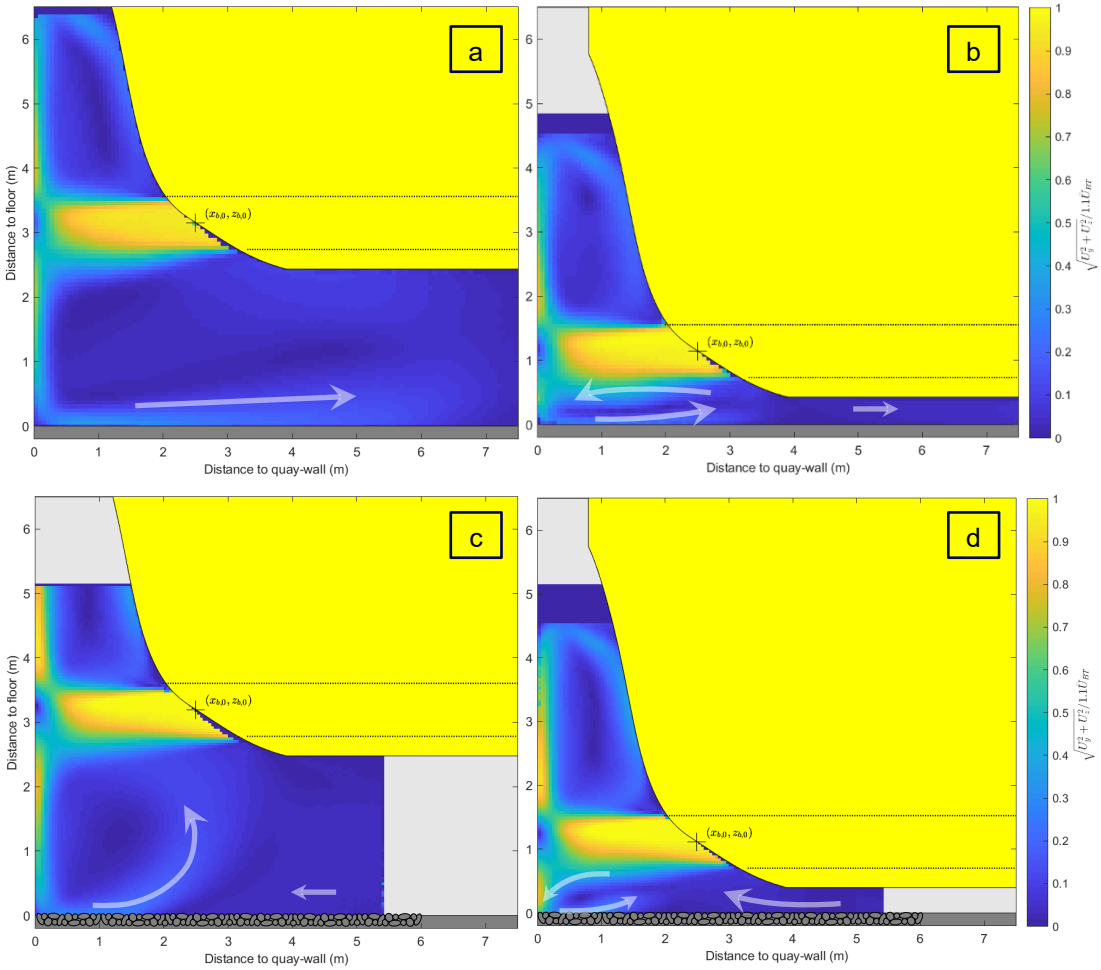

Figure 7.36 Time-averaged flow patterns in the x,z plane for Δx = 0.8m, for smooth and rough beds for different UKC for BT2. a: smooth bed, UKC 2.5m (test 107); b: smooth bed, UKC = 0.5 m (test 291); c: fixed rock, UKC = 2.5 m (test 308) and d: fixed rock, UKC = 0.5m (test 316). Map of the normalized velocity magnitude.

Regarding the magnitude of the maximum velocity near the bed, Figure 7.37 shows that in the presence of a rough bed not only the maximum measured velocities in the x-direction are lower than for smooth bed, for both UKC's tested, but also the velocity decay is quicker with a rough bed. The largest difference in the maximum velocity is observed for UKC = 0.5 m (Figure 7.37, right). The maximum normalized velocity amounts to 0.34 for UKC = 0.5 m for rough bed, whereas for a smooth bed situation almost a twice as high velocity was measured (0.63 with PIV, 0.70 with EMS's). The turbulence intensity measured for these tests show also a slight decrease in the presence of roughness, the maximum measured value being around 20% for a rough bed. For smooth bed the value could go up to 30%.

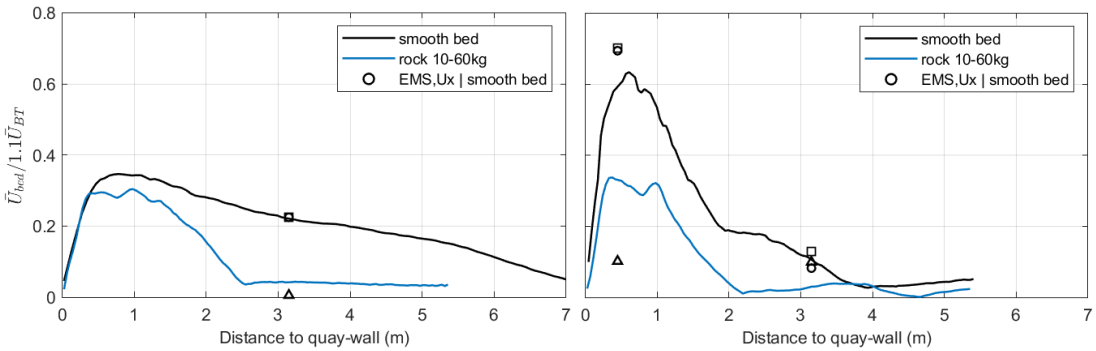

Figure 7.37 Decay of the maximum U_x velocity component (PIV) near the bed for smooth and rough bed, for different under-keel clearances: UKC = 2.5m, tests 107 and 308 (left) and UKC = 0.5m, tests 291 and 316 (right).

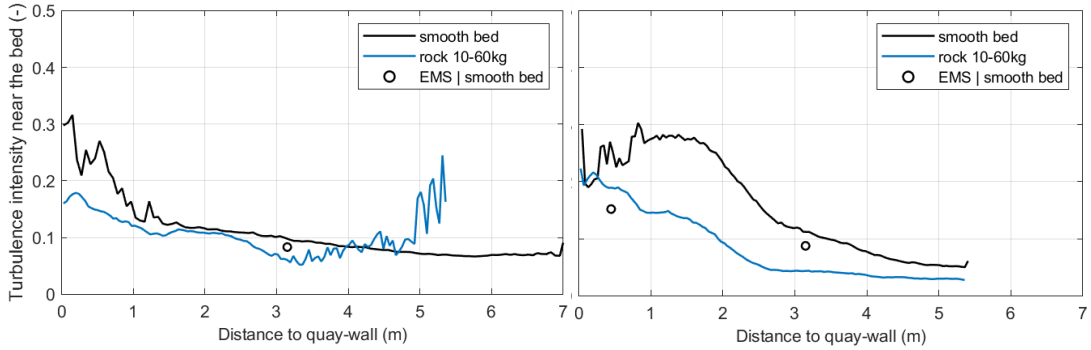

Figure 7.38 Decay of the maximum turbulence intensity (PIV, TI based on U_x and U_z components) near the bed for smooth and rough bed, for different under-keel clearances: UKC = 2.5m, tests 107 and 308 (left) and UKC = 0.5m, tests 291 and 316 (right).

Figure 7.39 illustrates the difference in flow patterns for smooth and rough beds (fixed rock, 10-60 kg), for a larger distance to the quay-wall (Δx = 3.0m), for the two extreme under-keel clearances tested: UKC = 2.5m (Figure 7.39 a,c) and UKC = 0.5m (Figure 7.39 b,d). In terms of flow patterns, the effect of the bed roughness is consistent to what was observed for a smaller quay-wall clearance. For a large UKC, there is little difference in flow patterns and in the maximum velocity near the bed (Figure 7.40, left) for different Δx. For the smallest UKC, the decay of the maximum velocity is even sharper for the larger Δx due to the interaction with the main jet; the main jet has a larger vertical spreading for this configuration.

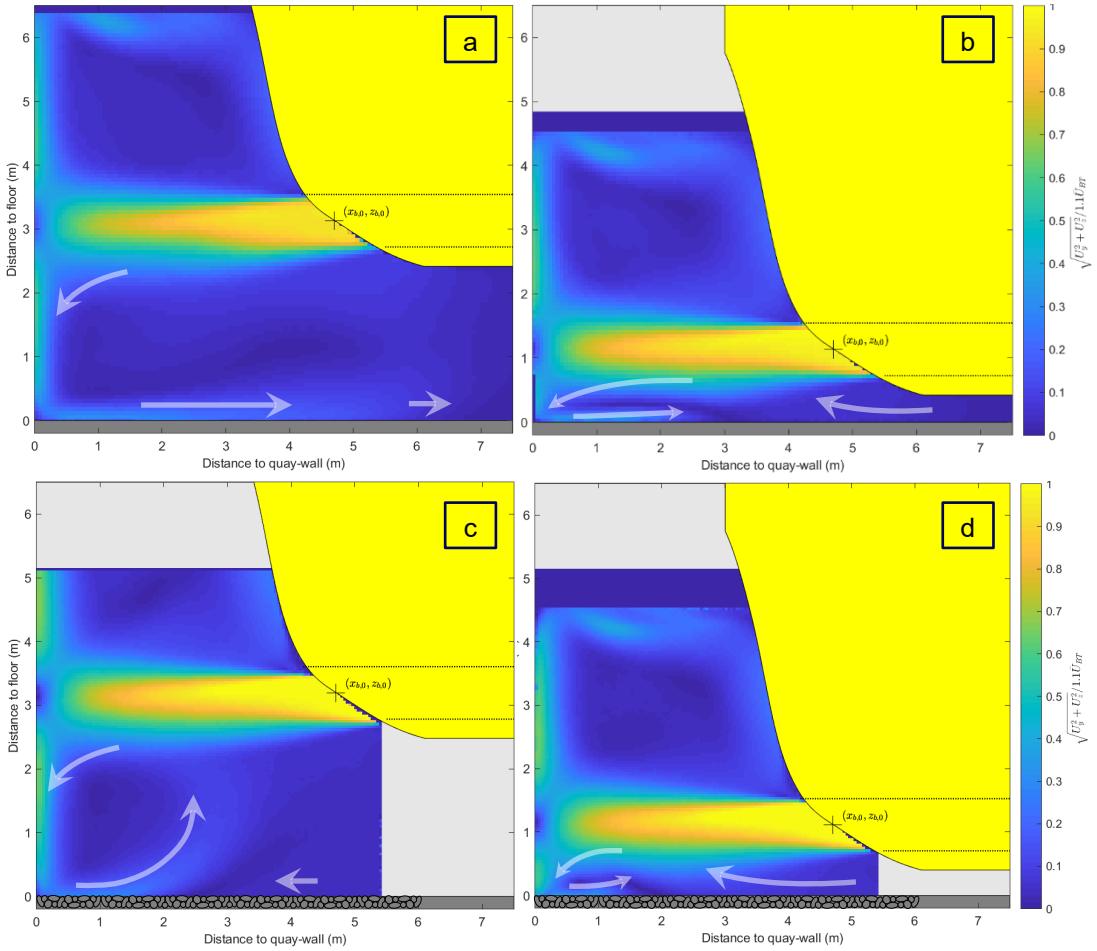

Figure 7.39 Time-averaged flow patterns in the x,z plane for Δx = 3.0m, for smooth and rough beds for different UKC for BT2. a: smooth bed, UKC = 2.5m (test 133); b: smooth bed, UKC = 0.5 m (test 142); c: fixed rock, UKC = 2.5 m (test 310) and d: fixed rock, UKC = 0.5m (test 318). Map of the normalized velocity magnitude.

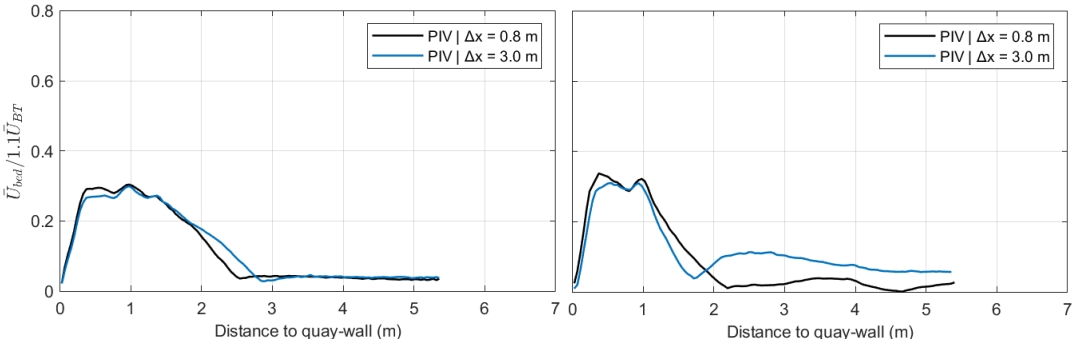

Figure 7.40 Decay of the maximum U_x velocity component (PIV) near the bed for rough bed, for varying Δx. UKC = 2.5m (tests 308 and 310, left) and UKC = 0.5m, (tests 316 and 318, right).

The circulation flow pattern observed in the plane Δy = 0m is also observed in the other measured parallel planes (Δy = 2.0m and -2.0m, see Figure 7.41). In the plane Δy = -2.0m the circulation pattern has a different shape than observed in the centerline of the jet, being more elongated, i.e., the return jet near the bed extends further towards the vessel and the upward motion is under an angle, leading to a separation point further away from the quay-wall. This results from the interaction of the rotational flow generated near the quay-wall with the

generalized flow towards the stern. In a three-dimensional view this would look like a spiraling flow towards the stern. Regarding the maximum velocity near the bed, the largest U_x values are found in the plane Δy = -2.0m (see Figure 7.42).

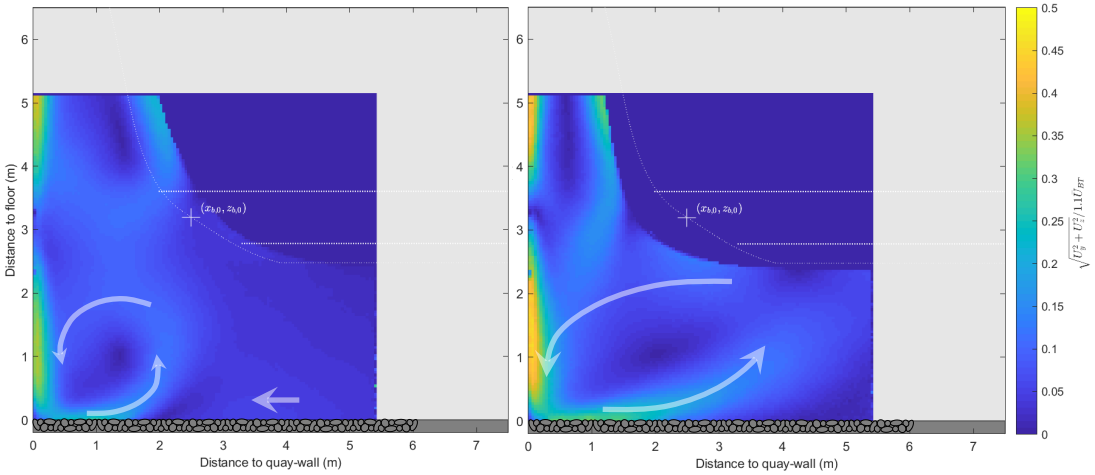

Figure 7.41 Time-averaged flow patterns in the x,z plane for rough bed (10-60kg rock), UKC = 2.5 m and Δx = 0.8 m. variation of the measurement plane (Δy). Left: Δy = 2.0m (test 303); right: Δy = -2.0m, (test 306). Map of the normalized velocity magnitude.

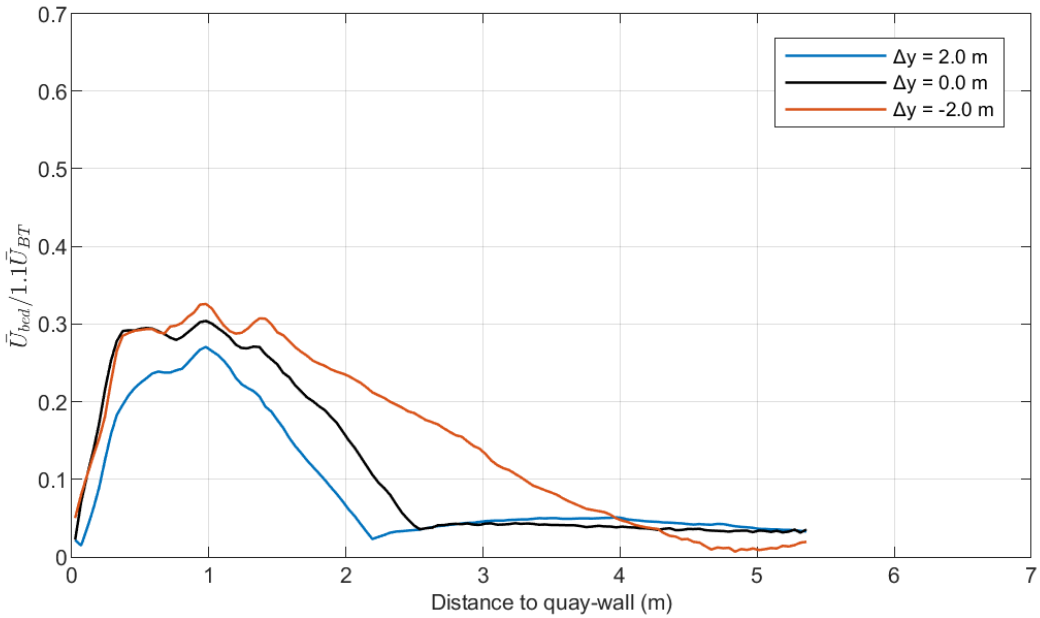

Figure 7.42 Decay of the maximum U_x velocity component (PIV) near the bed for rough bed, UKC = 2.5m, for a variation of Δy: Δy = 2.0 m (test 303), Δy = 0.0 m (test 308) and Δy = -2.0 m (test 306).

7.3 Results from deformation tests

For the tests where loose rock was used the deformation of the rock protection was assessed both qualitatively and quantitatively by using underwater cameras and stereophotography. Figure 7.43 presents the resulting deformation for the test performed with an UKC = 2.5 m. This figure shows that the largest deformation occurs very close to the quay-wall, slightly towards the stern of the vessel. The maximum measured deformation (scour) is in the order of 20 mm, m.s. (~0.3 m, p.s.) after a 30 min (m.s., representative for almost 2 hours on prototype scale) measurement in the model. Adjacent to the scour area there is accretion of rock material, deposited in a path parallel to the wall, right underneath the port side of the vessel. Based on the videos captured with the cameras it was observed that most deformation occurs during the

first 5 minutes (m.s.) of the test. Figure 7.44 shows snapshots captured before and after the test for two of the used cameras.

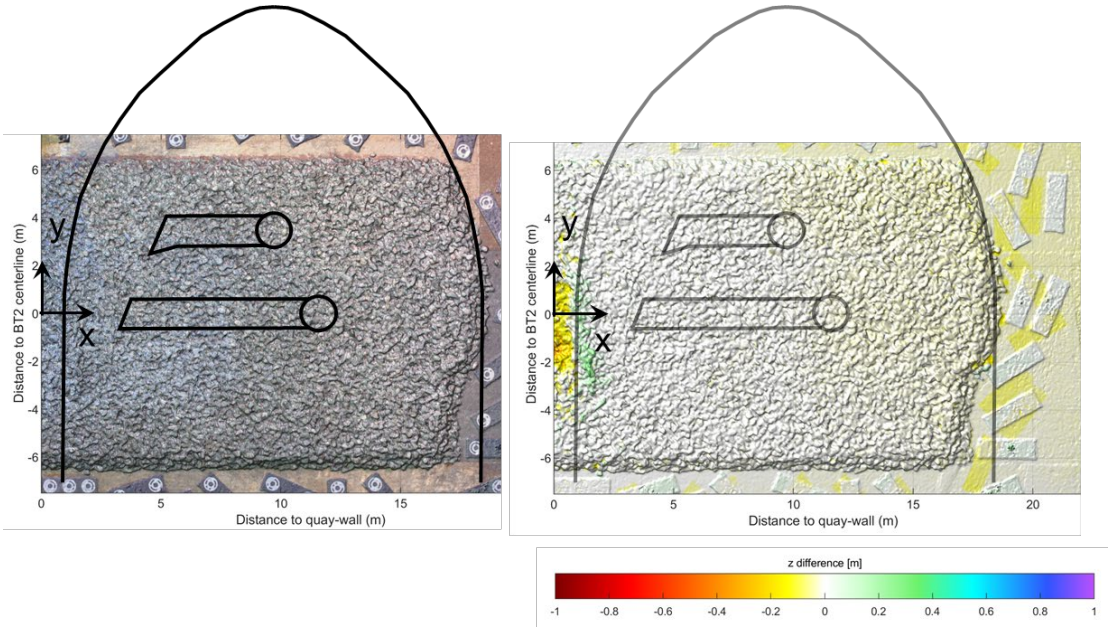

Figure 7.43 Color image at the end of the test (left) and bathymetry difference plot (right) from stereophotography measurement for the test performed with UKC = 2.5 m.

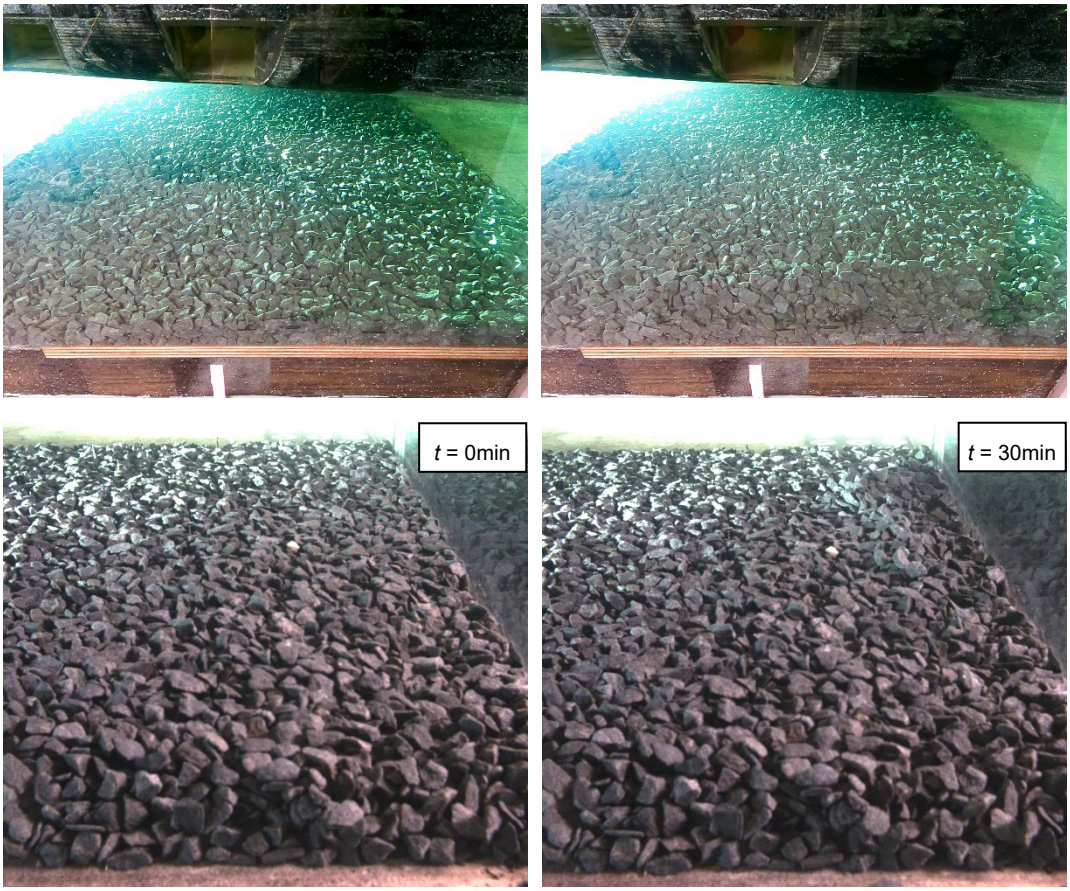

Figure 7.44 Snapshots from the GoPro (top) and Cam1 (bottom) at the start and end of the test with UKC = 2.5 m. Time in model scale.

Figure 7.45 presents the results from the stereophotography measurements for the test performed with UKC = 0.5 m. In this test the wooden bed became exposed within the first minute (m.s.) after turning on the propeller. Most of the observed deformation occurs within the first 5 minutes (m.s.) of the test. The eroded region developed over 4 m, from y = -2 m to 2 m, in a region very close to the quay-wall, roughly the same area as seen also for UKC = 2.5 m. In the first stages, scour develops earlier in a region towards the stern of the vessel; over time, it progresses also towards the bow, ending with a relatively more symmetric shape relative to the centerline of the active propeller (BT2). Figure 7.46 shows four snapshots taken with the GoPro camera illustrating the evolution of the scour hole over time. Figure 7.47 shows a photo before and after the test from the perspective of cam 1.

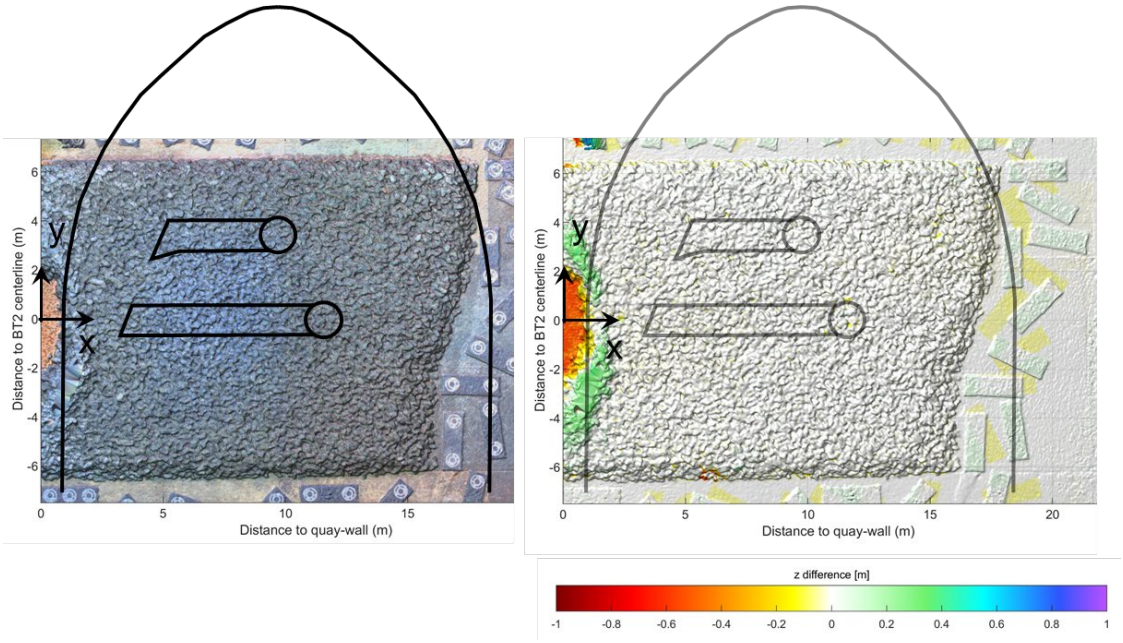

Figure 7.45 Color image at the end of the test (left) and bathymetry difference plot (right) from stereophotography measurement for the test performed with UKC = 0.5m.

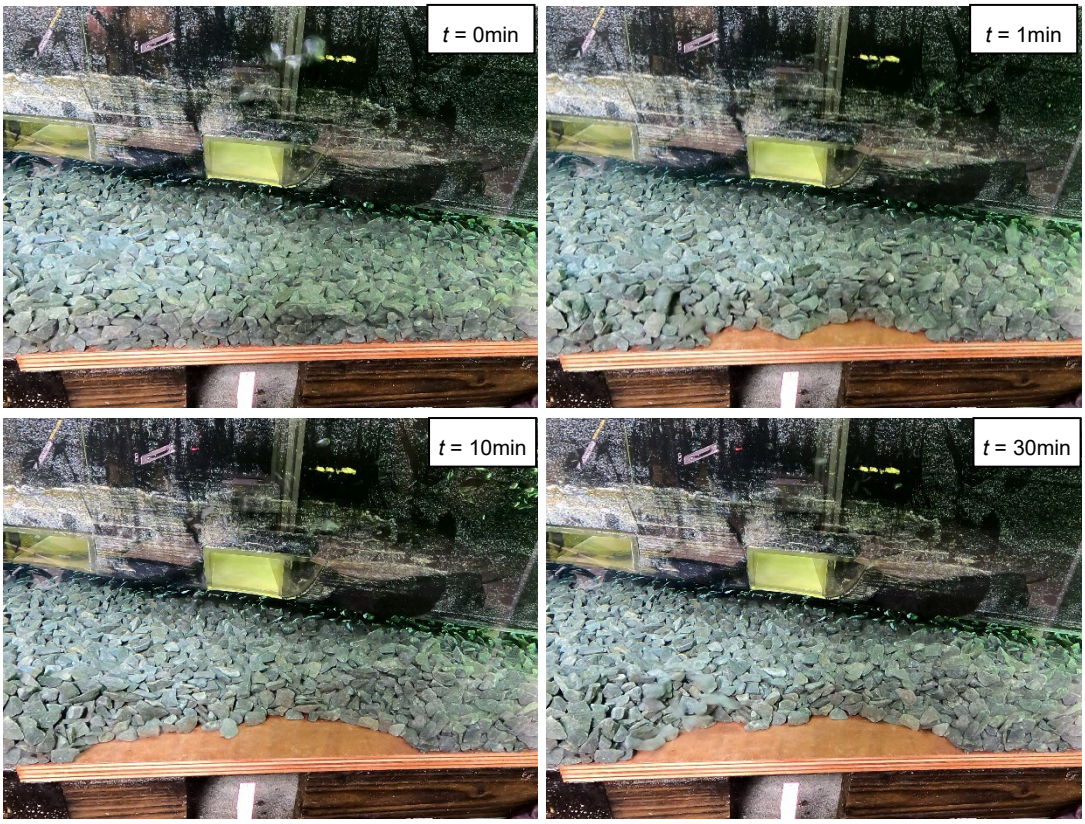

Figure 7.46 Snapshots from the GoPro at four instants of the with UKC = 0.5 m. Time in model scale.

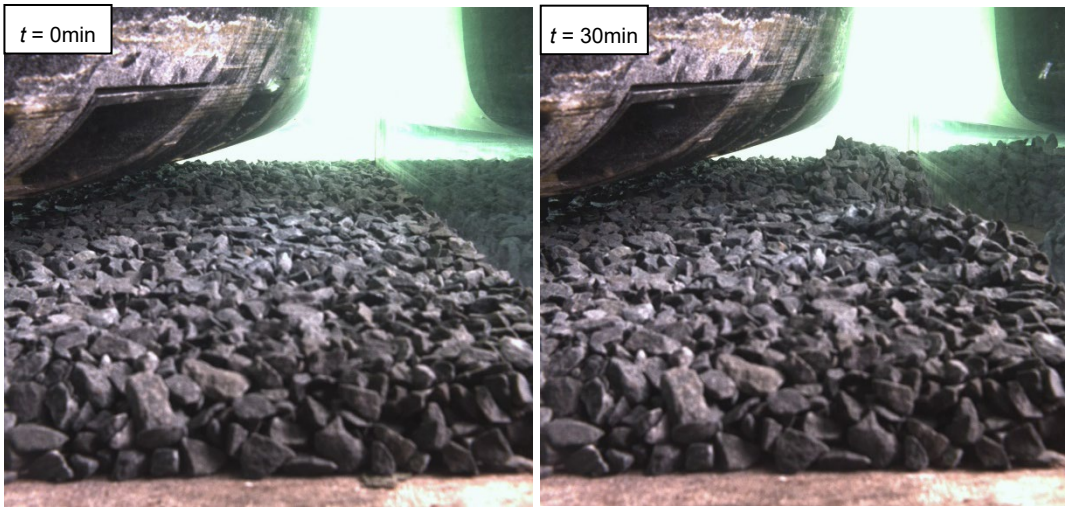

Figure 7.47 Snapshots from Cam1 at the start and end of the test with UKC = 0.5 m. Time in model scale.

8 Comparison with guidelines

In this chapter the results from the tests are compared with the Dutch and German formulations presented in the literature (ref. [4]). The updated version of the German formulations which will be included in a new version of the PIANC guidelines (update of [4], currently in print. Information based on personal communication with Henk Verheij, co-chairman of the corresponding PIANC working group) is here used and is described below.

Dutch method - maximum flow velocity near the bed

$$U_{b,max} = 1.0 U_0 \frac{D_t}{h_{BT}} \quad \text{for} \quad 1.0 < \frac{L_{BT}+x_b}{h_{BT}} < 1.8$$

$$U_{b,max} = 2.8 U_0 \frac{D_t}{L_{BT}+h_{BT}+x_b} \quad \text{for} \quad \frac{L_{BT}+x_b}{h_{BT}} \geq 1.8$$

In the above expressions, $U_{b,max}$ is the maximum horizontal velocity near the bed, U_0 is the efflux velocity, D_t the diameter of the thruster, h_{BT} the height of the thruster axis above the bed, L_{BT} is the quay-wall clearance measured from the outlet of the bow thruster channel and x_b the distance from the quay-wall in the x-direction.

In this formulation we use the following:

- D_t = 1.3 m (inlet diameter of the thruster, see section 2.3)
- h_{BT} = UKC + 0.715 m (mid height bow thruster channel plus hull thickness underneath vessel)
- L_{BT} = Δx + 2.89 m (distance in x-direction from the quay-wall to mid height bow thruster BT1 at the outlet, see section 5.1)
- L_{BT} = Δx + 1.84 m (distance in x-direction from the quay-wall to mid height bow thruster BT2 at the outlet, see section 5.1)

German method - maximum flow velocity near the bed

$$U_{axis,wall} = U_0 \quad \text{for} \quad \frac{L_{BT}}{D_t} < 1.9$$

$$U_{axis,wall} = 1.9 \cdot U_0 \left(\frac{L_{BT}}{D_t}\right)^{-1.0} \quad \text{for} \quad \frac{L_{BT}}{D_t} > 1.9$$

$$U_{b,max} = U_{axis,wall} \cdot min\left\{a_L \left(\frac{h_{BT}}{D_t}\right)^{-1.15}, 1\right\} \quad \text{with} \quad a_L = 10.6 \left(\frac{L_{BT}}{D_t}\right)^{-1.0}$$

In the above expression $U_{axis,wall}$ is the velocity in the thruster axis at the position of the quay-wall. The German method gives with $U_{b,max}$ an indication of the U_x velocity at the at the point of intersection of the quay-wall and the bed (x_b = 0).[1]

In the figures below it should be noted that Dutch guidelines provide an estimation for the maximum horizontal velocity (x and y components combined), whereas in the PIV

[1] BAW, 2010, [6], also provides an expression for the decay of the bed velocity away from the quay wall, specifically: $U_{b,max,x} = U_{b,max} * ((L+h_{BT})/(L+h_{BT}+x_b))^{1.62}$. It should be noted that, following BAW,2010, $U_{b,max}$ in that expression should be based on the above Dutch method evaluated at x_b=0 m. As the decay expression of BAW, 2010 was not yet included in [4], the scale model measurement results are not compared to this expression in the present version of this report. It is foreseen that this will be done at a later stage when results will be published in a paper.

measurements only one horizontal component was measured (U_x). For this reason, in Appendix B also the results from the EMS sensors are presented since they measure both U_x and U_y components. The figures below summarize the comparison between the tests and the guidelines.

In most cases, for small quay-wall clearance, German method gives larger values than the Dutch method.

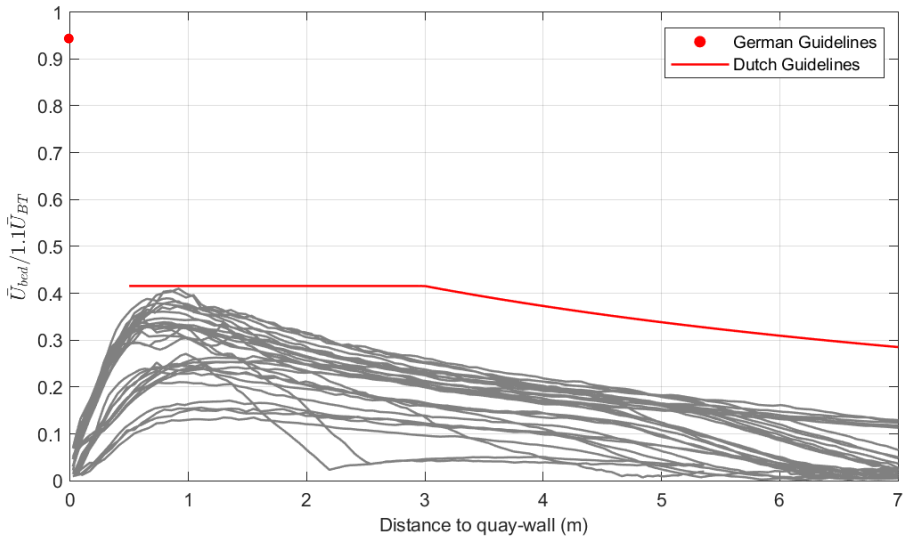

Figure 8.1 Decay of maximum velocity measured near the bed with PIV (U_x) and comparison with guidelines (U_b). Tests performed with BT2 active, Δx = 0.8 m and UKC = 2.5 m, all remaining parameters variable.

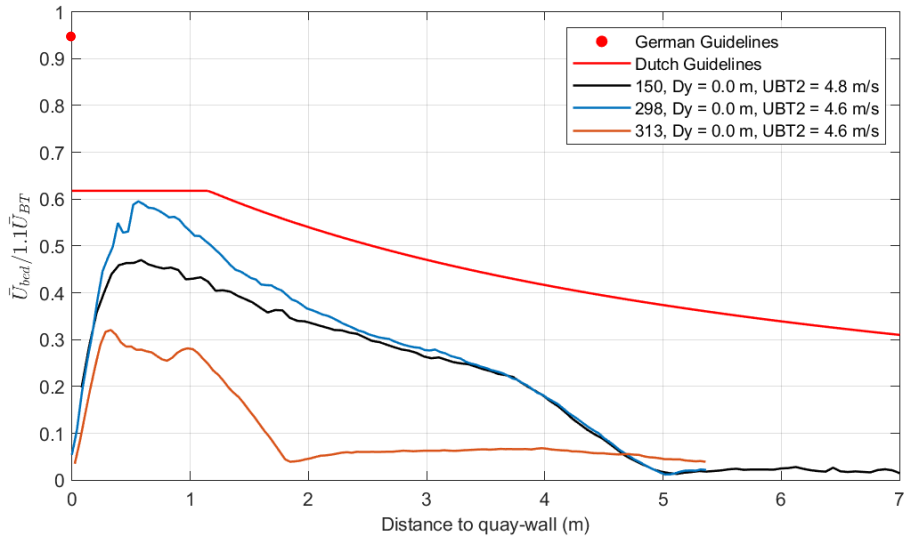

Figure 8.2 Decay of maximum velocity measured near the bed with PIV (U_x) and comparison with guidelines (U_b). Tests performed with BT2 active, Δx = 0.8 m and UKC = 1.5 m, all remaining parameters variable.

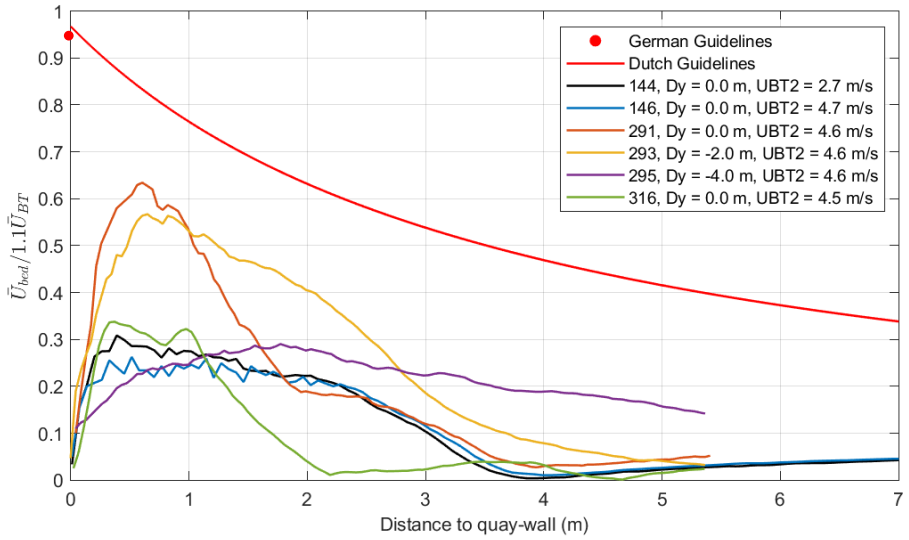

Figure 8.3 Decay of maximum velocity measured near the bed with PIV (U_x) and comparison with guidelines (U_b). Tests performed with BT2 active, Δx = 0.8 m and UKC = 0.5 m, all remaining parameters variable.

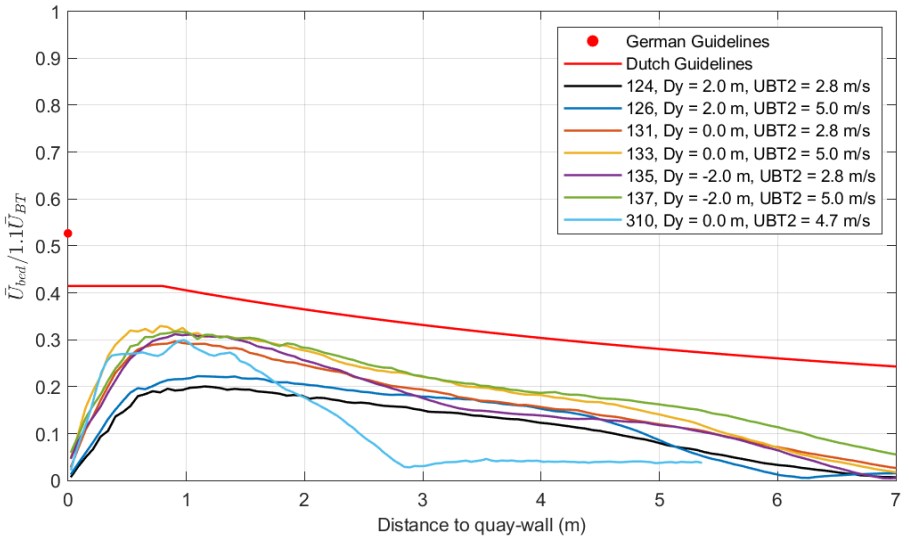

Figure 8.4 Decay of maximum velocity measured near the bed with PIV (U_x) and comparison with guidelines (U_b). Tests performed with BT2 active, Δx = 3.0 m and UKC = 2.5 m, all remaining parameters variable.

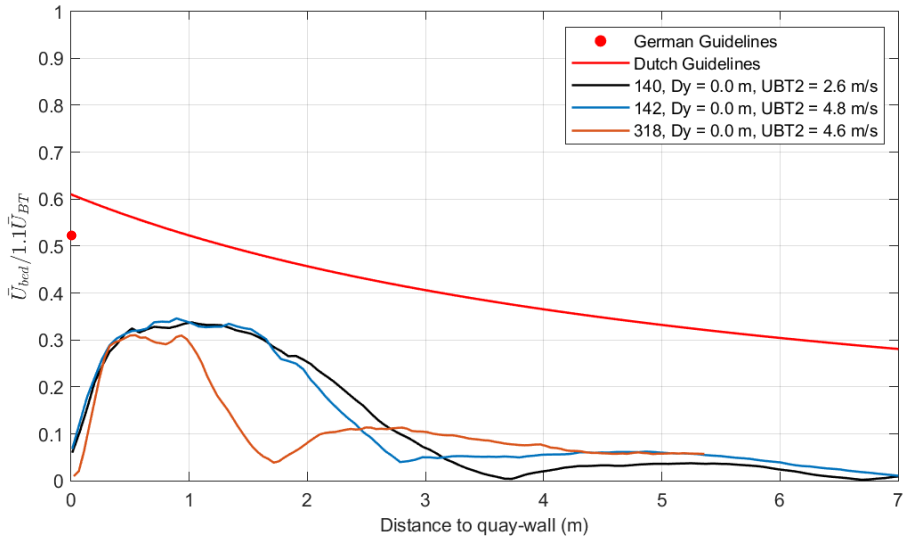

Figure 8.5 Decay of maximum velocity measured near the bed with PIV (U_x) and comparison with guidelines (U_b). Tests performed with BT2 active, Δx = 3.0 m and UKC = 0.5 m, all remaining parameters variable.

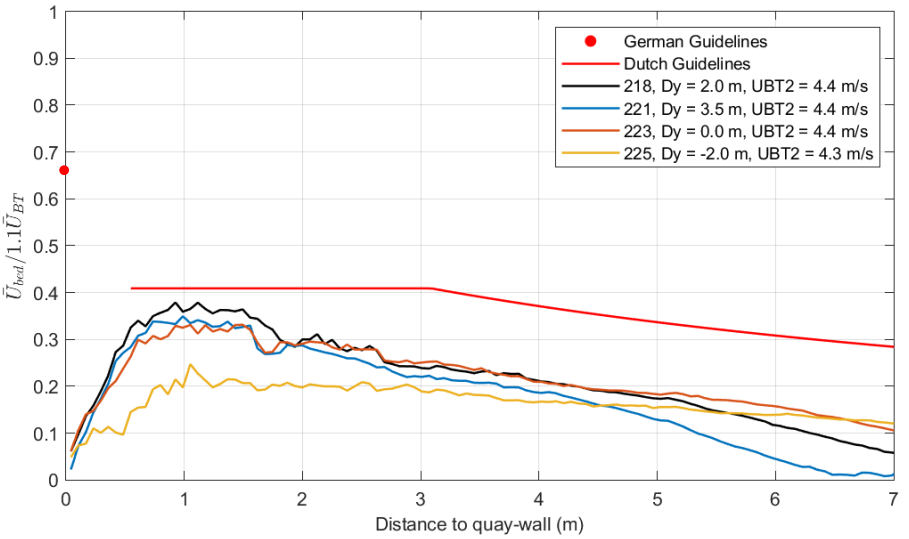

Figure 8.6 Decay of maximum velocity measured near the bed with PIV (U_x) and comparison with guidelines (U_b). Tests performed with BT1 active, Δx = 0.8 m and UKC = 2.5 m, all remaining parameters variable.

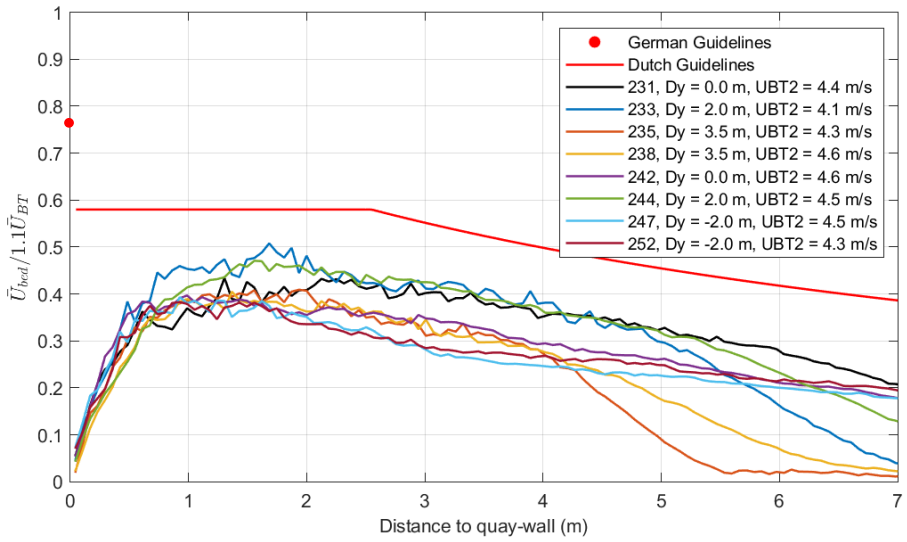

Figure 8.7 Decay of maximum velocity measured near the bed with PIV (U_x) and comparison with guidelines (U_b). Tests performed with BT1 and BT2 active, Δx = 0.8 m and UKC = 2.5 m, all remaining parameters variable.

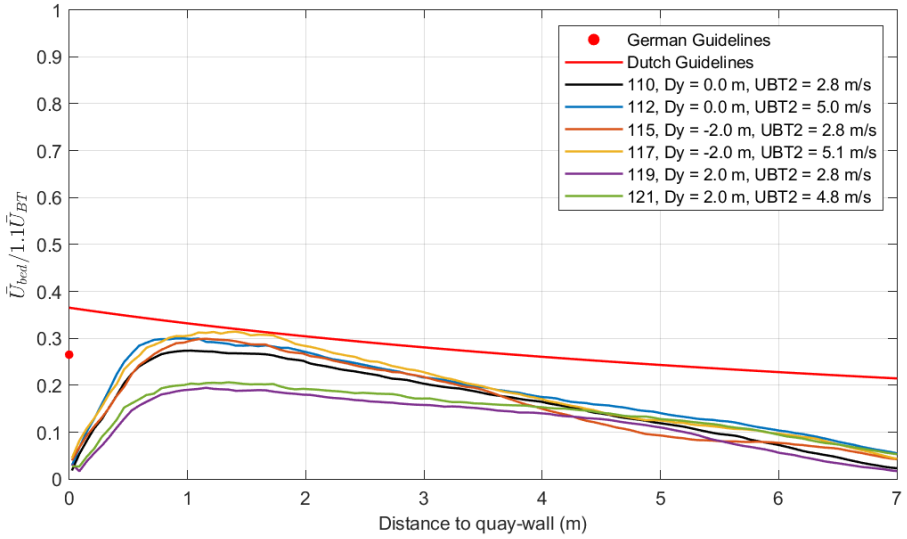

Figure 8.8 Decay of maximum velocity measured near the bed with PIV (U_x) and comparison with guidelines (U_b). Tests performed with BT2 active, Δx = 5.0 m and UKC = 2.5 m, all remaining parameters variable.

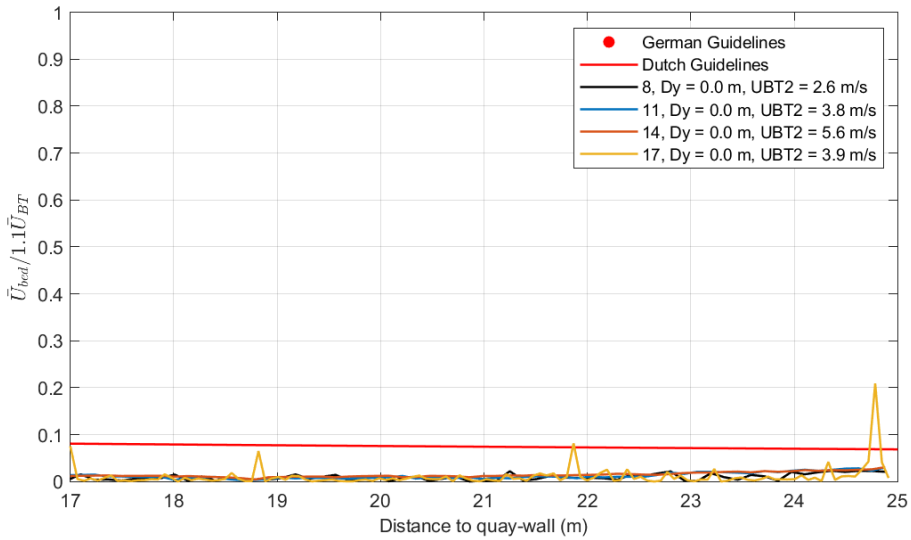

Figure 8.9 Decay of maximum velocity measured near the bed with PIV (U_x) and comparison with guidelines (U_b). Tests performed with BT2 active, Δx = 23 m and UKC = 2.5 m, all remaining parameters variable.

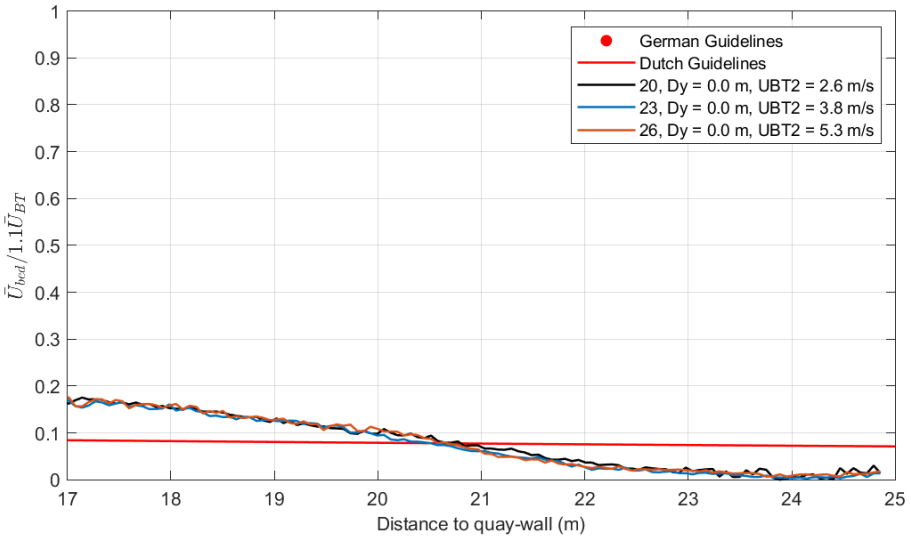

Figure 8.10 Decay of maximum velocity measured near the bed with PIV (U_x) and comparison with guidelines (U_b). Tests performed with BT2 active, Δx = 23 m and UKC = 0.5 m, all remaining parameters variable.

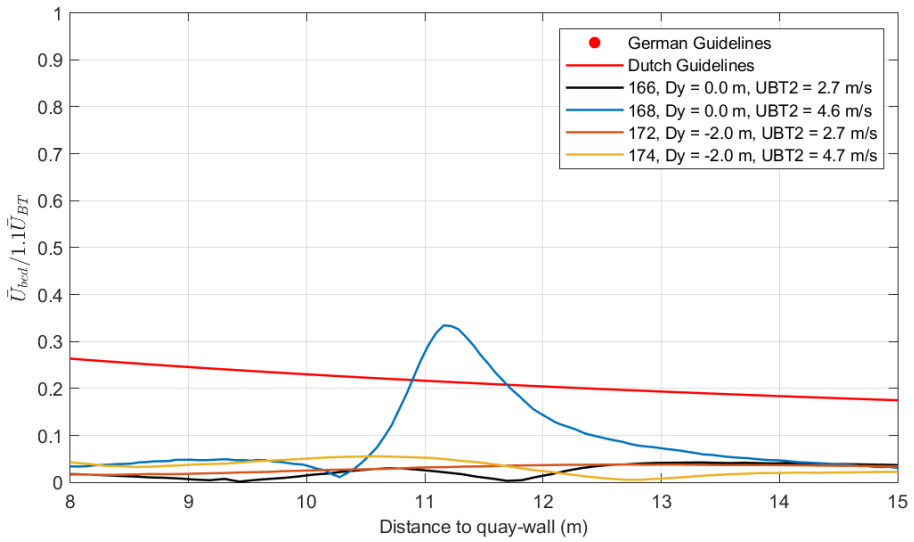

Figure 8.11 Decay of maximum velocity measured near the bed with PIV (U_x) and comparison with guidelines (U_b). Tests performed with BT2 active, Δx = 0.8 m and UKC = 2.5 m (FOV2), all remaining parameters variable.

This global comparison shown above seems to suggest that the Dutch formulations are more appropriate to estimate maximum near bed velocities and have a wider application range than the German method. Considering the large number of variations included in the comparisons above, it is possible to draw some general conclusions. The Dutch formulations in the design guidelines [4] tend to predict the maximum near-bed flow magnitude fairly well. In most cases the guidelines are slightly conservatively - which is actually desirable -, with exception of underneath the vessel, near the inlet. The decay of the near-bed flow velocity farther away from the quay wall seems to be predicted too conservatively by the design guidelines in most cases, i.e., the measured velocities decay faster than predicted.

These observations suggest that for these type of bow thrusters the extent of bed protections could be optimized. Near the quay wall (say within the first 5 m) the present design guidelines perform well, but farther away from the quay wall lighter or less bed protection may be adequate. At a later stage, we foresee to formulate recommendations for improvement of the current design guidelines based on this extensive model dataset.

9 Comparison with field measurements

As mentioned in Section 5.2, an one-to-one comparison between the scale model tests and the field measurements in Ghent [1] is not straightforward. Within the TKI-SOP research project, a comparison was made by an intern working at DEME (Maxence Jordan). His results were presented to and shared with the CROW propeller jet working group.

For the ease of further future analysis Table 9.1 shows corresponding field and scale model tests.

Table 9.1 Overview of the tests performed in the field [1] (Test ID in first column) and their corresponding tests performed within the present scale model research (Test ID in last column).

ID test field measurement	Subtest	Active thruster	Vessel position	Δx (m)	Δy (m)	UKC (m)	Power load	Test ID scale model
2	a	2	1	0.8	0.0	2.5	low	PIVSOP105
2	b	2	1	0.8	0.0	2.5	medium	PIVSOP055
2	c	2	1	0.8	0.0	2.5	high	PIVSOP107 PIVSOP300
3	c	1	1	0.8	0.0	2.5	high	PIVSOP223
4	c	1&2	1	0.8	0.0	2.5	high	PIVSOP231
5	a	2	2	0.8	2.0	2.5	low	PIVSOP063
5	b	2	2	0.8	2.0	2.5	medium	PIVSOP065
5	c	2	2	0.8	2.0	2.5	high	PIVSOP099
9	c	1	2	0.8	2.0	2.5	high	PIVSOP218
10	b	1&2	2	0.8	2.0	2.5	medium	PIVSOP233
12	c	1	4	0.8	3.5	2.5	high	PIVSOP221
13	a	2	4	0.8	3.5	2.5	low	PIVSOP070
13	b	2	4	0.8	3.5	2.5	high	PIVSOP102
14	c	1&2	4	0.8	3.5	2.5	high	PIVSOP235
15	a	2	3	0.8	-2.0	2.5	low	PIVSOP077 PIVSOP079
15	b	2	3	0.8	-2.0	2.5	high	PIVSOP096
16	c	1&2	3	0.8	-2.0	2.5	high	PIVSOP252
17	b	1&2	6	0.8	1.75	2.5	high	PIVSOP233
18	b	1&2	7	3	1.75	2.5	high	PIVSOP254
19	a	2	7	3	1.75	2.5	medum	PIVSOP124
19	b	2	7	3	1.75	2.5	high	PIVSOP126

It should be noted that the *Power load* in the 8th column of Table 9.1 is only an indication for the relative propeller power used within that test group. Since the produced thruster outflow velocity in the scale model (converted to prototype scale) is lower than obtained in the field

tests[2] , high-, medium- or low-power load conditions will not automatically lead to similar absolute magnitudes of the efflux velocity when comparing field and scale model conditions.

For example, in the “high” power load reference scale model test condition PIVSOP107, an efflux velocity U_0=1.1U_{BT}= 5.3 m/s is obtained. If this is compared to field test 2c, in which also a “high” power load (i.e.: 90%) was applied, there an efflux velocity of 8.03 m/s was assumed (see [1]). In field test 2a however, in which a low power load (25%) was applied, an efflux velocity of 5.08 m/s was expected, which is much more comparable to the PIVSOP107 condition.

So, for comparing absolute flow velocities, a comparison between low-power field test conditions and high-power scale model conditions seems most appropriate. The grouping as presented in Table 9.1 should therefore only be used for relative comparisons.

[2] See also Section 3.5. In the scale model, a less efficient propeller was selected based on practical considerations. This leads to a lower efflux velocity for a given propeller rotation rate and/or applied engine power, than compared to the actual bow-thruster that was used in the field tests.

10 Conclusions and recommendations

In order to optimize design guidelines for bed protections it was desired to better understand the flow generated by a transversal bow thruster that is reflected off a vertical quay wall. To this end, highly detailed velocity measurements have been carried out in a physical scale model. The objective of the measurements is to improve design guidelines of bed protections in order to reduce uncertainties and potentially save materials and reduce costs during construction of bed protections. Furthermore, the measurement data is aimed to serve as benchmark validation data for numerical models, thereby enhancing the possibilities for applying these models in detailed bed protection designs in the future.

The present report summarizes physical scale model tests performed to visualize and characterize the flow field generated by a bow thruster. In these measurements, the transverse flow induced by a 4-channel bow thruster of an inland vessel has been measured. Several systematic variations have been performed to gain better understanding of the most important parameters for design of bed protections. The variations considered in the present research include:

- Quay wall clearance
- Under keel clearance
- Applied propeller power
- Use of multiple propellers
- Influence of bed roughness
- Fixed or mobile bed

10.1 Conclusions

The dataset that has been obtained within this research project is extensive and characterizes flow induced by a transverse bow thruster in very high detail. Summarizing the main findings of the measurements, the following results have been found:

- **Flow distributio**n:
  The location of the maximum flow velocity is found in a plane approximately 2 m aft of the bow thruster outlet; this was confirmed by the field measurements. It is likely that the geometrical asymmetry of the bow channel outlet plays a major role in the flow distribution.

- **Underkeel and wall clearance:**
  A low UKC gives the higher velocities near the quay wall than high UKC values, but for low UKC values the near bed flow velocity reduces faster farther away from the quay wall. Regarding quay-wall clearance, the maximum flow velocities near the bed also occur for the smallest clearances.

- **Variation in RPM:**
  The efflux velocity increases with increasing applied propeller power of the bow thruster as expected. The influence of the rotational speed of the thruster on the spatial flow patterns is generally limited.

- **Multiple propellers:**
  According to the design guidelines [4] it is expected that, compared to a single propeller, the maximum near bed flow velocity increases by a factor $\sqrt{2} \approx 1.41$ when

two propellers are active simultaneously. The test results indeed confirm this trend, although the velocity increase is generally slightly smaller. Also, the influence of the rotation direction of the thrusters has been investigated, but its effect is small.

- **Bed roughness:**
  The largest near-bed flow velocities are observed for smooth beds. Bed roughness leads to overall lower flow velocities near the bed and an even sharper velocity decay away from the quay-wall.

  Bed roughness changes the flow pattern of the reflected jet: For a smooth bed the return jet is mainly horizontal. Above a bed protection with larger roughness the return jet towards the vessel is diverted more upwards; measurements for a rough bed showed a clear recirculation pattern in a confined area near the quay-wall; this is also visible in the deformation test videos (rocks recirculating near the window).

- **Bed deformation:**
  Deformation tests have been performed on a schematized bed protection with loose rocks to show initiation of bed deformation.

- **Design guidelines:**
  The Dutch method as defined in present design guidelines (ref. [4]) predicts the magnitude of max horizontal velocity near the bed well for most tested situations. The difference between measurements and the German method (ref. [4]) is larger.
  - Near the quay wall the Dutch method provides a good prediction of the maximum near bed flow velocity, being generally slightly conservative (but not being overly conservative);
  - The overall measured velocity decreases faster away from the quay-wall than predicted by the Dutch method;
  - When the vessel is very far away from the quay-wall (e.g. 23 m), for a low UKC the measured velocities are higher than predicted. This is observed with one propeller, see Figure 8.10, and using the formulas for a reflected jet the difference between measurements and guidelines is even larger with two propellers (test 275, Fig I). In this situation the results should better be compared to the formulations for a free propeller jet (see [4], Eq. 8.36) instead of for a reflected jet;
  - Present design guidelines do not provide a description of the flow right below the inlet suction point of the 4-channel type bow-thruster. Alternative formulas/literature should be used to estimate this effect.

- **Measurement technique:**
  The applied measurement technique (Particle Image Velocimetry, PIV) provides a lot of information about the spatial distribution of the flow. Such information proved to be very useful for interpretation of field measurement results. It also forms a solid basis for comparison to numerical simulations. Furthermore, such spatial information on flow patterns was indispensable for understanding the trends of near-bed flow velocities found under different conditions;

  Some attention points on the applied measurement technique that should be considered:
  - PIV only measured one horizontal velocity component (u or v) and guidelines (Dutch formulation) consider two horizontal components (u and v, together providing the horizontal velocity magnitude). Independent velocity measurements using an EMS-sensor show that v-component is usually much lower than u-component, but not always negligible (especially in planes away from the jet

centreline, e.g. see tests 293, 295 Fig I). It is not expected that this aspect will change the main findings of the research;

- Accurate turbulence intensities are difficult to measure with low-resolution PIV. In some tests it showed to be problematic to measure accurately near the bed (e.g.: not enough seeding present) and then found turbulence intensity values can become unrealistically high. In several tests this has been checked by repeating the measurements with a higher PIV resolution. Where necessary, a warning has been given within the present report to carefully interpret the presented results.

10.2 Recommendations

The following recommendations for follow-up work are suggested:

- The measurement results seem to suggest that the near bed velocity decay is generally faster than predicted by the Dutch design guidelines. Based on the extensive measurement dataset it is expected that it will be possible to derive a more suitable decay line, potentially leading to material savings in the design of bed protections. This analysis task is planned to be executed in in the near future;

- Exploratory deformation tests have been performed. It is recommended to do follow-up deformation tests using a more realistic schematization of a bed protection with sand underneath (scour tests) to see the evolution of the scour hole over time;

- In the physical scale model test global loads on the vessel have been measured. Also during the field measurements described in [1], mooring loads have been measured. These measurements should be further explored, and it could be investigated whether such load measurements can provide reliable estimates of propeller outflow velocity, providing a relatively easy measurement alternative to direct flow measurements in the field;

- It is recommended to verify the findings of the present research in the field by performing a pilot in which it is tested if a bed protection with a limited width remains stable under normal operation conditions. In these field tests also the relation between applied propeller power and efflux velocity U_0 should be verified.

11 References

[1] Tukker, J.W.T. (2021) Decay of bow thruster induced near-bed flow velocities at a vertical quay wall. Master Thesis, Technical University of Delft.

[2] Blaaw HG and van de Kaa EJ (1978) Erosion of bottom and sloping banks caused by the screw race of maneuvering ships. Delft Hydraulics Laboratory, Delft, the Netherlands, publication number 202.

[3] Raaijmakers, T.C., Liefhebber, F., Hofland., B., Meys, P. (2012), Mapping of 3D-bathymetries and structures using stereophotography through an air-water-interface, Proceedings Coastlab12, 2012, Ghent, Belgium.

[4] PIANC report 180 (2015). Guidelines for protecting berthing structures from scour caused by ships. ISBN 978-2-87223-223-9.

[5] Bakker W (2021) PIV measurement of the Calibration of a flush EMS, Research Report (internal report), Deltares, Delft.

[6] BAW, 2010, Principles for the Design of Bank and Bottom Protection for Inland Waterways (GBB), Code of Practice, Karlsruhe · March 2011 · ISSN 2192-9807

[7] MARIN, 2023, CFD calculations on channel type bow thrusters, 33178-2-MO, February 22, 2023, version 0.1 (Draft report).

A Tables with results

In the tables below the “PIVSOP” prefix is omitted in the test ID for simplification purposes. All tests were performed with BT2 active and with a channel wall (wooden wall) placed in the basin, except when otherwise indicated.

A.1 Initial test series

Table A1 - Results of the tests performed for field of view 1 (FOV1).

Test ID	Δx (m)	Δy (m)	UKC (m)	UBT (m/s)	PIV				EMS-1 (m/s)	EMS-2 (m/s)	EMS-3 (m/s)	F1x (kN)	Fx_{total} (kN)	RPM (-)	Note
					Ux,max jet (m/s)	Ux,max bed (m/s)	Ux,max / 1.1 UBT (-)	TI max bed (-)							
029	0.8	0.0	2.4	2.6	2.74	0.91	0.32	0.26	0.59	0.47	0.03	0.5	0.0	451	No wall*
052				2.6	2.80	0.98	0.34	0.33	0.63			2.4	1.5	450	Rep 029
105				2.6	2.63	0.95	0.33	0.15	0.57	0.42		1.5	1.6	445	Rep 029,052
032				3.9	4.17	1.44	0.34	0.38	1.06			6.4	5.8	618	
040				3.7	5.15	1.74	0.33	0.29		0.65	0.04	4.1	3.0	648	Rep 032
055				3.8	4.15	1.50	0.36	0.30	0.96			5.7	3.8	648	Rep 032, 040
037				4.7	4.10	1.35	0.33	0.35		0.79	0.05	6.8	4.9	804	No wall
057				4.8	5.22	2.00	0.38	0.21	1.29	0.79	0.03	8.2	6.8	798	Rep 037
107				4.8	4.96	1.82	0.35	0.32	1.18	0.74		7.9	7.1	800	Rep 037,057
060				4.9	5.31	1.88	0.35	0.51				12.2	10.3	760	w/ ladder
150			1.4	4.8	5.21	2.46	0.47	0.51	1.22	0.35		5.8	3.0	770	
162			1.0	4.8	5.20	2.32	0.44	0.48	1.40	0.52		2.8	-2.0	777	
144			0.4	2.7	2.82	0.90	0.31	0.43	0.37	0.34		0.1	0.9	428	
146				4.7	5.19	1.36	0.26	0.87	0.72	0.58		2.9	1.8	760	
070		3.5	2.4	2.8		0.41	0.13	0.36	0.29			1.4	1.5	428	
072				3.7		0.62	0.15	0.36	0.51			4.5	3.6	649	
074				4.6		0.79	0.16	0.38	0.67			6.6	5.4	825	
102				4.7		0.89	0.17	0.15	0.70	0.27		7.4	8.3	801	Rep 074
063		2.0	2.4	2.7		0.64	0.21	0.40	0.39	0.15	0.03	2.5	0.7	436	
065				3.8		0.97	0.23	0.37	0.65	0.29	0.03	2.5	0.3	646	
067				4.9		1.37	0.25	0.39	0.90			9.2	8.0	760	
099				4.7		1.29	0.25	0.25	0.85	0.37		8.8	9.3	802	Rep 067
077		-2.0	2.5	2.6		1.10	0.38	0.30	0.68			2.3	2.2	452	
079				3.7		1.68	0.41	0.32	1.04			5.4	4.7	650	
082				4.7		2.08	0.41	0.35	1.37			7.2	8.2	801	
096				4.8		1.95	0.37	0.42	1.36	0.54		8.7	8.8	797	Rep 082
085		-4.0	2.5	2.5		0.67	0.24	0.12	0.65			1.6	1.5	462	
091				2.6		0.71	0.25	0.10	0.69	0.21	0.03	1.4	1.7	446	Rep 085
087				3.6		1.03	0.26	0.16	1.01			2.9	3.7	675	
093				4.7		1.37	0.27	0.19	1.36	0.47	0.05	8.3	7.3	795	
131	3.0	0.0	2.4	2.8	2.86	0.91	0.30	0.17	0.57	0.04		4.4	4.4	423	
133				5.0	5.43	1.81	0.33	0.44	1.19	0.13		13.4	14.4	771	
154			1.4	4.8	5.29	2.09	0.39	0.29	1.38	0.17		11.9	11.2	774	
158			0.9	4.8	5.28	2.02	0.38	0.37	1.32	0.14		12.1	11.2	766	
140			0.4	2.6	2.80	0.98	0.34	0.27	0.11	0.16		2.4	3.4	437	
142				4.8	5.20	1.81	0.35	0.27	0.21	0.27		11.2	11.7	778	
124	3.0	2.0	2.4	2.8		0.61	0.20	0.39	0.47	0.02		3.7	4.3	425	
126				5.0		1.23	0.22	0.34	1.04	0.11		13.3	14.8	765	
135		-2.0	2.5	2.8		0.95	0.31	0.15	0.50	0.04		3.5	4.3	423	
137				5.0		1.76	0.32	0.34	1.25	0.07		12.9	14.8	761	

*channel wall installed just before test 052

Data not available Sensor not working

Table A1 (continuation) - Results of the tests performed for field of view 1 (FOV1).

Test ID	Δx (m)	Δy (m)	UKC (m)	UBT (m/s)	PIV				EMS-1 (m/s)	EMS-2 (m/s)	EMS-3 (m/s)	F1x (kN)	Fx_{total} (kN)	RPM	Note
					Ux,max jet (m/s)	Ux,max bed (m/s)	Ux,max / 1.1 UBT (-)	TI max bed (-)							
110	5.0	0.0	2.4	2.8	2.83	0.84	0.27	0.14	0.61	0.04		4.6	5.3	425	
112				5.0	5.19	1.65	0.30	0.15	1.19	0.07		15.3	18.4	753	
119		2.0		2.8		0.60	0.19	0.10	0.53	0.03		4.2	5.4	423	
121				4.8		1.08	0.21	0.20	1.00	0.04		14.1	16.8	791	
115		-2.0		2.8		0.92	0.30	0.15	0.64	0.03		2.6	5.3	423	
117				5.1		1.75	0.31	0.25	1.30	0.07		14.6	18.6	746	

Data not available Sensor not working

Table A2 - Results of the tests performed for field of view 2 (FOV2).

Test ID	Δx (m)	Δy (m)	UKC (m)	UBT (m/s)	PIV				EMS-1 (m/s)	EMS-2 (m/s)	EMS-3 (m/s)	F1x (kN)	Fx_{total} (kN)	RPM	Note
					Ux,max jet (m/s)	Ux,max bed (m/s)	Ux,max / 1.1 UBT (-)	TI max bed (-)							
166	0.8	0.0	2.5	2.7	0.77	0.13	0.04	0.14	0.61	0.02		2.3	2.5	423	
168				4.6	3.68	1.69	0.33	0.13	1.13	0.77		7.2	6.1	802	
172		-2.0		2.7		0.11	0.04	0.03	0.71	0.01		2.3	2.2	423	
174				4.7		0.29	0.06	0.07	1.31	0.29		8.4	7.2	776	

Data not available Sensor not working

Table A3 - Results of the tests performed for field of view 3 (FOV3).

Test ID	Δx (m)	Δy (m)	UKC (m)	UBT (m/s)	PIV				EMS-1 (m/s)	EMS-2 (m/s)	EMS-3 (m/s)	F1x (kN)	Fx_{total} (kN)	RPM	Note
					Ux,max jet (m/s)	Ux,max bed (m/s)	Ux,max / 1.1 UBT (-)	TI max bed (-)							
008	23.1	0.0	2.4	2.6	2.95	0.07	0.02	0.52	0.03	0.13	0.01	4.8	5.2	411	
011				3.8	4.51	0.13	0.03	0.14	0.10	0.19	0.01	11.4	12.8	622	
014				5.6	5.93	0.19	0.03	0.08	1.06	0.06	0.03	21.8	24.1	831	Free jet tests
020			0.5	2.6	2.77	0.53	0.19	0.57	0.25	0.40	0.43	2.4	0.9	409	No channel wall
023				3.8	4.22	0.75	0.18	0.42	0.36	0.53	0.56	8.1	6.0	620	
026				5.3	5.86	1.11	0.19	0.53	0.51	0.73	0.73	15.1	12.9	833	

Table A4 - Results of the tests performed for field of view 4 (FOV4).

Test ID	Δx (m)	Δy (m)	UKC (m)	UBT (m/s)	PIV				EMS-1 (m/s)	EMS-2 (m/s)	EMS-3 (m/s)	F1x (kN)	Fx_{total} (kN)	RPM	Note
					Ux,max jet (m/s)	Uy,max bed (m/s)	Uy,max / 1.1 UBT (-)	TI max bed (-)							
178	0.8	0.0	2.5	2.7	n.a	0.90	0.31	0.14	0.58	0.31		2.7	2.5	426	
180				4.9	n.a	1.72	0.32	0.13	1.16	0.13		10.9	9.0	755	
183				2.6	n.a	1.15	0.40	0.36	0.57	0.27		2.6	2.7	427	
186				4.9	n.a	2.29	0.42	0.37	1.17	0.04		10.7	9.1	743	
189	3.0			2.6	n.a	1.70	0.60	0.40	0.53	0.01		2.6	3.7	432	
191				4.4	n.a	2.75	0.56	0.45	1.08	0.01		10.6	11.7	774	

Data not available Sensor not working

A.2 Additional test series

Table A5 - Results of the tests performed with BT1 and BT1 and BT2 simultaneously active, smooth bed.

Test ID	Δx (m)	Δy (m)	UKC (m)	Active thruster	Dir. rotation (BT1 / BT2)	UBT (m/s)	PIV				EMS-1 (m/s)	EMS-2 (m/s)	EMS-3 (m/s)	F1x (kN)	Fx_{total} (kN)	RPM
							Ux,max jet (m/s)	Ux,max bed (m/s)	Ux,max / 1.1 UBT (-)	TI max bed (-)						
221	0.8	3.5	2.5	BT1	CCW	4.4	4.30	1.68	0.35	1.05	1.04	0.01	1.77	7.9	10.3	753
218		2.0				4.4	3.60	1.82	0.38	0.73	1.17	0.12	1.81	11.6	10.4	755
223		0.0				4.4	1.60	1.60	0.33	0.91	1.27	0.01	1.88	11.2	10.1	754
225		-2.0				4.3	1.17	1.17	0.25	1.18	1.14	0.21	1.62	9.1	9.9	757
231	0.8	0.0	2.5	BT1&BT2	CCW/CW	4.4	4.92	2.09	0.43	1.15	2.05	0.96	1.90	20.8	18.8	751
242					CW/CW	4.6	5.18	1.99	0.40	0.69	1.82	0.62	2.13	15.8	21.1	746
235		3.5			CCW/CW	4.3	4.08	1.93	0.41	0.94	1.54	0.22	1.95	16.2	19.1	751
238					CW/CW	4.6	4.43	2.03	0.40	0.79	1.60	0.08	1.82	10.6	21.2	747
233		2.0			CCW/CW	4.1	3.31	2.27	0.51	1.63	1.87	0.40	1.64	16.5	18.3	759
244					CW/CW	4.5	2.62	2.35	0.47	0.76	1.99	0.21	1.40	20.7	21.1	747
252		-2.0			CCW/CW	4.3	1.82	1.82	0.38	1.08	1.46	0.88	2.14	16.5	18.8	747
247					CW/CW	4.5	1.94	1.94	0.39	1.11	1.42	0.75	2.25	16.9	19.6	747
263		2.0	1.5		CCW/CW	4.4	3.75	2.62	0.55	0.96	1.90	0.46	2.59	8.6	5.7	765
267			0.4		CCW/CW	2.4	1.83	1.14	0.42	0.43	0.36	0.19	1.34	6.5	5.2	449
269			0.4		CCW/CW	4.1	3.21	2.07	0.46	0.53	0.58	0.41	2.31	15.3	14.7	766
254	3.0	2.0	2.5	BT1&BT2	CCW/CW	4.3	3.60	2.03	0.43	0.37	1.76	0.26	1.30	19.3	21.3	754
272			0.4			4.4	3.26	1.22	0.25	0.44	0.38	0.63	1.66	15.3	18.1	766
278	23.1	2.0	2.5			4.8	3.87	0.78	0.15	0.72	1.30	0.56	1.04	28.9	30.7	765
275			0.4			4.5	3.10	2.49	0.50	0.29	0.41	0.56	1.46	20.1	22.6	793

Table A6 - Results of the repeated tests in the additional test series, after moving EMS closer to the wall and increasing PIV resolution.

Test ID	Δx (m)	Δy (m)	UKC (m)	Active thruster	UBT (m/s)	PIV				EMS-1 (m/s)	EMS-2 (m/s)	EMS-3 (m/s)	F1x (kN)	Fx_{total} (kN)	RPM	Note
						Ux,max jet (m/s)	Ux,max bed (m/s)	Ux,max / 1.1 UBT (-)	TI max bed (-)							
201	0.8	0.0	2.5	BT2	4.5	n.a.	n.a.	n.a.	n.a.	1.24	0.74	2.07	7.4	6.1	730	Only EMS
206			1.5		4.7	n.a.	n.a.	n.a.	n.a.	1.53	0.38	3.39	5.5	2.6	742	
209			0.5		4.7	n.a.	n.a.	n.a.	n.a.	0.64	0.8	3.56	3.1	1.3	753	
291	0.8	0.0	0.4	BT2	4.6	5.14	3.18	0.63	0.30	0.65	0.69	3.52	3.1	0.9	772	PIV tests with higher res.
293		-2.0			4.6	2.84	2.84	0.57	0.42	0.88	0.26	4.56	2.5	0.6	774	
295		-4.0			4.6	1.47	1.47	0.29	0.23	1.48	0.10	3.30	2.6	0.1	769	
298		0.0	1.4		4.6	5.27	3.02	0.60	0.31	1.51	0.34	3.27	5.7	2.3	785	
300			2.4		4.4	4.99	1.89	0.39	0.16	1.19	0.76	2.02	8.0	5.7	814	

Table A7 - Results of the tests performed with fixed rock (10-60 kg).

Test ID	Δx (m)	Δy (m)	UKC (m)	UBT (m/s)	PIV				F1x (kN)	Fx_{total} (kN)	RPM	Note
					Ux,max jet (m/s)	Ux,max bed (m/s)	Ux,max / 1.1 UBT (-)	TI max bed (-)				
308	0.8	0.0	2.5	4.7	5.45	1.56	0.30	0.48	11.7	12.3	778	10-60kg fixed rock
313			1.4	4.6	5.37	1.64	0.32	0.34	10.6	11.8	774	
316			0.4	4.5	5.29	1.65	0.34	0.22	10.7	11.6	817	
303		2.0	2.5	4.7	1.49	1.39	0.27	0.23	9.2	12.6	775	
306		-2.0		4.7	1.73	1.67	0.33	0.27	11.4	12.4	778	
310	3.0	0.0	2.5	4.7	5.40	1.54	0.30	0.38	18.0	18.7	773	
318			0.4	4.6	5.35	1.58	0.31	0.23	14.6	16.3	773	

Table A8 - Results of the tests performed with rock.

Test ID	Δx (m)	UKC (m)	UBT (m/s)	Rock material	Max deformation (scour) (m)
A01	0.8	2.5	3.8	10-60 kg	n.a. (fixed bed)
B01	0.8	0.5	3.8	10-60 kg	n.a. (fixed bed)
C01	0.8	2.5	3.8	90-250 mm	0.3 m
D01	0.8	0.5	3.8	90-250 mm	0.6 m

B Overview figures

C Model thruster specs

D Calibration acoustic flow meter

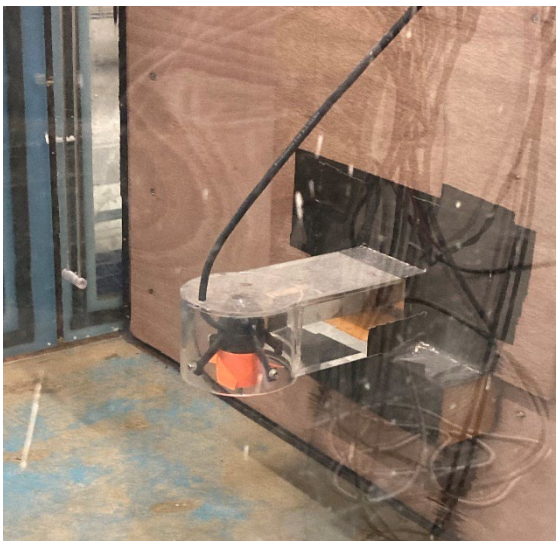

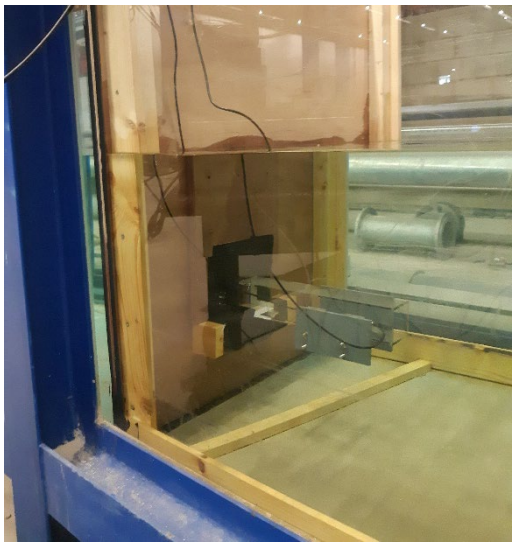

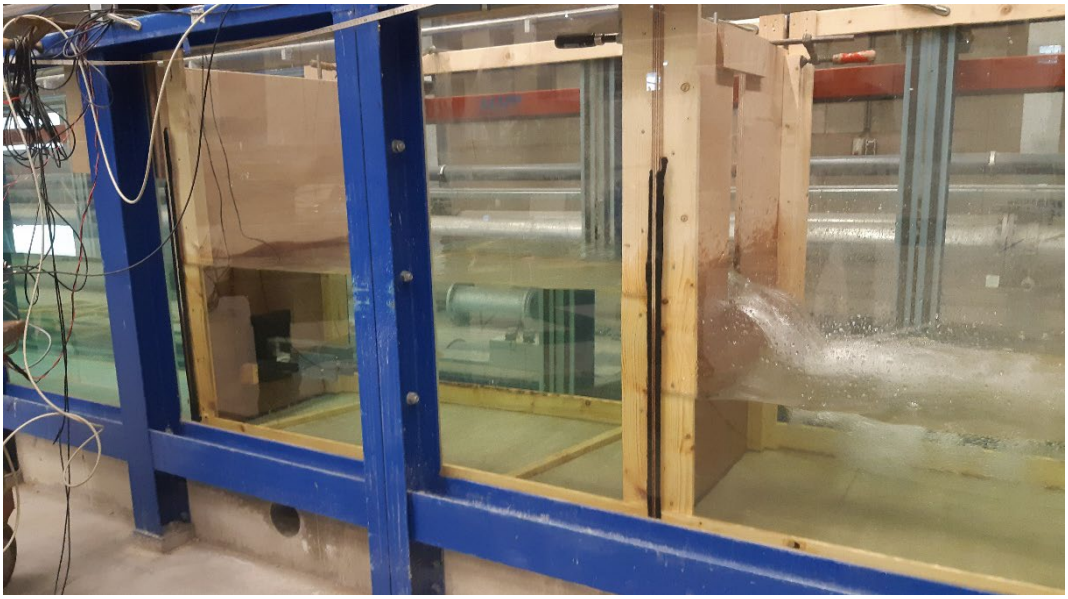

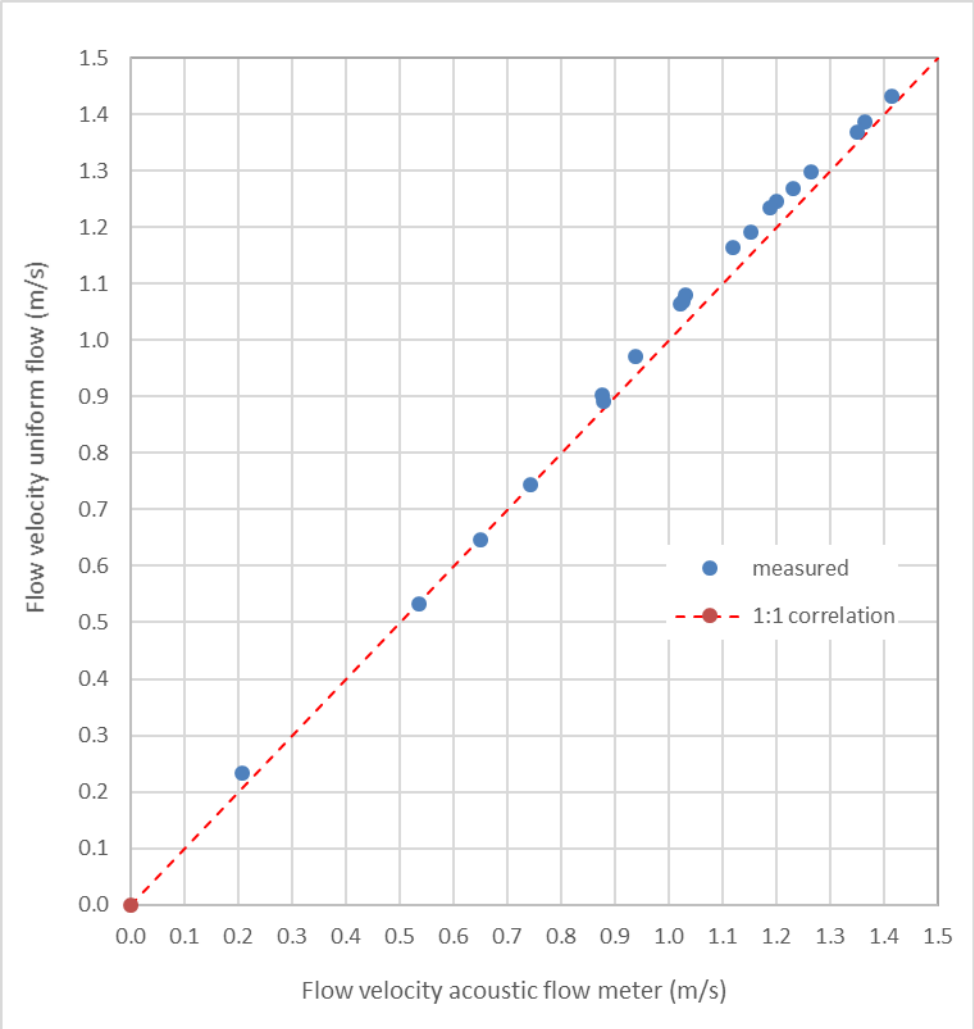

The average deviation between uniform (bow thruster channel cross-sectional averaged) flow velocity and the velocity measured by the acoustic flow meter is -2.4%. Meaning that, for the expected flow range, the acoustic flow meter measures on average 2.4% lower flow velocities than the actual mean flow velocity. Therefore, a correction is applied to the flow velocity measured by the acoustic flow meter (U_{AFM}) to obtain the actual mean outflow velocity of the bow thruster: $U_{BT} = 1.024\ U_{AFM}$.

E Overview of instrumentation

Measurement		Instruments					Calibration	DAQ Channel
		Device			Amplifier			
type	nr.	type	ID-nr.	range	type	ID-nr.		
	EMS-1							
Velocity X	S1	EMS E40	01.00.381	1 m/s	PEMS	02.00.375	V	1
Velocity Y	S2	EMS E40	01.00.381	1 m/s	PEMS	02.00.375	V	2
	EMS-2							
Velocity X	S1	EMS E40	01.00.382	1 m/s	PEMS	02.00.371	V	3
Velocity Y	S2	EMS E40	01.00.382	1 m/s	PEMS	02.00.371	V	4
	EMS-3							
Velocity X	S1	EMS E40	01.00.383	2.5 m/s	PEMS	02.00.369	V	5
Velocity Y	S2	EMS E40	01.00.383	2.5 m/s	PEMS	02.00.369	V	6
	KRM-1							
Force X	FX1	K3D60a 50N	01.06.355	50N	Scaime	02.06.533	5 N/V	7
Force Y	FY1	K3D60a 50N	01.06.355	50N	Scaime	02.06.534	5 N/V	8
Force Z	FZ1	K3D60a 50N	01.06.355	50N	Scaime	02.06.537	5 N/V	9
	KRM-2							
Force X	FX2	K3D60a 50N	01.06.373	50N	Scaime	02.06.539	5 N/V	10
Force Y	FY2	K3D60a 50N	01.06.373	50N	Scaime	02.06.540	5 N/V	11
Force Z	FZ2	K3D60a 50N	01.06.373	50N	Scaime	02.06.542	5 N/V	12
	KRM-3							
Force X	FX3	K3D60a 50N	01.06.374	50N	Scaime	02.06.543	5 N/V	13

Force Y	FY3	K3D60a 50N	01.06.374	50N	Scaime	02.06.544	5 N/V	14
Force Z	FZ3	K3D60a 50N	01.06.374	50N	Scaime	02.06.545	5 N/V	15
pressure	D1	RPOP001D6A	01.05.412	60 mB	Scaime	02.06.547	- 6 mB/V	16
pressure	D2	24PCEFA6D	01.05.494	30 mB	Scaime	02.06.501	3 mB/V	**25**
pressure	D3	RPOP001D6A	01.05.414	60 mB	Scaime	02.06.549	6 mB/V	18
pressure	D4	RPOP001D6A	01.05.415	60 mB	Scaime	02.06.550	- 6 mB/V	19
pressure	D5	RPOP001D6A	01.05.416	60 mB	Scaime	02.06.551	- 6 mB/V	20
pressure	D6	RPOP001D6A	01.05.463	60 mB	Scaime	02.06.552	6 mB/V	21
pressure	D7	24PCEFA6D	01.05.490	30 mB	Scaime	02.06.553	3 mB/V	22
pressure	D8	24PCEFA6D	01.05.492	30 mB	Scaime	02.06.554	3 mB/V	23
pressure	D9	24PCEFA6D	01.05.493	30 mB	Scaime	02.06.500	3 mB/V	24
pressure	D10	RPOP001D6A	01.05.413	60 mB	Scaime	02.06.548	6 mB/V	**17**
Discharge	Q1	Katronic	01.10.131	2.5 m/s	2-10V	0-2.5 m/s	-0.625 l/V	26
RPM	R1						380rpm/V	27
Level	LVL	Temposonic	01.11.257	1.2 m			1.3906-0.303693m/V	28
Trigger	PIV						1	32

Deltares is an independent institute for applied research in the field of water and subsurface. Throughout the world, we work on smart solutions for people, environment and society.

Deltares

www.deltares.nl